A transcription factor network dictates neuronal cell fate decisions in the zebrafish dorsal diencephalon

By

Sataree Khuansuwan

Dissertation

Submitted to the Faculty of the

Graduate School of Vanderbilt University

in partial fulfillment of the requirements

for the degree of

DOCTOR OF PHILOSOPHY

in

Biological Sciences

December, 2014

Nashville, Tennessee

Approved:

Joshua T. Gamse, Ph.D.

James G. Patton, Ph.D.

Wenbiao Chen, Ph.D.

Kevin Ess, M.D., Ph.D.

Douglas G. McMahon, Ph.D.

For my better half, Joshua Clanton

and

For my aunt Bussakorn

ACKNOWLEDGEMENTS

This work would not have been possible without the financial support from Vanderbilt University Medical Center Program in Developmental Biology training grant, Vanderbilt University Biological Sciences department, Gisela Mosig travel fund, Dissertation Enhancement grant from Vanderbilt University Graduate School, and funding support from National Institutes of Health.

I am extremely grateful to the current and past members of my dissertation committees for giving me guidance, shepherding my research goals, and teaching me invaluable lessons throughout the years. I thank Joshua T. Gamse, James G. Patton, Wenbiao Chen, Kevin C. Ess, Douglas G. McMahon, Jason R. Jessen, and Christopher V. Wright for their support. I am extremely appreciative of Jim Patton for not only allowing me into the Interdisciplinary Graduate Program, but also for his support over the years, and for providing me a scientific home when I needed one. I extend immense gratitude to my mentor, Joshua Gamse, for creating a great scientific community for me to work in and for always believing in me and allowing me to grow both personally and professionally.

Throughout my tenure at Vanderbilt and in the lab, I had the privilege to work alongside many wonderful people whom I believe have made me not only a better scientist, but also a better person. I thank Leslie Maxwell and Angela Titus in the Biological Sciences Department office and Kim Kane in the Program in Developmental Biology. For excellent fish care and lab maintenance, I thank Erin Booton, Gena Hockensmith, and Qiang Guan. My rotation mentor, Robert Taylor, has been a great role

model and a wonderful person to work with. Additionally, I thank Joshua Clanton, Simon Wu, Benjamin Dean, Nancy Hernandez, and Caleb Doll for providing input on my research and for being awesome lab mates. I also considered it a great privilege to mentor the two undergraduates: Christopher Bulow and Michelle Shen, whom, among other things, helped me maintain my ever-growing fish lines.

I am extremely thankful for my friend Xuan-Mai Vien, my mother Daraneerat Thaveeratrangsee, and for Joshua Clanton and his family. Joshua Clanton has not only been a great lab partner, he has also been the greatest friend and a wonderful life partner. I am fortunate and grateful that he has allowed me to come into his life. I could not ask to share my world with a better person.

I am indebted to my late aunt Bussakorn Rajvongs for opening up her home to me when I had no where to turn, for always believing in me when I did not have the strength to believe in myself, for showing me true kindness, and for being such a wonderful person I now strive to become. I would not be here without her.

TABLE OF CONTENTS

LIST OF TABLES

Table **Page**

LIST OF FIGURES

Figure **Page**

ABBREVIATIONS

ANR	anterior neural ridge
BMP	Bone morphogenetic protein
bp	base pairs
BrdU	Bromodeoxyuridine
Ca^{2+}	calcium ions
cDNA	complementary DNA
CNS	central nervous system
Cyc	Cyclops
dpf	days post fertilization
EdU	5-Ethynyl-2'-deoxyuridine
FACS	fluorescence activated cell sorted
Fgf	Fibroblash growth factor
Flh	Floating head
fsi	frequent-situs-inversus
hpf	hours post fertilization
IPN	interpeduncular nucleus
ISHCR	*in situ* hybridization chain reaction
Kctd	Potassium channel tetramerization domain
KV	Kupffer's vesicle
LH	Left heart and left sided parapineal organ
LLPM	left lateral plate mesoderm
MHB	Midbrain-Hindbrain boundary
MO	morpholino
MRI	magnetic resonance imaging
Ndr2	Nodal-related 2
NIC	non-injected controls
Nr2e3	Nuclear receptor subfamily 2, group E, member 3
PCR	polymerase chain reaction
PD	Parkinson's disease

PGC	primordial germ cells
PI	propidium iodine
Pitx2	Paired-like homeodomain 2
PLG	Phase Lock Gel
RH	Right heart and right sided parapineal organ
RNA-seq	RNA sequencing
rpm	round per minute
RT-PCR	Reverse transcription polymerase chain reaction
Shh	Sonic hedgehog
Six3	SIX homeobox 3
Sox1a	Sex determining y-box transcription factor
Spw	Southpaw
ss	somites stage
Tbx2b	T-box containing transcription factor 2b
TGFβ	Transforming growth factor beta
WT	wild-type; wildtypes
ZLI	zona limitans intrathalamica

CHAPTER 1

INTRODUCTION

Early patterning in the vertebrate brain

The formation of the vertebrate brain begins with the specification of the neuroectoderm from the presumptive epidermis during gastrulation. As development proceeds, the neuroectoderm converges and extends, lengthening into a flat plane of cells called the neural plate (Dworkin and Jane, 2013). In a process often referred to as primary neurulation, the neural plate folds and invaginates to form the neural tube. Then, regions of the anterior neural tube are specified toward a distinct set of fates based on their anterior-posterior and dorsal-ventral position (Wurst and Bally-Cuif, 2001).

Initially, the anterior neural tube forms three vesicles that will become the three early divisions of the vertebrate brain: the prosencephalon (forebrain), mesencephalon (midbrain), and rhombencephalon (hindbrain) (Wurst and Bally-Cuif, 2001). The prosencephalon will develop into the telencephalon, diencephalon, and their derivatives. The mesencephalon gives rise to the tectum and optic lobes. The rhombencephalon will develop into the cerebellum, medulla, and brain stem. Much of this brain regionalization is influenced by the formation of two "organizing centers" known as the Midbrain-Hindbrain boundary (MHB) and the rostral-organizing center. These organizing centers are groups of cells that secrete morphogens that can, through the initiation, maintenance, and shaping of transcription factor networks, dictate the fate of cells in a particular region of the developing brain (Dworkin and Jane, 2013; Suzuki-Hirano and Shimogori, 2009).

Distinct differences exist in the details of early brain patterning in vertebrates. However, this process and the molecules involved are quite well conserved. The best known organizing center of the brain, the MHB, which is sometimes called the isthmic organizer, secretes multiple Fibroblast growth factors (Fgf), as well as Wnt1 (Dworkin and Jane, 2013; Wurst and Bally-Cuif, 2001). These morphogens exert powerful effects on the surrounding mesencephalon and rhombencephalon. Rhombencephalic regions exposed to high levels of Fgf signaling near the MHB will become the cerebellum (Wurst and Bally-Cuif, 2001). Moderate to low Fgf activity specifies the medulla and other brain stem fates (Wurst and Bally-Cuif, 2001). The mesencephalon regions closest to the MHB will give rise to the tectum (Dworkin and Jane, 2013).

Morphogens are also secreted from the rostral-organizing center. Fgf from a specific group of cells directly anterior to the presumptive anterior prosencephalon called the anterior neural ridge (ANR) act in concert with sonic hedgehog (Shh) from the prechordal plate underlying the neuroectoderm to specify the anterior and ventral region of the telencephalon (Danesin and Houart, 2012; Suzuki-Hirano and Shimogori, 2009). More posterior regions of the prosencephalon become the diencephalon (Wurst and Bally-Cuif, 2001). Once specified, Shh signaling from a region called the zona limitans intrathalamica (ZLI) helps define the future compartment identity within the diencephalon, which consists of thalamus, subthalamus, hypothalamus, and epithalamus (Puelles, 2007).

Functional lateralization in the human brain

Functional lateralization between the left and right hemispheres of the human brains has long been described. The discoveries of Broca's and Wernicke's areas in the mid-late 1800s demonstrated that speech and language development are predominantly controlled by the left hemisphere (Toga and Thompson, 2003). In the 1960s, observations made by Richard Sperry and Michael Gazzaniga in split-brain patients, whose two hemispheres cannot communicate due to resection of the corpus callosum, showed that each of the hemispheres is specialized for different tasks (Sperry, 1961). While both hemispheres can perform any task to some degree, the left hemisphere is more specialized for language development and tool usage, while the right hemisphere is more specialized for processing visual-spatial information. This lateralization of brain functions is believed to allow for humans to more efficiently multi-task by preventing duplication of functions or simultaneous initiation of incompatible responses from the two hemispheres (Vallortigara and Rogers, 2005).

It has also been shown that reduced or reversed brain asymmetries are linked to neurological disorders including schizophrenia, dyslexia, autism, and depression. Reduced asymmetry in the planum temporale volumes (the brain regions important for speech and language development; normally larger in the left hemispheres of most right handed individuals) has been associated with increased severity of symptoms for schizophrenia (Oertel et al., 2010). Individuals with reduced hemispheric asymmetries tend to have deficits in written and oral language skills associated with dyslexia (Leonard and Eckert, 2008; Sun et al., 2010). Whole brain MRI studies revealed that boys with autism, in addition to having larger cortical volumes overall, show general trends toward

an asymmetric increase in the left cortex. However, the volumes of the corpus callosum remain unchanged despite the altered cortical volumes, suggesting a reduced interhemispheric communication (Herbert et al., 2005). Male patients with severe depression exhibit smaller left hippocampal volumes (Kronmüller et al., 2009).

Furthermore, the progression of certain neurodegenerative diseases is asymmetric. Greater atrophy, neuronal loss, and more abnormal protein precipitates in the language dominant hemisphere have been documented in patients with Alzheimer's disease (Mesulam et al., 2014). Parkinson's disease (PD) is marked by asymmetric onset on motor dysfunction. Moreover, asymmetrical lateral ventricular enlargement, a non-specific marker for neurodegeneration, is greater and displays a faster rate of enlargement in the contralateral to symptom onset side in PD subjects (Lewis et al., 2009). Thus, it is important to understand the molecular mechanisms that underlie the development of asymmetric brain formation, as well as how asymmetry is maintained.

Lateralized brain functions in other animals

Until as recently as the 1970s, it was widely believed that brain asymmetry is a feature unique to humans (Vallortigara et al., 1999). However, recent work in animal models has demonstrated that both structural and functional brain asymmetries likely exist throughout the animal kingdom (Vallortigara and Rogers, 2005). In chicks, the left hemisphere is responsible for differentiating pebbles from grain and for both short and long term memory; the right hemisphere is responsible for responding to predator attacks, recognition of other chicks, and control of copulation, as well as short term memory

(Rogers, 2008). Functional lateralization of the zebrafish brain has also been documented, as discussed below.

Lateralization of the nervous system is not restricted to vertebrates, but rather is found throughout the animal kingdom. The evolutionary conservation of this attribute suggests an important selective advantage. For examples, in the round worm *Caenorhabditis elegans*, the left and right AWC neurons are different at the molecular level and detect different sets of odors (Taylor et al., 2010); in social bees, the right antenna has more receptors and is used for learning and for short term memory, while the left antenna is used for long term memory (Rogers, 2014). Interestingly, lateralization of receptor number in the right antenna is not observed in solitary mason bees (Anfora et al., 2010), suggesting that lateralization provides advantage at the population level in social animals.

The zebrafish dorsal diencephalon as a model for asymmetric brain development

While asymmetries have been well documented in all vertebrate brains analyzed (reviewed by Concha and Wilson (2001)), very little is known about the molecular mechanisms that control how these asymmetries arise during development. Over the past two decades, the zebrafish (*Danio rerio*) has emerged as a great model to study brain development due to its transparent embryos, relatively simple brain, rapid development, plentiful genetic tools, high fecundity, and the ability to perform high throughput behavioral testing.

The best-studied asymmetric region of the zebrafish brain is the dorsal diencephalon. Also known as the epithalamus, it lies at the top of the third ventricle and

is comprised of bilaterally paired dorsal habenular nuclei and the pineal complex (Figure 1). The habenular nuclei are two clusters of neurons and associated neuropil that reside just anterior to the telencephalon in the forebrain. These neurons arise from the neuroepithelium that lines the third ventricle of the epithalamus, (Aizawa et al., 2007; Concha et al., 2003). The pineal complex develops as an evagination of the diencephalic roof plate during development and is comprised of the pineal and parapineal organ (Concha and Wilson, 2001). The parapineal organ is formed by precursors that initially reside within the pineal anlage. They later migrate to the left side, adjacent to the pineal organ (Concha et al., 2003; Gamse et al., 2003).

Based on cytoarchitecture, neural connectivity, and molecular characterization, the zebrafish habenulae can be subdivided into dorsal and ventral regions. Briefly, the zebrafish ventral habenula sends projection into the median raphe and has been shown to be homologous to the mammalian lateral habenula, an important brain region that controls motor and cognitive behaviors through the modulation of dopaminergic and serotonergic neuronal activities (Amo et al., 2010). The zebrafish dorsal habenulae are analogous to the mammalian medial habenulae, and send projections into the interpeduncular nucleus (IPN) of the midbrain region (Aizawa et al., 2005; Gamse et al., 2005). While the ventral habenula is symmetric (Amo et al., 2010), the dorsal habenular nuclei exhibit robust left-right asymmetries in zebrafish and will be further discussed.

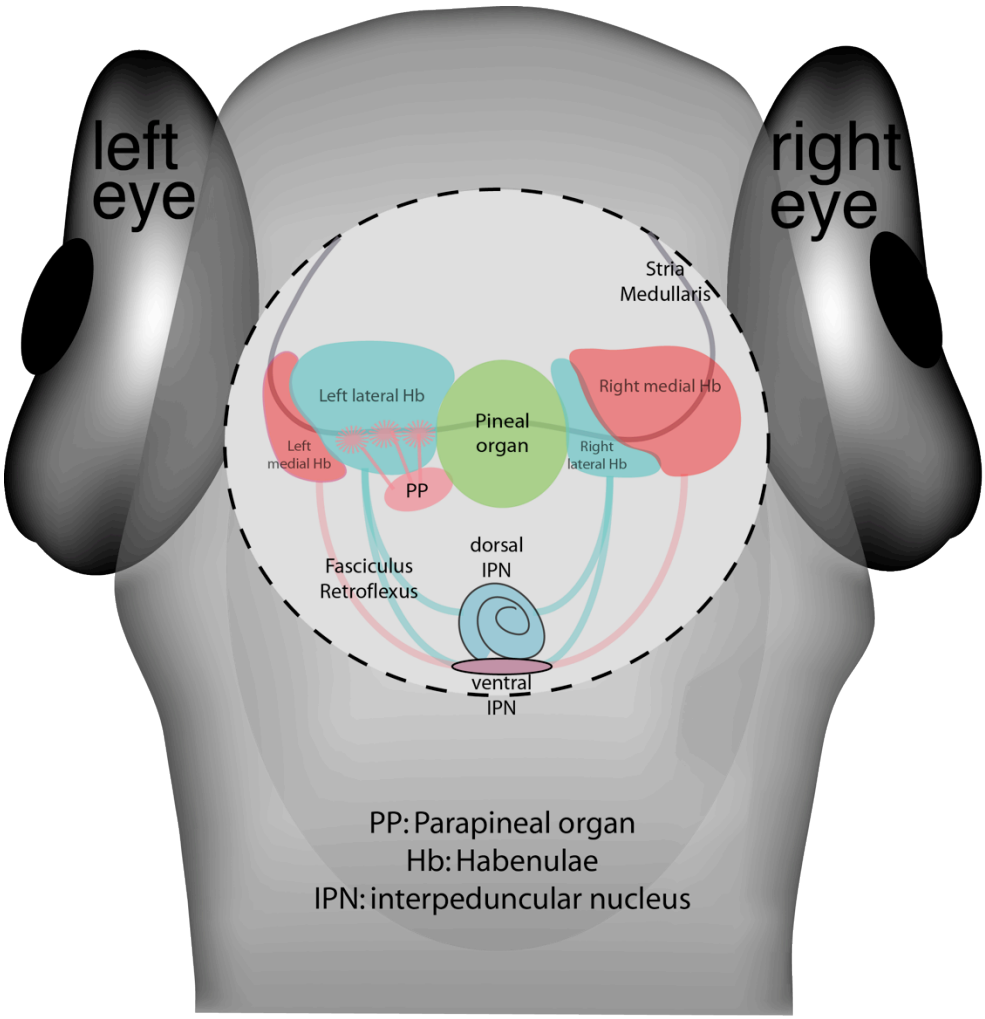

Figure 1: The zebrafish dorsal diencephalon exhibits left-right asymmetry. A schematic of a 4 days post fertilization zebrafish dorsal diencephalon (epithalamus), dorsal view. The zebrafish epithalamus is comprised of a medially located pineal organ and a left sided parapineal organ (PP). The PP organ sends projections into the flanking habenular (Hb) nucleus, influencing asymmetry in gene expression and neuropil density between the left and right Hb nuclei. Hb nuclei are subdivided into lateral and medial subnuclei. Hb nuclei receive afferent inputs from the anterior forebrain via stria medullaris and send projections into their midbrain target, the interpeduncular nucleus (IPN), via fasciculus retroflexus. Lateral Hb send projections into both the dorsal and ventral aspects of the IPN, while medial Hb project exclusively into the ventral IPN. Figure is modified from Snelson CD and Gamse JT, “Building an asymmetric brain: Development of the zebrafish epithalamus,” Seminars in Cell & Developmental Biology 20, 491-497 (2009).

The dorsal habenulae are posterior forebrain structures and are part of a relay system that receives input from the anterior forebrain through the stria medullaris and sends projections into the IPN of the midbrain region through the fasciculus retroflexus (Sutherland, 1982). Left-right differences in neuropil density, gene expression, and efferent connectivity are prominent between the dorsal habenular nuclei. Greater neuropil density is observed in the left dorsal habenula as compared to the right (Concha et al., 2000). At the molecular level, expression of the potassium channel tetramerization domain proteins Kctd12.1 and Kctd12.2 is asymmetric; they are more highly expressed in the left and right habenular nuclei, respectively (Gamse et al., 2005). While efferents from the Kctd12.1+ neurons project mostly into the dorsal subnucleus of the IPN (and to a lesser extent the ventral IPN), Kctd12.2+ neurons exclusively project to the ventral subnucleus of the IPN (Gamse et al., 2005). The development of these asymmetries is dependent on the presence of the parapineal organ (Concha et al., 2003; Gamse et al., 2003). If parapineal placement is right sided (reversed), asymmetries within the habenular nuclei are also reversed (Gamse et al., 2003). In zebrafish larvae that lack a parapineal organ, asymmetry is reduced and both habenular nuclei send their efferents into the ventral subnucleus of the IPN instead (Snelson et al., 2008b).

The pineal organ, which acquired its name through its resemblance to a pine cone, is an important neuroendocrine organ that secretes melatonin which modulates sleep-wake cycle in response to circadian stimuli (Cahill, 1996; Fodor et al., 2013; Gamse et al., 2002; Jiang et al., 2014; Stockhammer et al., 2010; Wells et al., 2013). Unlike in mammals, the pineal organ of teleosts, as well as reptiles, amphibians, lampreys, and embryonic birds, can directly sense light and serves as a photosensory organ in some

species (Bertolucci and Foà, 2004; Mano and Fukada, 2007). In larval zebrafish, no asymmetry is observed in the pineal organ itself. However, asymmetry is observed in the adult zebrafish pineal stalk, which is positioned to the left of midline (Liang et al., 2000). Adjacent to the pineal organ is the parapineal organ, which is comprised of a small cluster of 10-12 neurons that typically resides on the left side of the brain. The neurons of the parapineal organ are specified in the anterio-medial region of the pineal anlage and subsequently migrate away from the midline to lie adjacent to the left habenula. While the parapineal organ's function is not well understood, the projections that it sends into the flanking habenular nucleus clearly influences the left-right differences observed between the habenular nuclei (Concha et al., 2000; Concha et al., 2003; Gamse et al., 2003; Ozsolak and Milos, 2011). Thus, the development of the unilaterally located parapineal organ is integral to the formation of left-right asymmetry in the zebrafish brain.

Parapineal organ development

Parapineal organ development occurs in several steps (Figure 2). Cells that will later migrate away from the midline to form the parapineal organ originate from within the pineal anlage and are morphologically indistinguishable from pineal precursors for much of their development (Clanton et al., 2013; Concha et al., 2003). BrdU labeling experiments indicate that most parapineal precursors are born by 18 somites stage (ss) (Snelson et al., 2008a). Although markers for newly specified parapineal precursors do not currently exist, by 24 hours post fertilization (hpf), lineage labeling experiments indicate that parapineal precursors are bilateral in origin and are located in the anterior-most region of the pineal anlage prior to their migration (Concha et al., 2003). By 26 hpf,

newly differentiated parapineal cells, indicated by *sox1a* expression, appear to be bilaterally located in the anterior pineal complex anlage (Clanton et al., 2013). These differentiated parapineal cells then begin to unilaterally migrate away from the pineal anlage to the left of the midline around 24-28 hpf. By 48 hpf, parapineal cells have completed their migration to their approximate final position, which is to the left of and ventral to the pineal organ and posterior and adjacent to the developing left habenular nucleus. By 50 hpf, the parapineal organ sends projections into the flanking habenular nucleus, influencing left-right differences observed between the habenular nuclei.

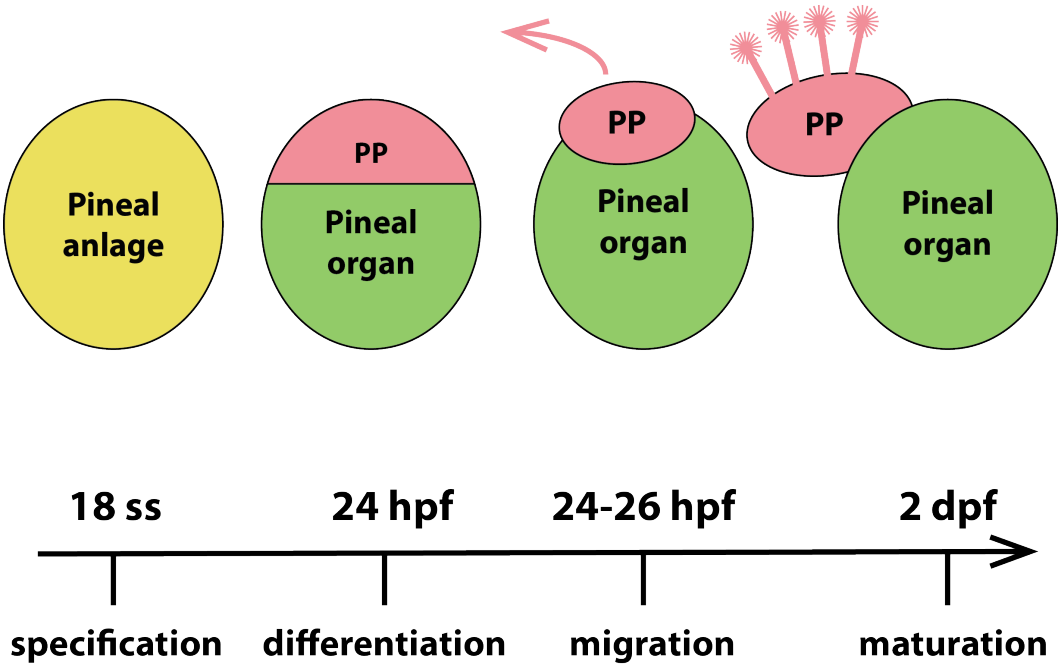

Figure 2: Parapineal organ development occurs in several steps.
Parapineal (PP) precursors are specified within the pineal anlage from an unknown developmental stage until about 18 ss, when most PP cells have been born. By 24 hpf, most, if not all of the specified PP cells accumulate in the anterior region of the pineal anlage. At this stage, PP cells also begin to turn on an early differentiation marker, *sox1a*. Starting around 24-26 hpf, PP cells initiate their leftward migration and a small outcropping of cells can be seen protruding from the pineal anlage. By 2 dpf, these mature parapineal neurons have mostly completed their migration to lie left of the pineal organ and begin to send projections into the flanking habenular nucleus.

Nodal and Fgf signaling defines laterality of the parapineal organ

Laterality of the parapineal organ depends on Nodal and Fgf signaling. Nodal, which belongs to the TGFβ superfamily, has been well documented in playing a role in asymmetric placement of internal organs and for inducing overall left-right asymmetries across multiple species (reviewed by Schier (2003) and Palmer (2004)). In the zebrafish epithalamus, Nodal signaling components are transiently expressed in the presumptive pineal organ, as well as habenular precursors directly ventral to it (Concha et al., 2000; Concha et al., 2003; Liang et al., 2000). Expression of Nodal related genes precede the onset of asymmetric migration of the parapineal organ.

Asymmetric expression of Nodal components is the result of an earlier symmetry-breaking event. In zebrafish, the symmetry-breaking event is thought to be induced by the left sided fluid flow generated by the rotation of cilia found on the dorsal forerunner cells of the transient embryonic "organ of asymmetry" known as the Kupffer's vesicle (KV) (Essner et al., 2005); KV is found at the tailbud at the end of gastrulation (Essner et al., 2002) and it is the zebrafish analog of the 'primitive node' structure (also known as the embryonic node in mice, Henson's node in chicks, and Spemann's organizer in amphibians). This left sided fluid flow allows for intracellular Ca^{2+} to more highly accumulate to the left of the KV (Sarmah et al., 2005) and for expression of *southpaw* (*spw*) to unilaterally localize to the left lateral plate mesoderm (LLPM) (Long et al., 2003). Through an unknown mechanism, a signal(s) generated by *spw* from the LLPM is transduced to the developing left epithalamus, where Nodal signaling is thought to be bilaterally repressed by the coordinated action of Wnt signaling and Six3 genes (*six3b/six7*) during mid- and early-somitogenesis stages (Carl et al., 2007; Inbal et al.,

2007). While *spw* itself is not expressed in the epithalamus, loss of *spw* function leads to an absence of Nodal signaling in the left epithalamus (Long et al., 2003), resulting in randomization of parapineal placement (Gamse et al., 2003). Once Nodal signaling is unilaterally de-repressed, expression of other Nodal signaling genes is transiently activated in the left epithalamus during late somitogenesis stages including *nodal related 2/cyclops* (*ndr2/cyc*) (Rebagliati et al., 1998; Sampath et al., 1998), the feedback inhibitor *lefty1/antivin* (Bisgrove et al., 1999; Thisse and Thisse, 1999), and the downstream effector *pitx2* (Campione et al., 1999; Essner et al., 2000). Furthermore, embryos that have a compromised midline structure (the physical and biochemical barrier that prevents signals from the left-of-midline to cross over to the right) have bilateral expression of *ndr2, lefty1,* and *pitx2* and randomized parapineal placement (Concha et al., 2000; Gamse et al., 2003). Thus, Nodal signaling is key in influencing the laterality of parapineal placement.

Regardless of laterality (left- or right-sided), placement of the parapineal organ has always been coordinated with induction of 'left' characteristics in the adjacent habenular nucleus (greater neuropil density and higher Kctd12.1 expression). Thus, the parapineal organ is thought to be a key modulator of left-right asymmetry formation. While it is clear that Nodal signaling influences the laterality of the parapineal placement, questions regarding whether or not Nodal influences formation of asymmetry itself is an interesting one and remains to be elucidated. Work by Roussigne and others showed that asymmetry within the habenular nuclei is observed prior to parapineal migration, and thus the initiation of habenular asymmetry is parapineal independent (2009). Further, blocking Nodal signaling through the use of the small molecule SB431542, which

inhibits TGFβ type I receptors, inhibits this early asymmetry formation in the habenular nuclei. Work from our lab also suggests that Nodal may influence this early asymmetry by controlling Fgf signaling (Benjamin J. Dean, unpublished), which has been shown to occur asymmetrically in the developing habenular nuclei (Clanton et al., 2013; Regan et al., 2009). However, some confounding results have also emerged. Embryos that lack *pitx2*, the downstream effector of Nodal signaling, show an increase of "left-ness" in the right habenula, leading to more symmetrical left and right habenular nuclei (Garric et al., 2014). As Nodal is normally left sided, loss of Nodal signaling is expected to cause more right sided characteristics in the left habenula, so this finding is paradoxical. Nonetheless, these studies suggest that some aspects of early habenular asymmetries depend on Nodal signaling and are parapineal independent.

To a lesser degree, Fgf signaling also influences laterality of the parapineal organ. As mentioned, Fgf signaling occurs in the presumptive habenular precursors. Fgf8a is expressed in the developing habenulae and is thought to be a chemotactic cue for parapineal cells (Regan et al., 2009). In concordance, parapineal precursors also express *fgf receptor4* (Clanton et al., 2013). Misexpression of Fgf8a can guide the directionality of parapineal migration in embryos that lack Nodal signaling (Regan et al., 2009). Conversely, reduction of Fgf8a causes parapineal cells to fail to migrate (Clanton et al., 2013; Regan et al., 2009).

In addition to Nodal and Fgf8a playing a clear role in inducing laterality of the parapineal placement, it has also been observed that reducing the temperature at which the zebrafish embryos are raised from 28.5°C to 22°C results in the randomization of parapineal placement and an increase in embryos with bilateral expression of *ndr2, lefty1*,

and *pitx2* (Liang et al., 2000). How this happens remains a mystery, but it could be that the coordinated action of *spw,* Wnt, and Six3 genes are temporally disrupted, as *spw* expression in the LLPM remains left sided in over 95% of the population raised at lower temperature (Liang et al., 2000).

Functional implications of zebrafish brain asymmetries

Recently, the behavioral implications of left-right brain asymmetries have begun to emerge in zebrafish. Unlike in humans and other animals with binocular vision (which both eyes are placed together and the two visual fields overlap), most fishes including zebrafish have monocular vision and can thus see two different field-of-views at once. Visual inputs from the left and right eyes are received in separate hemispheres, each specializing in different tasks. Thus, it is not surprising that zebrafish exhibit preferential eye usage; as this allows them to multitask, e.g. look out for predators while feeding. The zebrafish preferentially uses its left eye (right hemisphere) when assessing familiar objects; and its right eye (left hemisphere) for controlled behaviors, such as approaching and biting objects and for looking at contraspecific in the 'mirror viewing' test (Barth et al., 2005; Domenichini et al., 2011).

The zebrafish *frequent-situs-inversus* (*fsi*) mutant exhibits laterality defects; a high percentage of mutants develop with concordant reversal of visceral and neuroanatomical asymmetries (Barth et al., 2005). Behavioral testing in *fsi* larva show that fishes with reversed laterality (RH, right heart and right sided parapineal organ) show some coordinated reversal in some behaviors but not others. Both LH (left heart and left sided parapineal organ) and RH *fsi* fishes take the same turn direction when emerging

into a new environment (Barth et al., 2005) and when they are startled (Barth et al., 2005; Facchin et al., 2009). However, LH and RH *fsi* show opposite eye usage while viewing their own reflection for the first time (LH preferentially uses its right eye; RH its left eye) (Barth et al., 2005). Compared to LH *fsi,* RH *fsi* larvae emerge from the start chamber more quickly when confronted with a novel object (Barth et al., 2005). A study that examined zebrafish larva that naturally have right sided parapineal organ made similar observations; fishes with reversed parapineal placement tend to be 'bolder' when inspecting a predator (Dadda et al., 2010). In addition to demonstrating some differences in lateralized behaviors, fish with reversed central nervous system (CNS) laterality also demonstrates navigational delay as well as reduced exploration in a swim test (Facchin et al., 2009).

The above data suggests that eye use preference is influenced by reversing the laterality of an otherwise developmentally normal epithalamus. Recent works suggest that asymmetries within the habenular nuclei are also important for certain behaviors. Asymmetric reduction of habenular function results in inappropriate escape responses in zebrafish. These fishes were trained to associate a flashing light with electrical shocks and would attempt to escape. Over several sessions, they developed freezing behavior and did not attempt to escape, a behavior that can be associated with learned helplessness (Agetsuma et al., 2010; Lee et al., 2010). More recently, two independent studies demonstrate that neuronal responses to visual and odor stimuli in the habenular nuclei are lateralized and parapineal dependent (Dreosti et al., 2014; Krishnan et al., 2014). Using a genetically encoded GCaMP5G, which fluoresces in response to neural activity, Dreosti and others showed that more neurons in the left habenula of wild-type (WT) larvae

respond to light as compared to the right habenula (2014). Conversely, certain odors evoke responses strongly in the right habenula but not the left. This neural activity profile is reversed if parapineal placement is reversed (right sided instead of left). Ablation of the parapineal organ results in strong neural response to odor in both habenulae but far fewer light responsive neurons in either habenula (Dreosti et al., 2014). This work provides the first direct link between asymmetric neural activities and parapineal laterality. Additionally, it suggests that afferent inputs from the forebrain to the habenular nuclei are influenced by the presence of the parapineal organ. While more work needs to be done in order to better understand the linkage between left-right brain asymmetries and behaviors, these studies offer a great starting point for researchers.

Molecular mechanisms of zebrafish pineal complex development

The zebrafish pineal complex is comprised of a medially located pineal organ and a left-sided parapineal organ. The development of these two structures is thought to be specified by distinct molecular mechanisms (Snelson et al., 2008a). In larval zebrafish, the pineal organ is comprised of photoreceptors (rods and cones) and projection neurons and is among the earliest brain regions to be defined during development (Masai et al., 1997). The first nascent signs of pineal anlage development occur by approximately bud stage (10 hfp) (Masai et al., 1997). At this time, the presumptive pineal anlage precursors are small, bilateral patches of cells on the lateral edges of the anterior neural plate that express the homeodomain transcription factor *floating head* (*flh*). By 8 ss (13 hpf), the two *flh*-expressing domains are brought together as the neural plate converges at the midline during neural tube formation, and fuse to form a contiguous pineal complex

anlage. Flh activity is required for the progression of pineal neurogenesis beyond 18 ss (Masai et al., 1997). In *flh* mutants, the pineal anlage domain is reduced (Masai et al., 1997; Snelson et al., 2008a).

The anterior boundary of the pineal anlage is controlled by Wnt/β-catenin signaling (Masai et al., 1997); the dorsoventral patterning is governed by BMP activity (Barth et al., 1999). Mutation of Axin1 causes disruption of β-catenin degradation, which results in overactivation of Wnt/β-catenin signaling. The telencephalon and eyes are reduced or absent in Axin1 mutants, while the pineal anlage domain is expanded anteriorly (Masai et al., 1997). In strong Bmp2a mutants, *flh* expressing pineal complex domain is expanded ventrally (Barth et al., 1999).

One of the major questions regarding pineal complex development is how each cell type in the pineal and parapineal becomes correctly specified. Some progress has been made to elucidate this question with respect to molecular mechanisms. Two main cell types found within the pineal organ are photoreceptors and projection neurons. Together, BMP and Notch activity regulate the decision between photoreceptor and projection neuron cell fates (Cau et al., 2008; Quillien et al., 2011). BMP signaling is necessary and sufficient to promote photoreceptor fate and it is required for the Notch-inhibition of projection neuron fate (Quillien et al., 2011). On the other hand, the T-box containing transcription factor 2b (Tbx2b) has been shown to be important for both parapineal specification and migration. Loss of Tbx2b function results in fewer parapineal cells. Additionally, the few remaining cells fail to migrate away from the midline (Snelson et al., 2008b). However, the identity of Tbx2b's downstream target

genes that control these aspects of parapineal development is currently unknown. In Chapter 2, experiments to identify these target genes will be discussed.

Regarding specification of pineal versus parapineal, work by Clanton and others has shown that Fgf8a is required for a group of bipotential pineal anlage cells to adopt parapineal fate (2013). Complete absence of Fgf8a results in cells that would have become parapineal cells to instead adopt a cone photoreceptor fate. In addition to its role in parapineal specification, Fgf8a has been shown to direct and influence the migratory ability of parapineal cells. Reduction of Fgf8a, particularly during the initiation of parapineal migration stage, leads to failure of parapineal migration (Clanton et al., 2013; Regan et al., 2009). Recent work by Garric and others also showed that loss of the Nodal target *pitx2c* gene leads to an increase in parapineal number (2014). Thus, several transcription factors and signaling molecules act together to produce the correct number of each cell type within the pineal complex.

While some aspects of cell type specification within the pineal complex have been described, it is still unclear whether there is a key factor which dictates the decision between pineal and parapineal fate. In chapter 3, I will discuss a network of transcription factors believed to dictate cell fate choices between pineal and parapineal cells.

The question of how photoreceptor cell fate is governed is also of interest. Aside from projection neurons, the pineal organ has two main photoreceptor subtypes: red/green cones and rods (Cau et al., 2008; Clanton et al., 2013; Lu et al., 2013). The mechanisms controlling the switch from production of cone photoreceptors (which are born first) to rod photoreceptors (which are born second) is not well understood (Emerson et al., 2013). Since the pineal organ shares morphological and functional

similarities with the retina (Mano and Fukada, 2007), it can be used as a model to study how the number of rod versus cone photoreceptors are correctly proportioned. This study has yielded some insight into the role of Tbx2b in specifying the correct number of rods versus cones. Preliminary results on this topic will be discussed in Chapter 4.

CHAPTER 2

IDENTIFICATION OF DIFFERENTIALLY EXPRESSED GENES DURING DEVELOPMENT OF THE ZEBRAFISH PINEAL COMPLEX USING RNA SEQUENCING

Published in *Developmental Biology*

Khuansuwan S., Gamse, J.T., Identification of differentially expressed genes during development of the zebrafish pineal complex using RNA sequencing. Dev. Biol. (2014). http://dx.doi.org/10.1016/j.ydbio.2014.08.015

Abstract

We described a method for isolating RNA suitable for high-throughput RNA sequencing (RNA-seq) from small numbers of fluorescently labeled cells isolated from live zebrafish (*Danio rerio*) embryos without using costly, commercially available columns. This method ensured high cell viability after dissociation and suspension of cells and gave a very high yield of intact RNA. We demonstrated the utility of our new protocol by isolating RNA from fluorescence activated cell sorted (FAC sorted) pineal complex neurons in wild-type and *tbx2b* knockdown embryos at 24 hours post fertilization. Tbx2b is a transcription factor required for pineal complex formation. We described a bioinformatics pipeline used to analyze differential expression following high-throughput sequencing and demonstrated the validity of our results using *in situ* hybridization of

differentially expressed transcripts. This protocol brings modern transcriptome analysis to the study of small cell populations in zebrafish.

Introduction

Gene expression profiling is an excellent starting point to study a large variety of biological mechanisms associated with specific developmental stages, mutations, and/or disease conditions (Fodor et al., 2013; Jiang et al., 2014; Stockhammer et al., 2010; Vesterlund et al., 2011; Wells et al., 2013). RNA sequencing (RNA-seq) has become an established method for transcriptome profiling, especially with the recent reduction of associated costs. As compared to more traditional methods, such as an oligonucleotide microarray, RNA-seq offers greater dynamic range and the ability to detect novel transcripts (Ozsolak and Milos, 2011), even at the single cell level (Grindberg et al., 2013; Tang et al., 2009; Treutlein et al., 2014; Vesterlund et al., 2011). The ability to use fluorescent markers and cell sorting for transcriptome profiling is a powerful advance that can overcome the limitations of using whole embryos or tissues, where changes in tightly regulated or localized transcripts can be masked by more broadly expressed genes. Isolating a small number of viable cells and obtaining good quality RNA suitable for downstream applications such as RNA-seq present its own challenges. Furthermore, the task of performing bioinformatic analysis on large data sets resulting from a single RNA-seq experiment can be intimidating when generating and analyzing transcriptome profiling data for the first time. This paper described methods used to isolate cells and extract high-quality RNA from the developing zebrafish pineal complex, which consists of a relatively small population of neurons in the brain, and a description of the

bioinformatic pipeline used to perform differential expression analysis between control and knockdown animals. Many of the techniques described are broadly applicable to other tissues or model systems.

The zebrafish pineal complex resides in the epithalamus and consists of the pineal and parapineal organs. The zebrafish pineal organ, which is made up of projection neurons and photoreceptors, is an important neuroendocrine organ that secretes melatonin in response to circadian stimuli (Cahill, 1996; Fodor et al., 2013; Gamse et al., 2002; Jiang et al., 2014; Stockhammer et al., 2010; Wells et al., 2013). Cell fate decisions between projection neurons and photoreceptors in the pineal organ are determined by the coordinated actions of BMP and Notch signaling (Cau et al., 2008; Quillien et al., 2011). However, the molecular mechanisms controlling photoreceptor subtype differentiation in the pineal organ remain to be elucidated. Adjacent to the pineal organ is the parapineal organ, a small cluster of 10-12 neurons that typically resides on the left side of the brain (Concha et al., 2000; Concha et al., 2003; Gamse et al., 2003; Ozsolak and Milos, 2011). The unilateral placement of the parapineal organ is integral to the development of left-right asymmetry in the zebrafish brain (Concha et al., 2003; Gamse et al., 2003). Thus, understanding the molecular mechanisms involved in pineal complex formation will elucidate pineal photoreceptor differentiation and is key to understanding left-right asymmetry formation in the zebrafish brain.

The T-box containing transcription factor 2b (Tbx2b) plays important roles during cell fate determination in the zebrafish central nervous system. We have shown that Tbx2b is essential for both parapineal migration and specification, as well as proper formation of the pineal organ (Snelson et al., 2008b). Tbx2b is also necessary for

inducing a bipotential population of pineal complex precursors that can give rise to either pineal cone photoreceptors or parapineal cells (Clanton et al., 2013). In the zebrafish retina, Tbx2b is required for UV cone specification (Alvarez-Delfin et al., 2009) and proper neuronal differentiation along the dorsal axis (Gross and Dowling, 2005). Thus, identification of Tbx2b responsive genes will elucidate its role in neuronal specification, differentiation, and migration. We sought to better understand pineal complex formation by comparing the transcriptomes of pineal complex cells between wild-type controls and *tbx2b* morphants during development by using RNA-seq. We have identified several genes that are under the control of Tbx2b and verified these results using *in situ* hybridization. Intriguingly, many of the Tbx2b responsive genes seemed to have more traditional roles in photoreceptor differentiation and function. Given the known roles of Tbx2b during parapineal development, these results implied that parapineal neurons might be a specialized form of photoreceptor. These data shed light on how cell identity within the pineal complex is defined.

Materials and methods

Zebrafish

Zebrafish were raised at 28.5°C on a 14/10 light/dark cycle. Embryos obtained from natural mating were staged according to hours post-fertilization (hpf). The wild-type strain AB* (Walker, 1999) and the transgenic strain Tg[*flhBAC*:*kaede*]^{vu376} (Clanton et al., 2013) were used.

Morpholino injections

Embryos at 1-2 cell stage were pressure injected with 1 nL of a *tbx2b* splice blocking morpholino (MO), 5' AAAATATGGGTACATACCTTGTCGT 3', (Snelson et al., 2008b) diluted with nuclease-free water (Ambion) to 6 mg/mL.

Tissue preparation

Using a dissecting microscope with a fluorescent filter set (Leica MZ16F), embryos from Tg[*flhBAC*:*kaede*]^{vu376} and AB* crosses were sorted to separate carriers and non-carriers of the transgene. Embryos were dechorionated using 1 mg/mL Pronase solution (Roche) diluted in egg water at 28.5°C for 5-15 minutes prior to the desired developmental stage. Petri dishes were coated with 1% agarose to avoid injury to the embryos. After most chorions had broken open, Pronase solution was rinsed out with several washes of egg water. Embryos were then placed back into the 28.5°C incubator until they reach the desired developmental stage. In order to obtain as many stage-matched embryos as possible, we used embryos from clutches fertilized at 1-2 hours intervals and staggered the dissection time accordingly.

Embryos were anesthetized with Tricaine methanesulfonate (Acros Organics) prior to dissection at 24 hpf. To prevent collection of notochord cells, (which, like pineal cells, are fluorescently labeled by the Tg[*flh*BAC:*kaede*]^{vu376} transgene) we manually dissected out the head tissue from embryos (Figure 3) in Ringer's solution using fine forceps (Dumont #5, Fine Science Tools). For deyolking of embryos, refer to Manoli and Driever (2012) for instructions. We routinely collected about 200 heads per experimental condition. Dissected head tissues were then placed into 1.5 mL Eppendorf tube

containing 1.0 mL of cold Ringer's solution without calcium or magnesium and containing EDTA (see recipe) and placed on ice. As more tissue and Ringer's solution was added during the collection process, Ringer's solution was removed as necessary to keep the total volume constant. Similar to the heads, the trunks from dissected Tg[*flh*BAC:*kaede*]^{vu376} embryos were placed into a 1.5 mL Eppendorf tube containing 1.0 mL of cold Ringer's solution on ice, and later used as a positive fluorophore control for fluorescence activated cell (FAC) sorting. Kaede-negative embryos were anesthetized and placed directly into a 1.5 mL Eppendorf tube containing 1.0 mL of cold Ringer's solution on ice, and later used as a negative control for FAC sorting.

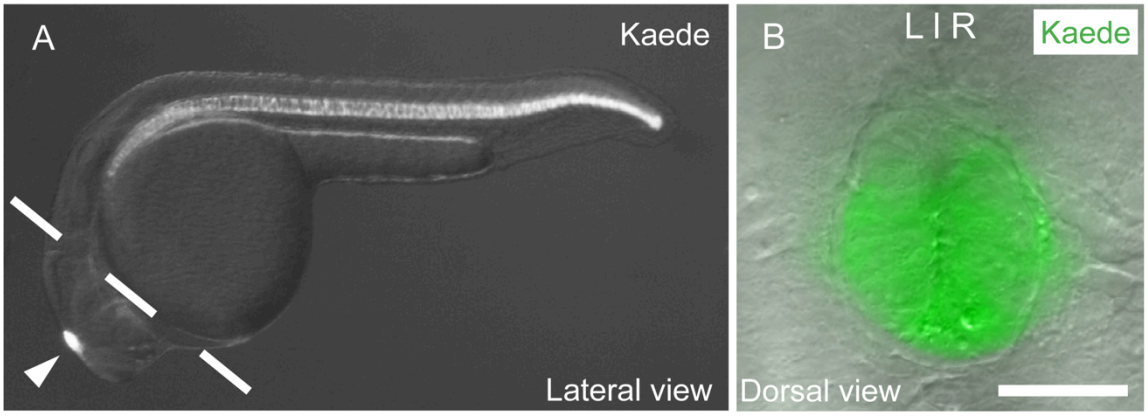

Figure 3: Expression pattern of Tg[*flhBAC*:*kaede*]^{vu376} at 24 hpf.
(A) Kaede was expressed in the notochord and the pineal complex (arrow head). Head tissues were isolated by manual dissection along the dashed line. (B) Dorsal view of the Tg[*flhBAC*:*kaede*]^{vu376} epithalamus showing the fluorescent Kaede channel overlaid on a DIC image. Scale bar: 30 μM

Tissue dissociation

After all tissue samples had been collected, each sample was washed 3 times with 1 mL of Dulbecco's PBS (D-PBS, Gibco). Care was taken to ensure that no samples were lost during washes. After the last D-PBS wash, as much D-PBS was removed as possible. Accumax cell dissociation enzyme mix (Innovative Cell Technologies) was added to each sample at a ratio of 0.5 mL of Accumax enzyme mix per 200 heads or 0.75 mL per 200 trunks. Additionally, 5 µL of 10KU/ml DNase I (Sigma) was added to each tube to alleviate cellular clumping during dissociation. Each tube was placed into a 37°C water bath for 30-60 minutes. During this time, dissociation was facilitated with gentle pipetting. Pipette tips with a filter barrier were always used to avoid contamination. Larger tissues (e.g. trunk tissue) took longer to dissociate. After the tissues were fully dissociated, each tube was removed from the water bath and placed on ice. Then, a volume of washing solution (see recipe) equal to the amount of Accumax solution used was added to each tube. With gentle pipetting as previously, no clumps of tissue were observed. In both of our sample conditions, heat shock proteins were activated at similar levels (Figure 4). Researchers are advised to look for alternative dissociation enzyme that would work at room temperature should their gene(s) of interest is activated as a response to heat shock condition.

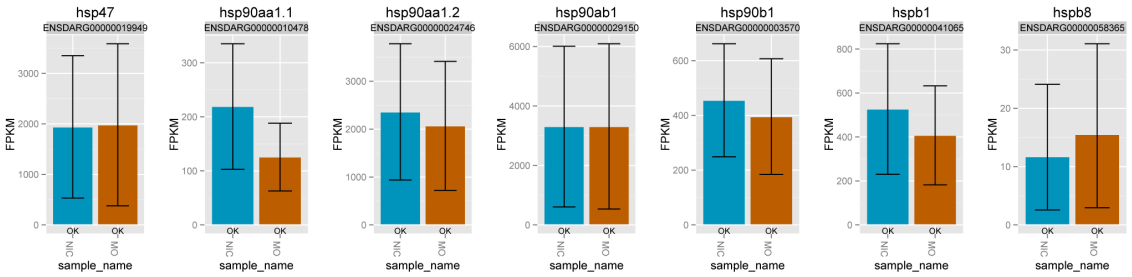

Figure 4: Heat shock proteins were activated at similar levels in both WT and morphant conditions.
Bar plots generated using CummeRbund software demonstrated FPKM values of different heat shock proteins in NIC (blue) were not different from *tbx2b* morphant (orange) samples.

Sample preparation for fluorescence-activated cell sorting

Each cell suspension sample was filtered through a 35 µM nylon mesh directly into a round bottom 12 x 75 mm Falcon collection tube (Becton Dickinson) (Figure 5). In order to obtain as much sample as possible, the tube used for dissociation was then rinsed once with 0.5 mL of full-strength washing solution and twice with diluted washing solution (see recipe); all of these rinses were subsequently filtered through the same nylon mesh into the collection tube. The dissociated cells were then pelleted using a tabletop centrifuge (Beckman X15R) at 1100 rpm (282 g) for 10 minutes at 4°C. The supernatant was removed and the pellet resuspended thoroughly with an appropriate amount of diluted washing solution to achieve a density of no greater than $5x10^6$ cells/ml which is appropriate for low pressure (100 µM nozzle) FAC sorting. The minimum sorting volume used was 300 µL. For the experimental sample (cells from transgenic embryo heads), the vital dye propidium iodide (PI, Sigma) was added at 1 µL per 1 million cells. Typically, we added 1 µL per 1 mL of cell suspension. The samples were

kept on ice prior to flow cytometry. Kaede positive cells were sorted directly into Trizol-LS (Life Technologies) using the BD FACS Aria II (VUMC Flow Cytometry Core, Nashville, TN). Our protocol yielded an average of 83.1 percent viable cells (N=8), ranging from 68.8-95.0 percent. On average, we collected 226 Kaede-positive cells per head (Figure 6).

For each FAC sorting experiment, the following controls were used: (1) negative, unstained sample (i.e. Kaede-negative embryos, no PI added); (2) PI compensation control (i.e. Kaede-negative embryos with PI viability dye added); (3) positive fluorophore control (i.e. Kaede-positive trunks, no PI added). Prior to running the experimental samples, we adjusted the gating of the FAC sorter using our positive compensation control with PI added so as not to lose any experimental sample.

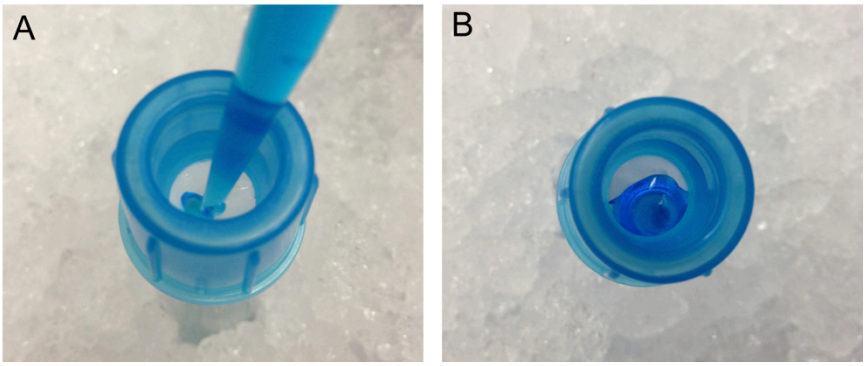

Figure 5: Each cell suspension sample was filtered through a 35 µM nylon mesh directly into a round bottom collection tube.
(A) A suspension of dissociated cells solution was filtered through a 35 µM nylon mesh into a round bottom 12 x 75 mm Falcon collection tube by direct pipetting through the mesh. (B) The solution may not pass entirely through the nylon mesh. This remaining solution will pass through the mesh during the centrifugation step. Dye has been added to the suspension for illustration purpose.

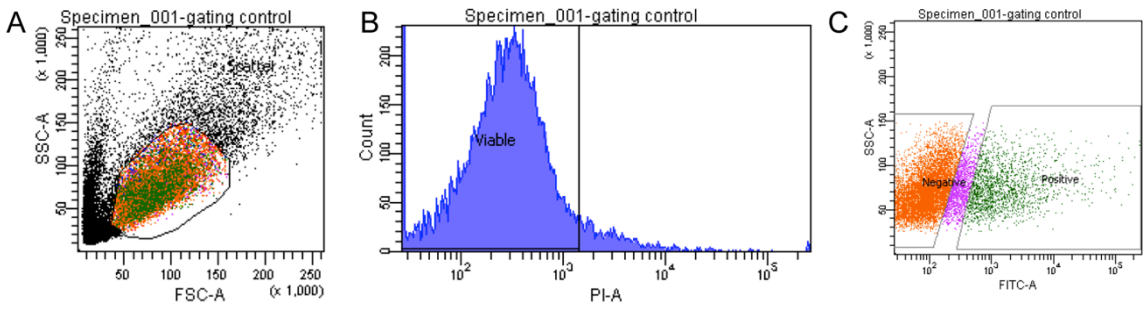

Figure 6: Fluorescence activated cell sorting of Kaede positive cells from head tissues dissociated from 24 hpf Tg[*flhBAC:kaede*]^{vu376} embryos.
(A) Cells first undergo forward scatter (FSC-A) and side scatter (SSC-A) analysis to be separated based on cell size and internal granularity, respectively. Only the cells from the selected colored region are subsequently sorted for viability. (B) Viable cells do not take up propidium iodine (PI-A). (C) Intact, viable cells then get sorted based on fluorescence intensity.

RNA extraction

All equipments used for RNA isolation were pretreated with RNAse Away (Molecular BioProducts). When required, the ratio of the Trizol-LS volume to the sample volume was brought up to 3:1 with addition of nuclease-free water. Cells were lysed by pipetting the mixture several times. RNA was extracted using Trizol-LS similar to the manufacturer's protocol, with one modification: we used Phase Lock Gel-Heavy tubes (PLG, Fisher) during the phase separation step.

Each PLG tube was prepared for use by centrifugation at 14,000 rpm (18,000 g; Beckman Coulter Microfuge 18 centrifuge) for 2 minutes at room temperature. 800 µL of cell lysate (in Trizol-LS) was added to a pre-spun PLG tube and incubated for 5 minutes at room temperature to allow for complete dissociation of nucleoprotein complexes. Chloroform was added to the PLG tube at a ratio of 200 µL per 1 mL of Trizol-LS plus sample mixture initially used. The tube was then shaken vigorously by hand (without

vortexing) for 15 seconds. Phase separation was achieved via centrifugation at 13,200 rpm (16,100 g; Eppendorf 5415D centrifuge) for 15 minutes at 4°C. The clear, aqueous top phase containing RNA, atop the PLG, was then transferred to a fresh tube via decanting or by using a pipette. Ice-cold isopropanol was added to the aqueous phase at a ratio of 500 µL per 1 mL Trizol-LS plus sample initially used, along with 3 µL of 20 mg/mL mussel glycogen (Roche, used as a carrier for the precipitation of nucleic acids). Samples were mixed by repeated inversion and incubated at room temperature for 10 minutes. To allow for precipitation of RNA, samples were incubated at -20°C for at least 1 hour (up to 16 hours). RNA was pelleted via centrifugation at 13,200 rpm (16,100 g; Eppendorf 5415D centrifuge) for 15 minutes at 4°C, resulting in a visible RNA pellet. The supernatant was discarded and the pellet was washed twice with 1 mL of ice-cold 75% ethanol. The location of the pellet was marked and the pellet was allowed to air-dry at room temperature; after drying the pellet became translucent. The pellet was resuspended with 20 µL of nuclease-free water plus 1 µL of RNase inhibitor (40 U/µL RNasin, Promega) at 55°C for 10 minutes. The sample was then gently pipetted to ensure complete resuspension of RNA. Because the subsequent RNA-seq includes a poly-A selection, there was no need to treat samples with DNase. RNA was stored at -80°C until needed.

RNA quantity was determined using the RNA assay program on a Qubit fluorometer (Life Technologies). Each FAC-sorted Kaede-positive cell yielded an average of 3.5 pg of RNA, ranging from 1.3-5.8 pg of RNA/cell (n=11). These values are similar to the yields obtained from neuronal cells in another study (Saxena et al., 2012). RNA quality and integrity were analyzed by capillary electrophoresis using the RNA

Pico chip on an Agilent 2100 Bioanalyzer. Our protocol typically yielded total RNA with RIN integrity values ranging from 6.0-8.5, with an average of 7.2 (n=14) (Figure 7). We observed improved RNA integrity values when we spent less time completing the RNA extraction process (Figure 7, Figure 8). In our hands, the use of a commercially available column (Purelink RNA Micro Kit, Invitrogen) led to a significant loss of total RNA (Figure 8), despite following the manufacturer's protocol precisely.

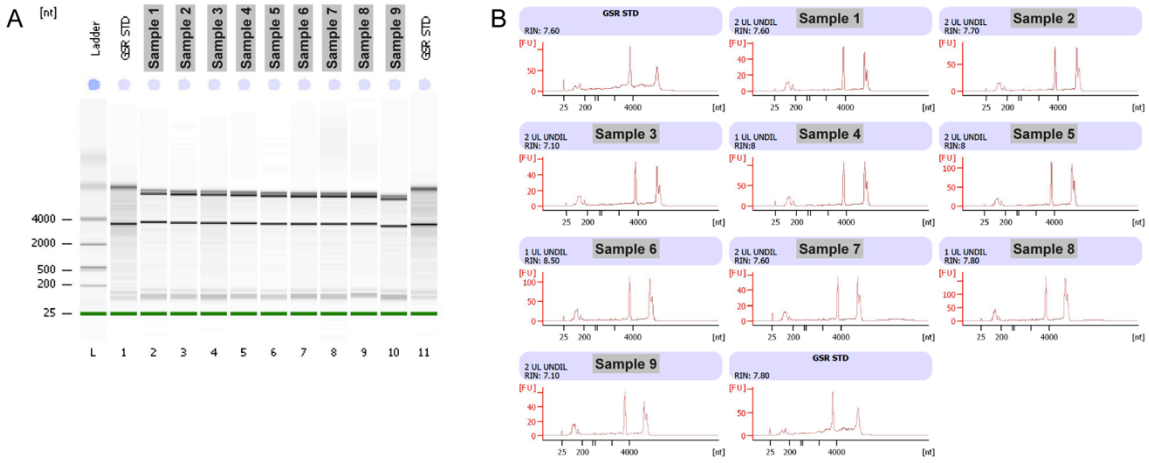

Figure 7: **A bioanalyzer report from FAC sorted samples.**
An example of bioanalyzer report from an RNA Pico chip for nine different FAC sorted samples extracted using our protocol and as quickly as possible. (A) L: ladder; Lane 1 and 11: Standard controls; Lane 2-10: sample 1-9. (B) Sharp ribosomal RNA peaks indicated that the quality of RNA extracted was consistently good (with RIN of 7.10 or greater), meaning that RNA was not significantly degraded.

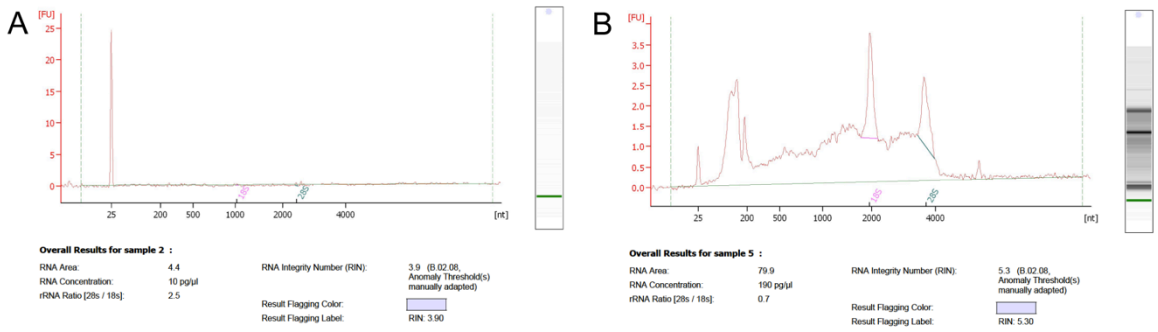

Figure 8: Bioanalyzer reports of total RNA from one FAC sorted sample using two different methods.
(A) Use of commercially available column yielded no usable RNA. (B) Use of our protocol (Trizol/Isopropanol) yielded greater quantity and quality RNA. RNA quality, quantity, and integrity were further improved with shorter RNA extraction process (Fig. 7).

cDNA library preparation and RNA-seq

cDNA sequencing libraries preparation and sequencing was performed by the Genome Sciences Resource at Vanderbilt University Medical Center (Nashville, TN) using the Illumina TruSeq RNA Sample Preparation Kit as previously described (Elmore et al., 2012; Venkateswaran et al., 2013). High-throughput RNA-seq was performed on four libraries (two control groups and two *tbx2b* knockdown groups) twice. Using the multiplexing strategy of the TruSeq protocol, each technical replicate, consisting of four libraries, was performed on one lane of the Illumina HiSeq 2000 utilizing version 3 chemistry. On average, 40 million 51-101 bp single-end reads were generated for each group, which should be sufficient to detect differentially expressed genes. A study performed in human and mouse tissues has shown that sequencing beyond the depth of 3 million reads does not increase transcript detection (Ramsköld et al., 2009). Others have concluded that cDNA sequencing with 30-40 million 25 bp reads is sufficient to detect

major splice isoforms for abundant and moderately abundant transcripts in mouse and that 1X coverage of the transcriptome can be achieved with 40 million 25 bp reads (Mortazavi et al., 2008).

Read mapping, differential expression analysis, and data visualization

Bioinformatic analysis was performed on a 64-bit MacBook Pro (Apple) running Mac OS X 10.8.5 with 8 GB of RAM. Raw 51 or 101 bp single-end reads generated from the Illumina HiSeq 2000 were first assessed for sequence quality using the FastQC software version 0.10.0 (http://www.bioinformatics.bbsrc.ac.uk/projects/fastqc/). Quality scores across all bases fell into the "very good quality" category (>28, Sanger/Illumina 1.9 encoding). Adapter sequences were removed using cutadapt software version 1.4.1 (Martin, 2011) (https://code.google.com/p/cutadapt/). Reads were trimmed to 40 or 80 bp, respectively, to remove bases of lower quality using trimmomatic software version 0.32 (Bolger et al., 2014). Each sequencing data set was independently mapped to the zebrafish genome with a bowtie2 index generated from Danio_rerio.Zv9.70 (Ensembl) downloaded from Illumina's iGenomes collection (https://support.illumina.com/sequencing/sequencing_software/igenome.ilmn) using the TopHat2 program (Kim et al., 2013) with novel splice discovery disabled. HiSeq 2000 libraries were aligned with the following options: "-p 2 -G genes.gft --no-novel-juncs" where genes.gft contains the Ensembl coding transcripts in GTF format downloaded from Illumina's iGenomes collection. On average, 89% of trimmed reads were mapped (83.7% uniquely mapped) to the genome.

Differentially expressed genes between control and *tbx2b* morphant pineal cell samples were identified by using Cuffdiff 2 program (Trapnell et al., 2013) with the following options: "-b genome.fa -p 2 -u -c 5 genes.gtf" where genome.fa is a multifasta file downloaded from Illumina's iGenomes collection. We used a 1.8-fold change in expression and an FDR adjusted p value (q value) of ≤ 0.05 as cut offs.

CummeRbund software was used to generate volcano plot and bar plots for expression levels for genes of interest (Goff et al., 2012). Volcano plot was generated using the following options: "alpha=0.05, showSignificant=T, xlimits=c(-12,12)".

For additional information on how to install and use TopHat, Cufflinks, and CummeRbund, see Trapnell et. al. (2012).

Raw and processed transcriptome sequencing data for all conditions and the associated biological and technical replicates have been deposited in the NCBI's Gene Expression Omnibus (GEO) database under accession number GSE61202.

Read mapping for individual tbx2b exons and data visualization

Raw 51 bp reads generated from the Illumina HiSeq 2000 were first assessed for sequence quality using the FastQC software version 0.10.0. Each fastq sequence data set was then converted to fasta format using the fq_all2std.pl script in the Maq software package, version 0.7.1 (http://maq.sourceforge.net/index.shtml). Reads were trimmed to 35 bp reads, each bp has a quality score of 35 or above from fasqc analysis, and aligned to each individual exon of Tbx2b gene obtained from Ensembl database (Zv9.65), allowing 3 mismatches using SeqMap software (Jiang and Wong, 2008) version 1.0.13, as previously described ((Gibbons et al., 2012), http://www-

personal.umich.edu/~jianghui/seqmap/). Normalized read counts for each exon in our data sets were calculated using the rSeq software, version 0.0.7 as previously described (Gibbons et al., 2012). Normalized read counts for each exon between controls and *tbx2b* knockdown conditions were compared in Microsoft Excel. Read coverage for Tbx2b gene is viewed using the genome browsing application Integrative Genomics Viewer (Robinson et al., 2011).

In situ hybridization

Whole-mount RNA *in situ* hybridization was performed as previously described (Gamse et al., 2003), using reagents from Roche Applied Bioscience. Embryos were hybridized to probe at 70°C in hybridization solution containing 50% formamide (Roche). Hybridized probes were detected using alkaline phosphatase-conjugated antibodies (Roche) and visualized by 4-nitro blue tetrazolium (NBT; Roche) and 5-bromo-4-chloro-3-indolyl-phosphate (BCIP; Roche). RNA probes (Table 1) were labeled using digoxygenin-UTP.

Table 1: Templates and enzymes used to synthesize antisense RNA probe

Plasmid name	Reference	Enzyme used to linearized plasmid	RNA polymerase
pBluescriptSK(-)-*gngt1*	GE Healthcare (Clone ID 4789083)	NotI	T7
pBluescriptSK(-)-*gngt2a*	GE Healthcare (Clone ID 4786786)	NotI	T7
pBS-SK-*oep*5A1	Zhang et al., 1998	HindIII	T3
pCR4-TOPO-*otomp/zomp-1*	Murayama et al., 2005	NotI	T3
pBS-*otx5*	Gamse et al., 2002	EcoRI	T7
pCRII-TOPO-*rdh5*	Nadauld et al., 2006	EcoRV	Sp6
pME18S-FL3-*rgra*	Open Biosystems (Clone ID 8123753)	PCR amplified. Forward primer: 5' TGCTCTAAAAGCTGCGGAAT 3' Reverse primer: 5' TAATACGACTCACTATAGGGGGGAGGTGTGGGAGGTTTT 3'	T7
pCRII-*tbx2b*	Snelson et al., 2008b	BamHI	T7

Imaging

Bright field images were obtained using Qcapture software (Qimaging) with a Retiga EXi *Fast* 1394 cooled monochrome-12 bit CCD camera (Qimaging) attached to a RGB color filter (Qimaging) mounted on a Leica DM6000B microscope with a 20X objective.

RT-PCR

First strand cDNA was generated using 1 µg total RNA, 200 ng random hexamers (Applied Biosystem), 1 µL of 10 mM dNTP (NEB), 4 µL of 5x first strand buffer (Invitrogen), 2 µL of 0.1 M DTT (Invitrogen), 1 µL of RNase inhibitor (Promega) and 1 µL of Superscript III reverse transcriptase (Invitrogen) in a 20 µL reaction. PCR was performed using 2 µL of cDNA from the RT reaction, with 30 rounds of amplification with annealing temperature of 60 °C and 90 seconds extension time. The following primers were used: *β-actin* 5' CCATGGATGAGGAAATCGCTGC 3' and 5' GTCACACCATCACCAGAGTCC 3' ; *flh* 5' GTACTGGCGAAAGCAGCAGTT 3' and 5' AGCAGATGCCAACAGAAAGC 3'; *no tail* 5' TGGAAATACGTGAACGGTGA 3' and 5' TCTGAATCCCACCGACTTTC 3'; *tbx2b* 5' TGTGACGAGCACTAATGTCTTCCTC 3' and 5' GCAAAAAGCATCGCAGAACG 3'.

Recipes

Ringer's solution-without calcium or magnesium, containing EDTA

Reagent	Amount per 500 mL	Final concentration
5 M NaCl	11.6 mL	116 mM
1 M KCl	1.45 mL	2.9 mM
1 M HEPES	2.5 mL	5 mM
0.5 M EDTA	1.0 mL	1 mM
ddH2O	483.45 mL	--

-Mix thoroughly, then filter sterilize. Stored at room temperature.

Wash Solution

- 30 µL of DNase I (10,000 units/mL in D-PBS)
- 4 mL D-PBS

Diluted Wash Solution

- 15 µL of DNase I (10,000 units/mL in D-PBS)
- 10 mL D-PBS

Results

FACS yields an enriched population of pineal complex cells

To isolate pineal cells, we used the Tg[*flh*BAC:*kaede*]^{vu376} transgenic line that expresses the fluorophore Kaede at high levels in the pineal complex and the notochord at 24 hpf (Figure 3A,B). To minimize the collection of unwanted Kaede-positive notochord cells, we resected head tissue, and then FAC sorted and collected dissociated Kaede-positive cells from the head tissue of transgenic embryos. RT-PCR for specific pineal and notochord markers was performed on cDNA synthesized from the FAC sorted Kaede-positive cells to ensure that we enriched for the desired pineal cell population and excluded notochord cells. As controls, we performed RT-PCR on cDNA synthesized from whole Tg[*flh*BAC:*kaede*]^{vu376} embryos and Kaede-negative cells from head tissue (Figure 9A,B, respectively). FAC sorted Kaede-positive cells from dissected head tissue showed high expression of *flh,* a marker present in the pineal complex and the notochord with barely detectable levels of the notochord-specific marker *no tail*. As expected, *tbx2b* was readily detected in the Kaede-positive cells.

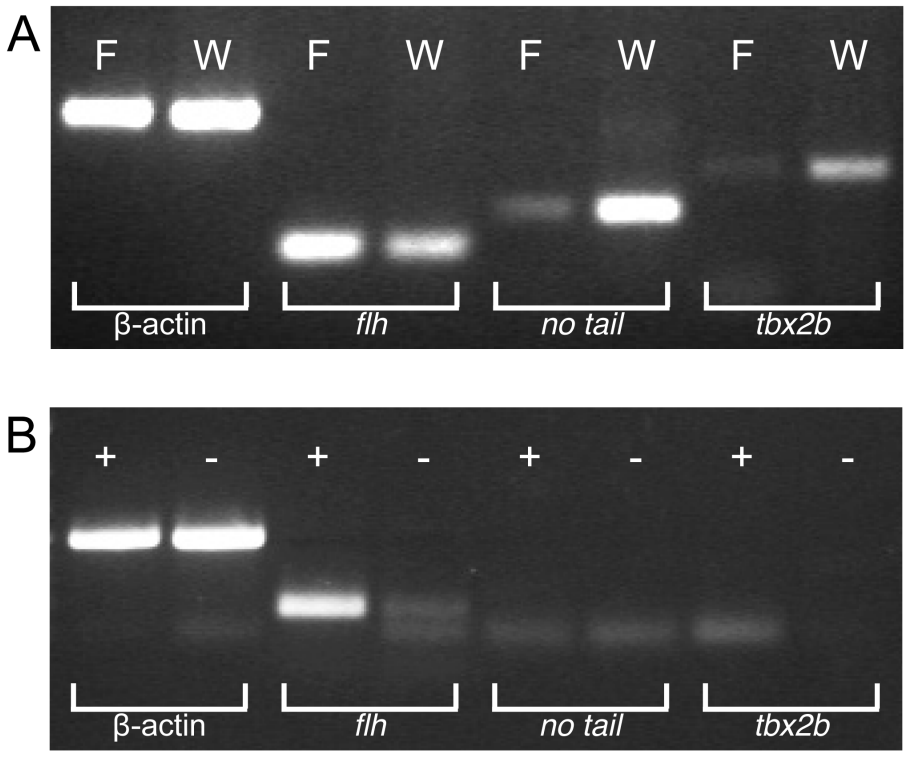

Figure 9: An enriched pineal cell population has been collected from FACS. (A) A gel image illustrating RT-PCR results from FAC sorted Kaede positive Tg[*flhBAC:kaede*]^{vu376} cells from head tissues (F) versus whole, wild-type, non-transgenic, embryos (W) at 18 hpf. FAC sorted sample showed enrichment of the pineal and notochord marker *flh*. *tbx2b* was detected at low levels in the FAC sorted sample. *no tail* (notochord marker) expression was observed in the FAC sorted sample indicating that the sample has some contamination from *flhBAC*:Kaede positive notochord cells. (B) A gel image illustrating RT-PCR results from FAC sorted Kaede positive (+) versus Kaede negative (-) cells from Tg[*flhBAC:kaede*]^{vu376} head tissues at 24 hpf. The pineal markers *flh* and *tbx2b* were highly expressed as compared to Kaede negative cells from surrounding head tissues. The notochord marker, *no tail*, was detected at a background level.

RNA-seq from small numbers of FAC sorted cells identifies pineal-specific genes affected by **Tbx2b** *loss-of-function*

With the ability to selectively enrich for pineal complex cells, we sought to identify pineal specific genes that are under the control of the transcription factor Tbx2b. In order to identify genes regulated by Tbx2b, we FAC sorted pineal cells as above in the presence or absence of an antisense morpholino that targets *tbx2b* (Snelson et al., 2008b). This morpholino is predicted to block inclusion of exon 3 from *tbx2b* primary transcripts, resulting in a frameshift and premature truncation of translated protein. To test the efficacy of the morpholino, we aligned RNA-seq reads for individual exons of *tbx2b* and found that the presence of exon 3 was reduced by 94.5% in *tbx2b* morphants, as compared to non injected controls (NIC) (aligned reads ratio of morphants:NIC=0.054, N=2). Other exons of *tbx2b* were unaffected (aligned reads ratio of morphants:NIC=1.007, N=2) (Figure 10).

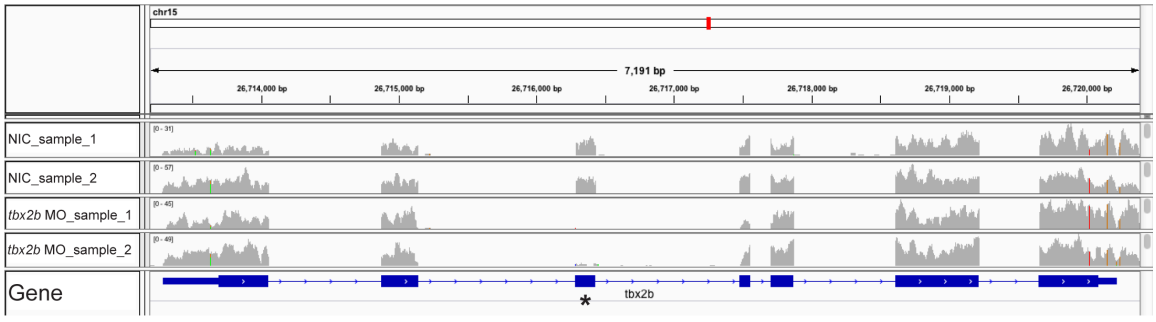

Figure 10: **Exon 3 was absent in *tbx2b* morphants.**
The read coverage of *tbx2b* gene viewed using the Integrative Genomics Viewer application showed a decrease in sequencing reads that align to exon 3 (asterisk) in *tbx2b* morphant (MO) samples as compared to non-injected control (NIC) samples.

Comparison of expression profiles in the presence or absence of *tbx2b* knockdown resulted in the identification of 83 genes that were significantly up (20/83) or down (63/83) regulated ($q \leq 0.05$) by more than 1.8 fold across all biological and technical replicates (Figure 11). By searching published literature, as well as Zfin.org and Biomart (Ensembl.org), expression data were available for 57 of 83 identified genes. Of these, 14/57 had pineal-specific expression patterns (Table 2, see Table 3 for a complete list) and 14/57 had broad expression patterns in the brain (Table 4). There has been no documented role for these genes during pineal complex development. At 24 hpf, approximately 284 genes showed specific expression in the pineal complex (BioMart, Ensembl.org using Prim5 and epiphysis as search terms). Therefore, Tbx2b function is required for appropriate expression of at least 4.9% of pineal specific genes during parapineal development.

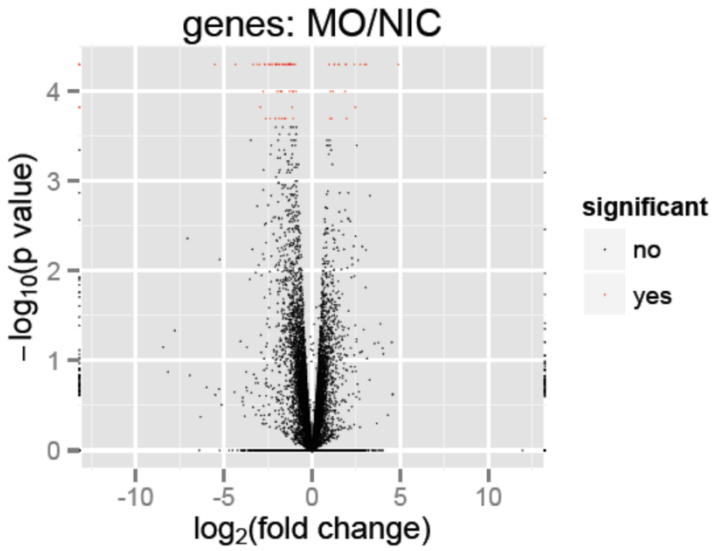

Figure 11: **Volcano plot revealed differentially expressed genes.**
Volcano plot revealed genes that were significantly different (represented by red marks, $q \leq 0.05$) between control and *tbx2b* morphant conditions.

Table 2: Differentially expressed genes between *tbx2b* morphants and controls with pineal specific expression

Gene Symbol	Description	Ensembl Gene ID	(*tbx2b* MO/NIC)[a]	*p*-value[b]	*q*-value[c]
otomp	otolith matrix protein	ENSDARG00000040306	-7.84	5.00E-05	0.0176
gngt1	guanine nucleotide binding protein (G protein), gamma transducing activity polypeptide 1	ENSDARG00000035798	-6.41	5.00E-05	0.0176
rlbp1b	retinaldehyde binding protein 1b	ENSDARG00000045808	-5.37	5.00E-05	0.0176
saga	S-antigen; retina and pineal gland (arrestin)	ENSDARG00000012610	-4.14	5.00E-05	0.0176
sagb	S-antigen; retina and pineal gland (arrestin) b	ENSDARG00000038378	-4.00	5.00E-05	0.0176
rgra	retinal G protein coupled receptor a	ENSDARG00000054890	-3.73	5.00E-05	0.0176
rcv1	recoverin	ENSDARG00000019902	-3.60	5.00E-05	0.0176
rdh5	retinol dehydrogenase 5 (11-cis/9-cis)	ENSDARG00000008306	-3.10	5.00E-05	0.0176
gngt2a	guanine nucleotide binding protein (G protein), gamma transducing activity polypeptide 2a	ENSDARG00000010680	-2.98	2.00E-04	0.0457
pde6g	phosphodiesterase 6G, cGMP-specific, rod, gamma	ENSDARG00000022820	-2.70	5.00E-05	0.0176
rbp4l	retinol binding protein 4, like	ENSDARG00000044684	-2.45	5.00E-05	0.0176
otx5	orthodenticle homolog 5	ENSDARG00000043483	-2.19	1.00E-04	0.0287
rpe65a	retinal pigment epithelium-specific protein 65a	ENSDARG00000007480	-2.06	1.00E-04	0.0287
fsta	Follistatin a	ENSDARG00000052846	2.87	5.00E-05	0.0176

[a] Fold change of FPKM values in *tbx2b* morphants versus non-injected controls; negative values denote reduction; positive values denote increase
[b] The uncorrected *p*-value of the test statistic
[c] The FDR-adjusted *p*-value of the test statistic

To validate our findings, we used *in situ* hybridization to examine the expression of 6 of the 14 pineal-specific genes in both NIC and *tbx2b* morphant embryos at 24 hpf. Of 6 genes tested, we found 100% concordance between our *in situ* data and our RNA-seq results (Figure 12A). We also performed *in situ* hybridization experiments for these 6 genes in *tbx2b*^{c144} mutants at 24 hpf (Figure 12B). Genes that showed the highest fold reduction in *tbx2b* knockdown condition from RNA-seq reads (Figure 12C, Table 2) also showed the highest reduction in expression as observed by *in situ* hybridization. By 36 hpf, the parapineal organ has migrated away from the midline and is located to the left of the pineal organ (Gamse et al., 2003). Of the 6 differentially expressed genes tested, *otx5* and *rdh5* were expressed in the migrating parapineal cells (Figure 13, 36 hpf). At a later stage, *otx5* was maintained in differentiated parapineal cells (Figure 13, 2dpf).

Table 3: List of differentially expressed genes between *tbx2b* morphants and controls

Gene Symbol	Description	Ensembl Gene ID	(*tbx2b* MO/NIC)[a]	*p*-value[b]	*q*-value[c]
hbae3	hemoglobin alpha embryonic-3	ENSDARG00000079305	-45.60	5.00E-05	0.0176
hbae1 (1 of 2)[d]	Hemoglobin alpha embryonic-1 (1 of 2)	ENSDARG00000089475	-38.23	5.00E-05	0.0176
hbae1 (2 of 2)[d]	Hemoglobin alpha embryonic-1 (2 of 2)	ENSDARG00000089124	-34.41	5.00E-05	0.0176
cdk19	Cyclin-dependent kinase 19	ENSDARG00000043858	-20.31	5.00E-05	0.0176
IAPP[d]	Islet amyloid polypeptide	ENSDARG00000074122	-11.19	1.50E-04	0.0400
mb	Myoglobin	ENSDARG00000031952	-10.15	5.00E-05	0.0176
tyrp1b	Tyrosinase-related protein 1b	ENSDARG00000056151	-8.67	5.00E-05	0.0176
otomp	Otolith matrix protein	ENSDARG00000040306	-7.84	5.00E-05	0.0176
si:ch211-113a14.19	Novel protein coding	ENSDARG00000075220	-7.66	1.50E-04	0.0400
si:ch73-304f21.1	Known protein coding	ENSDARG00000087407	-6.85	1.00E-04	0.0287
rgs5b	regulator of G-protein signaling 5b	ENSDARG00000017860	-6.43	5.00E-05	0.0176
gngt1	Guanine nucleotide binding protein (G protein), gamma transducing activity polypeptide 1	ENSDARG00000035798	-6.41	5.00E-05	0.0176
si:ch211-154o6.3	Known protein coding	ENSDARG00000090538	-6.21	2.00E-04	0.0457
dct	Dopachrome tautomerase	ENSDARG00000006008	-5.50	5.00E-05	0.0176
si:ch211-134a4.2[d]	Known protein coding	ENSDARG00000087076	-5.41	1.50E-04	0.0400
rlbp1b	Retinaldehyde binding protein 1b	ENSDARG00000045808	-5.37	5.00E-05	0.0176
LRRIQ4	leucine-rich repeats and IQ motif containing 4	ENSDARG00000017720	-5.24	2.00E-04	0.0457
cyp8b1[d]	Cytochrome P450, family 8, subfamily B, polypeptide 1	ENSDARG00000053068	-5.19	5.00E-05	0.0176
oca2	Oculocutaneous albinism II	ENSDARG00000061303	-5.10	5.00E-05	0.0176
tyrp1a	tyrosinase-related protein 1a	ENSDARG00000029204	-4.79	5.00E-05	0.0176
pmelb	Premelanosome protein b	ENSDARG00000033760	-4.24	5.00E-05	0.0176
cyp46a1	Cytochrome P450, family 46, subfamily A, polypeptide 1	ENSDARG00000012137	-4.22	2.00E-04	0.0457
saga	S-antigen; retina and pineal gland (arrestin) a	ENSDARG00000012610	-4.14	5.00E-05	0.0176
zgc:112234	Known protein coding	ENSDARG00000091066	-4.10	5.00E-05	0.0176
npas4a	Neuronal PAS domain protein 4a	ENSDARG00000055752	-4.05	5.00E-05	0.0176
prl	Prolactin	ENSDARG00000037946	-4.02	5.00E-05	0.0176
sagb	S-antigen; retina and pineal gland (arrestin) b	ENSDARG00000038378	-4.00	5.00E-05	0.0176
neurod6a	Neurogenic differentiation 6a	ENSDARG00000040008	-3.95	1.00E-04	0.0287
rgra	Retinal G protein coupled receptor a	ENSDARG00000054890	-3.73	5.00E-05	0.0176
txnipb	Thioredoxin interacting protein b	ENSDARG00000070000	-3.69	5.00E-05	0.0176
BX511021.1	Novel protein coding	ENSDARG00000070406	-3.64	2.00E-04	0.0457
rcv1	Recoverin	ENSDARG00000019902	-3.60	5.00E-05	0.0176
b3gnt5b	UDP-GlcNAc:betaGal beta-1,3-N-acetylglucosaminyltransferase 5b	ENSDARG00000004396	-3.54	1.00E-04	0.0287
tpi1a	Triosephosphate isomerase 1a	ENSDARG00000025012	-3.42	1.00E-04	0.0287
FP017249.1	Known protein coding	ENSDARG00000069685	-3.31	1.00E-04	0.0287
rergla	RERG/RAS-like a	ENSDARG00000019396	-3.29	2.00E-04	0.0457
PGBD4	piggyBac transposable element derived 4	ENSDARG00000092846	-3.25	5.00E-05	0.0176
rdh5	Retinol dehydrogenase 5 (11-cis/9-cis)	ENSDARG00000008306	-3.10	5.00E-05	0.0176
pou5f1	POU domain, class 5, transcription factor 3	ENSDARG00000044774	-3.07	5.00E-05	0.0176
gngt2a	Guanine nucleotide binding protein (G protein), gamma transducing activity polypeptide 2a	ENSDARG00000010680	-2.98	2.00E-04	0.0457
si:dkey-251i10.2	Known protein coding	ENSDARG00000093957	-2.91	5.00E-05	0.0176
hist2h2l	Histone 2, H2, like	ENSDARG00000068996	-2.87	5.00E-05	0.0176
dmrt2a	Doublesex and mab-3 related transcription factor 2a	ENSDARG00000015072	-2.81	2.00E-04	0.0457
pde6g	Phosphodiesterase 6G, cGMP-specific, rod, gamma	ENSDARG00000022820	-2.70	5.00E-05	0.0176
socs1	Suppressor of cytokine signaling 1a	ENSDARG00000038095	-2.57	5.00E-05	0.0176
pvalb8	Parvalbumin 8	ENSDARG00000037790	-2.53	5.00E-05	0.0176
rbp4l	Retinol binding protein 4, like	ENSDARG00000044684	-2.45	5.00E-05	0.0176
gadd45bb	Growth arrest and DNA-damage-inducible, beta b	ENSDARG00000013576	-2.45	5.00E-05	0.0176
slc6a2	Solute carrier family 6 (neurotransmitter transporter, noradrenalin), member 2	ENSDARG00000016141	-2.44	1.00E-04	0.0287
h1fx	H1 histone family, member X	ENSDARG00000054058	-2.40	5.00E-05	0.0176
dmrt3a	Doublesex and mab-3 related transcription factor 3a	ENSDARG00000035290	-2.40	5.00E-05	0.0176
slc22a7a	Solute carrier family 22 (organic anion transporter), member 7a	ENSDARG00000056028	-2.37	5.00E-05	0.0176
cyr61	Cysteine-rich, angiogenic inducer, 61	ENSDARG00000023062	-2.33	5.00E-05	0.0176
CU019646.2	Novel protein coding	ENSDARG00000091234	-2.33	5.00E-05	0.0176
fabp7a	Fatty acid binding protein 7, brain, a	ENSDARG00000007697	-2.30	5.00E-05	0.0176
socs3a	Suppressor of cytokine signaling 3a	ENSDARG00000025428	-2.21	5.00E-05	0.0176
otx5	Orthodenticle homolog 5	ENSDARG00000043483	-2.19	1.00E-04	0.0287
cebpb	CCAAT/enhancer binding protein (C/EBP), beta	ENSDARG00000042725	-2.19	1.50E-04	0.0400
h1f0	H1 histone family, member 0	ENSDARG00000038559	-2.12	2.00E-04	0.0457
cxcl-c1c	Chemokine (C-X-C motif) ligand C1c	ENSDARG00000075045	-2.08	5.00E-05	0.0176
rpe65a	Retinal pigment epithelium-specific protein 65a	ENSDARG00000007480	-2.06	1.00E-04	0.0287
aqp1a.1	Aquaporin 1a, tandem duplicate 1	ENSDARG00000023713	-1.94	5.00E-05	0.0176
zgc:55733	Known protein coding	ENSDARG00000022579	-1.88	1.00E-04	0.0287
clec14a	C-type lectin domain family 14, member A	ENSDARG00000026751	1.95	5.00E-05	0.0176
tmem88a	Transmembrane protein 88 a	ENSDARG00000056920	2.02	2.00E-04	0.0457
tie2	TEK tyrosine kinase, endothelial	ENSDARG00000028663	2.07	1.00E-04	0.0287
fli1b	Friend leukemia integration 1b	ENSDARG00000040080	2.15	2.00E-04	0.0457
lmo2	LIM domain only 2 (rhombotin-like 1)	ENSDARG00000095019	2.26	1.00E-04	0.0287
tal1	T-cell acute lymphocytic leukemia 1	ENSDARG00000019930	2.39	5.00E-05	0.0176
etv2	Ets variant gene 2	ENSDARG00000053868	2.42	5.00E-05	0.0176
CU041398.1	Novel protein coding	ENSDARG00000089082	2.83	5.00E-05	0.0176
fsta	Follistatin a	ENSDARG00000052846	2.87	5.00E-05	0.0176
f5	Coagulation factor V	ENSDARG00000055705	3.68	1.00E-04	0.0287
si:dkey-204l11.1	Known processed transcript	ENSDARG00000079403	3.74	5.00E-05	0.0176
trh	Thyrotropin-releasing hormone	ENSDARG00000006868	3.80	5.00E-05	0.0176
tnnt2a	Troponin T2a, cardiac	ENSDARG00000020610	3.87	2.00E-04	0.0457
mmp13a	Matrix metalloproteinase 13a	ENSDARG00000012395	5.27	5.00E-05	0.0176
5_8S_rRNA	5.8S ribosomal RNA	ENSDARG00000081218	5.45	1.50E-04	0.0400
myl7	Myosin, light polypeptide 7, regulatory	ENSDARG00000019096	6.62	5.00E-05	0.0176
vmhc	Ventricular myosin heavy chain	ENSDARG00000079564	7.84	5.00E-05	0.0176
cmlc1	Cardiac myosin light chain-1	ENSDARG00000032976	8.40	5.00E-05	0.0176
CD109	CD109 molecule	ENSDARG00000060609	29.53	5.00E-05	0.0176
SNORD14[e]	Small nucleolar RNA SNORD14	ENSDARG00000082008	1042.26	2.00E-04	0.0457

[a] Fold change of FPKM values in *tbx2b* morphants versus non-injected controls; negative values denote reduction; positive values denote increase
[b] The uncorrected *p*-value of the test statistic
[c] The FDR-adjusted *p*-value of the test statistic
[d] FPKM value of morphant condition is arbitrarily changed from 0 to 0.1
[e] FPKM value of control condition is arbitrarily changed from 0 to 0.1

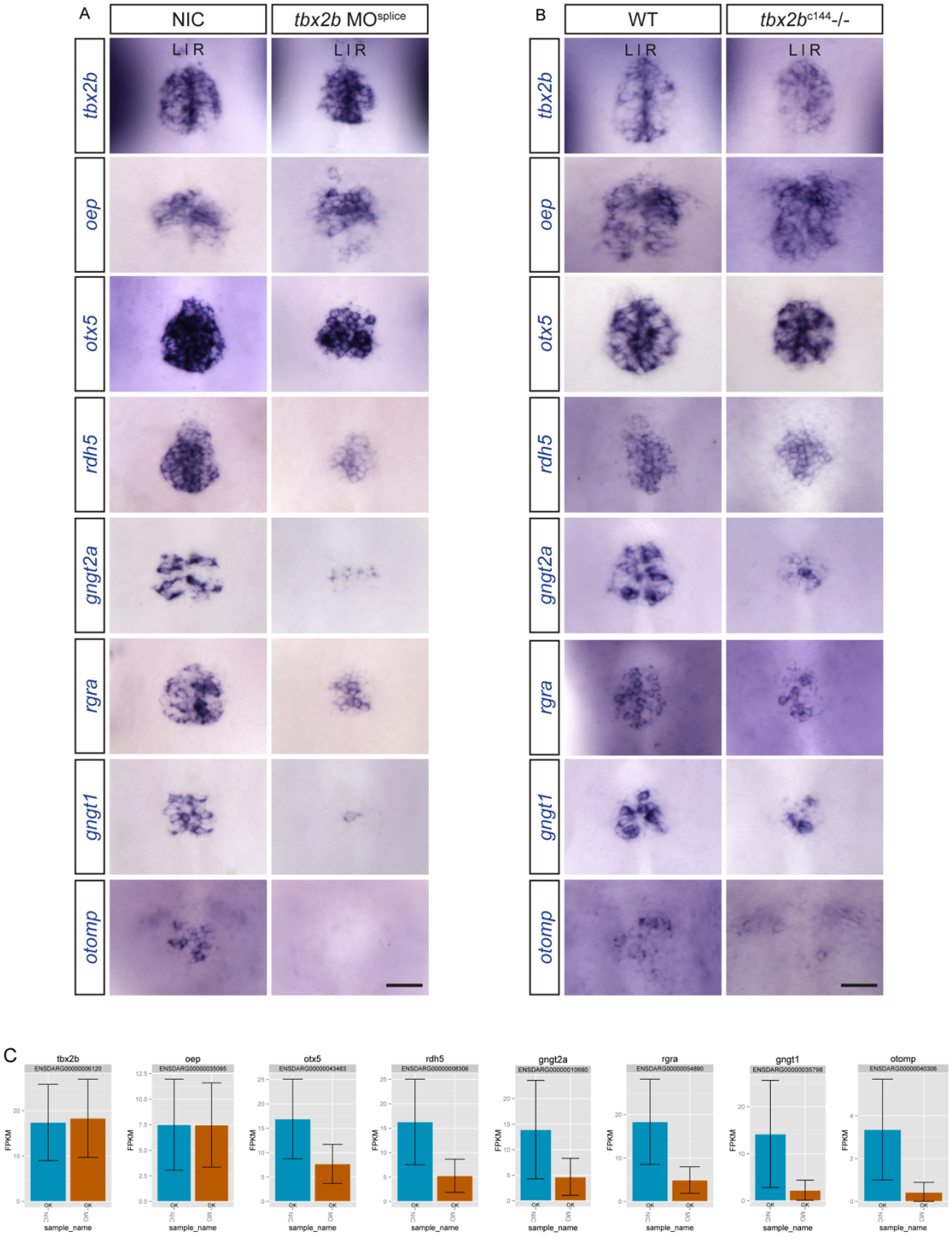
A
NIC
tbx2b MOsplice
L I R
tbx2b
oep
otx5
rdh5
gngt2a
rgra
gngt1
otomp
B
WT
tbx2bc144-/-
C
FPKM
sample_name
OK
ENSDARG00000006120
ENSDARG00000035095
ENSDARG00000043483
ENSDARG00000008306
ENSDARG00000010680
ENSDARG00000054890
ENSDARG00000035798
ENSDARG00000040306

Figure 12: **Differentially expressed genes identified from RNA sequencing experiments were validated using *in situ* hybridization.** At 24 hpf, expression of *otx5, rdh5, gngt2a, rgra, gngt1,* and *otomp,* shown to be downregulated in *tbx2b* morphant pineal transcriptome as compared to controls by 2.2, 3.1, 3.0, 3.7, 6.4, and 7.8 fold, respectively, were reduced in *tbx2b* morphant (A) and *tbx2b*^{c144}-/- (B) pineal complex as compared to NIC or WT. *tbx2b* and *oep*, displayed no significant change in FPKM values from RNA seq experiments (C), and were used as controls. (A and B) Dorsal view of the epithalamus at 24 hpf. Scale bar: 30 μM

Table 4: Differentially expressed genes between *tbx2b* morphants and controls with broad expression in the brain

Gene Symbol	Description	Ensembl Gene ID	(*tbx2b* MO/NIC)[a]	*p*-value[b]	*q*-value[c]
rgs5b	regulator of G-protein signaling 5b	ENSDARG00000017860	-6.43	5.00E-05	0.0176
tpi1a	Triosephosphate isomerase 1a	ENSDARG00000025012	-3.42	1.00E-04	0.0287
pou5f1	POU domain, class 5, transcription factor 3	ENSDARG00000044774	-3.07	5.00E-05	0.0176
hist2h2l	Histone 2, H2, like	ENSDARG00000068996	-2.87	5.00E-05	0.0176
gadd45bb	Growth arrest and DNA-damage-inducible, beta b	ENSDARG00000013576	-2.45	5.00E-05	0.0176
h1fx	H1 histone family, member X	ENSDARG00000054058	-2.40	5.00E-05	0.0176
dmrt3a	Doublesex and mab-3 related transcription factor 3a	ENSDARG00000035290	-2.40	5.00E-05	0.0176
cyr61	Cysteine-rich, angiogenic inducer, 61	ENSDARG00000023062	-2.33	5.00E-05	0.0176
fabp7a	Fatty acid binding protein 7, brain, a	ENSDARG00000007697	-2.30	5.00E-05	0.0176
socs3a	Suppressor of cytokine signaling 3a	ENSDARG00000025428	-2.21	5.00E-05	0.0176
h1f0	H1 histone family, member 0	ENSDARG00000038559	-2.12	2.00E-04	0.0457
zgc:55733	Known protein coding	ENSDARG00000022579	-1.88	1.00E-04	0.0287
lmo2	LIM domain only 2 (rhombotin-like 1)	ENSDARG00000095019	2.26	1.00E-04	0.0287
etv2	Ets variant gene 2	ENSDARG00000053868	2.42	5.00E-05	0.0176

[a] Fold change of FPKM values in *tbx2b* morphants versus non-injected controls; negative values denote reduction; positive values denote increase
[b] The uncorrected *p*-value of the test statistic
[c] The FDR-adjusted *p*-value of the test statistic

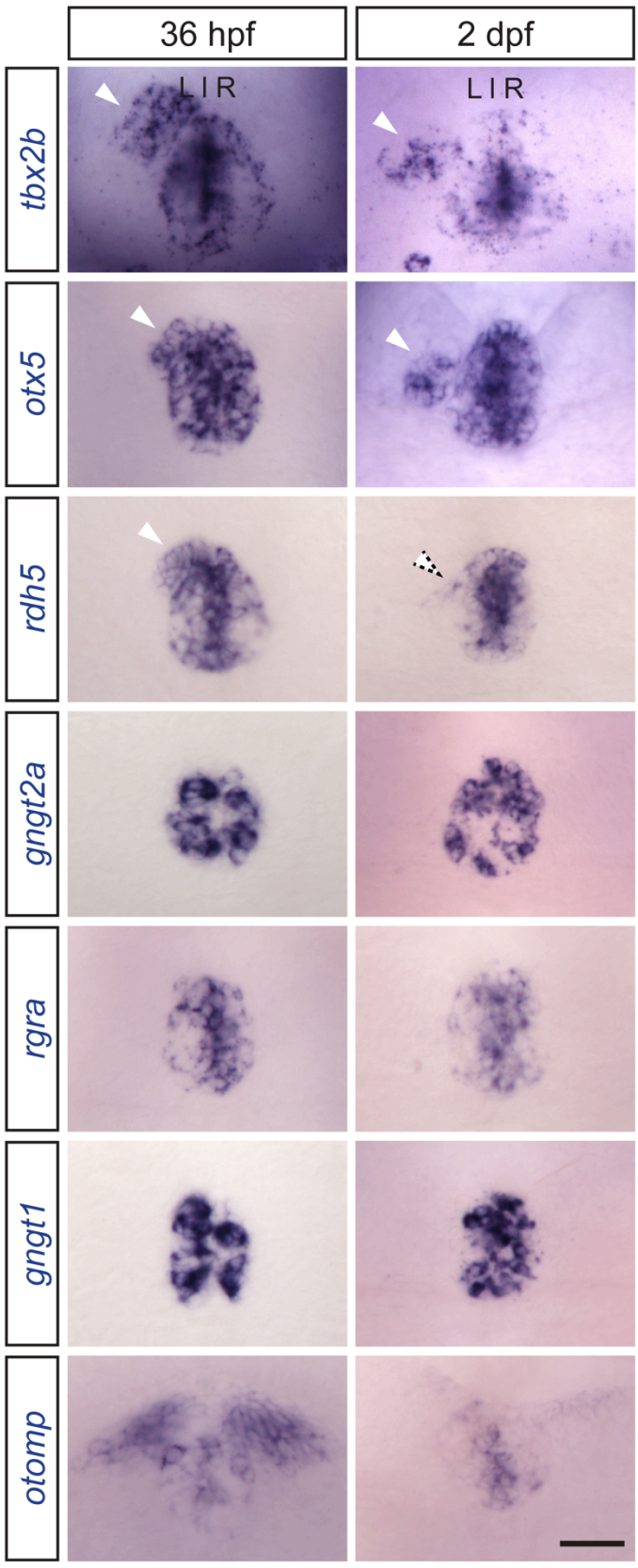
36 hpf
2 dpf
L I R
L I R
tbx2b
otx5
rdh5
gngt2a
rgra
gngt1
otomp

Figure 13: Tbx2b responsive genes displayed distinct expression patterns. At 36 hpf, *tbx2b, otx5,* and *rdh5* were expressed throughout the pineal and parapineal organs (arrowheads). At 2 dpf, *tbx2b* and *otx5* expression was maintained in differentiated parapineal cells (arrowheads), but *rdh5* was downregulated (dotted arrowhead). *rgra, gngt1,* and *gngt2a* were only expressed in the pineal organ. *otomp* was expressed in only a small population of pineal cells and was also expressed in the habenular nuclei. *tbx2b* expression was maintained throughout parapineal development and was used as a control. Images are dorsal views of the epithalamus of wild-type embryos at indicated stages. Scale bar: 30 μM

Discussion

High-throughput cDNA sequencing (RNA-seq) has emerged as a powerful tool for gene expression profiling. This technique is replacing microarrays because RNA-seq provides a larger dynamic range, requires less starting material, and allows detection of novel transcripts. Despite the high sensitivity, however, this technique can still be difficult to perform when analyzing small numbers and/or dispersed populations of cells. Additionally, researchers are faced with the challenge of analyzing large data sets generated by these experiments. Using 24 hpf zebrafish embryos, we have described the methods that we used to isolate a small number of pineal complex cells from each embryo and extract high quality RNA suitable for RNA-seq experiments. We also described how we utilized a simple bioinformatics pipeline using readily available open-source programs to obtain differential gene expression data between two experimental conditions; in this case, the pineal transcriptomes between wild-type and *tbx2b* morphants. We were able to identify 83 genes with 1.8 fold or more significant change in expression. Focusing on genes that have specific expression in the pineal complex, we have identified 14 genes that were differentially and significantly regulated. We verified 6 of these findings via *in situ* hybridization.

Our experiments enabled the identification of 14 genes that have restricted expression within the pineal complex and are differentially expressed between *tbx2b* morphants and WT. Intriguingly, these genes have not been shown to participate in pineal complex development. However, most of these genes do participate in photoreceptor differentiation and function within the retina. This is of potential interest, as pineal and retinal photoreceptors share similar features and may have evolved from a common

ancestral cell type (Mano and Fukada, 2007). *rlbp1b* is expressed in zebrafish Müller glia cells and has been shown to be important for normal cone vision (Collery et al., 2008; Fleisch et al., 2008). Loss of *rpe65a* or rod arrestins, results in altered rod outer segment morphology (Schonthaler et al., 2007) or reduced photoresponse recovery of the rod photoreceptor (Renninger et al., 2011; Xu et al., 1997), respectively. Furthermore, *rdh5* and *rbp4l* are important for retinal cell differentiation (Nadauld et al., 2006; Nagashima et al., 2009; Nagashima et al., 2010). In mouse, rhodopsin regeneration is dependent on Rgr, the *rgra* homolog (Chen et al., 2001). Lastly, recoverin, encoded by the *rcv1 gene,* participates in the visual cycle (Stryer, 1991). A role for Tbx2b in pineal photoreceptor formation and function is unexpected as mutation of *tbx2b* does not lead to a reduction in Arr3a or rhodopsin expression in red/green cone cells or rod outer segments (Clanton et al., 2013; Snelson et al., 2008b). However, our results are consistent with known roles of Tbx2b in promoting particular cone fates in the zebrafish retina (Alvarez-Delfin et al., 2009). Together, these findings suggest novel roles of Tbx2b in pineal photoreceptor formation and function. Additionally, these results suggest that the parapineal may be a specialized form of photoreceptor.

It has been shown that prenylation of G protein gamma subunits is necessary to facilitate directed migration of primordial germ cells (PGC) (Mulligan and Farber, 2011; Mulligan et al., 2010). The parapineal organ also migrates directionally. Therefore, it is reasonable to predict that the molecular mechanisms controlling parapineal migration are similar to those controlling PGC migration. Our current study has identified two genes affected by Tbx2b that encode G protein gamma subunits, *gngt1* and *gngt2a.* We are currently investigating the roles of these two genes in parapineal migration.

Although we have shown the power of FAC sorting plus RNA-seq to reveal novel gene targets of Tbx2b in the developing pineal complex, we are aware of experimental limitations. The zebrafish pineal complex anlage is composed of approximately 30-32 pineal complex cells by 24 hpf (Masai et al., 1997; Quillien et al., 2011), but we isolated an average of 226 cells/embryo. Since the number of cells that we FAC sorted from each Tg[*flh*BAC:*kaede*]^{vu376} head exceeded the number of pineal cells, we were likely not working with a 100% pure population; rather, we were working with a highly enriched population of pineal cells. Having ruled out the inclusion of significant numbers of Kaede expressing notochord cells (Figure 9A,B), we concluded that many non-pineal cells from the brain have been collected and subsequently analyzed. Nevertheless, we did achieve significant enrichment of our desired cell types with an approximate 17-fold enrichment of pineal cells as compared to using total head tissue. Kaede-positive pineal cells normally constitute about 0.85% of total population of head tissues. Post FAC sorting, pineal cells constitute about 14.2% of the sorted population. One constraint on the ability to better enrich the desired population is the transgene used to label pineal cells, *flh:Kaede*. In preparation for FAC sorting experiments, one should fully characterize the expression of the transgene used to mark cells. Using high resolution imaging, we found weakly expressing Kaede-positive cells in the telencephalon. In any given embryo, these cells express Kaede at a much lower level than cells in the pineal complex. However, the absolute level of transgene expression varies from embryo to embryo. Cells with a low absolute level of Kaede expression could be pineal cells from embryos with overall low transgene expression, or telencephalic cells from embryos with overall high transgene expression. Collecting only the highest expressing population of Kaede-positive cells

(pineal cells from embryos with high expression of the transgene) would have resulted in extremely low yields. Therefore, a transgenic line with less embryo-to-embryo variation is needed in order to obtain a more pure population of pineal complex cells. Alternatively, the use of two transgenes with different fluorophores with expression that overlaps only in the tissue to be isolated (in this case, the pineal) could be used.

Despite collection of extraneous cells by our FAC sorting protocol, it was nevertheless successful in identifying differentially expressed genes in the pineal, as confirmed by *in situ* hybridization. It is also important to note that in the head, Tbx2b is only expressed in the pineal complex (which is Kaede positive) and in the eyes (which are Kaede negative), and as a transcription factor it is predicted to act cell autonomously. Therefore, although we were capturing some telencephalic cells in our sample, we did not expect that gene expression in those cells would be significantly changed by loss of Tbx2b function, and therefore would not affect our list of differentially expressed genes.

We used cuffdiff to identify differentially expressed genes, using two biological replicates. However, increasing the number of biological replicates (three or greater) is strongly suggested, as it should yield fewer false positives and false negatives. Additionally, there are other widely used tools available for differential expression analysis including DESeq (Anders and Huber, 2010) and EdgeR (Robinson et al., 2009).

Tbx2b has been shown to be crucial for the development of the pineal and parapineal organs (Snelson et al., 2008b); its role in parapineal formation makes it important for the establishment of left-right asymmetries in the zebrafish brain (Gamse et al., 2003; Gamse et al., 2005). Identifying downstream targets of Tbx2b should pinpoint the genes involved in pineal complex development including the specification and

migration of parapineal cells. We used *tbx2b* morphants because of the challenges of rapidly identifying a sufficient number of *tbx2b* homozygous mutant embryos, as they are morphologically indistinguishable from their siblings at 24 hpf. However, we were convinced that we have successfully knocked down Tbx2b using the morpholino. Not only does treatment with this concentration of morpholino phenocopy *tbx2b*^{c144} parapineal defects (Snelson et al., 2008b), but we found that it almost completely eliminated the presence of exon 3 in *tbx2b* transcripts, leading to a premature truncation of nearly all Tbx2b protein in the treated embryos (this study). Our current study looked at the 24 hours post fertilization stage of development, which is just prior to parapineal and pineal photoreceptor differentiation as well as parapineal migration. Our results have yielded genes that may be involved in pineal photoreceptor formation and function, as well as genes that may have roles in parapineal migration. In order to identify genes responsible for parapineal specification, we believe this experiment should to be repeated at an earlier time point, such as 15-18 hpf when parapineal specification occurs (Snelson et al., 2008a).

Aside from its roles in parapineal and UV cone development, Tbx2b has also been shown to be involved in other important biological processes including neuronal differentiation in the dorsal retina (Gross and Dowling, 2005), atrioventricular canal formation in the heart (Chi et al., 2008), and notochord formation (Fong et al., 2005). While our differential expression data came from comparing the transcriptomes between WT and *tbx2b* morphant pineal complex cells, it would be interesting to explore our list for Tbx2b responsive genes that also function in retina, heart, and/or notochord formation. In particular, such genes could lead to insight into human health, since Tbx2 is a putative

modifier of two human syndromes caused by mutation in related T-box genes, ulnar-mammary syndrome (Tbx3) and 22q11.2 deletion syndrome (Tbx1) (Jerome-Majewska et al., 2005; Mesbah et al., 2012).

Acknowledgements

We thank the following: Leah Potter and Mark Magnuson's laboratory (VUMC) for sharing protocols, suggestions, and reagents relating to cell dissociation; John Gibbons, David Rinker, Xiaofan Zhou and Antonis Rokas's laboratory for guidance on transcriptome data analysis; the Vanderbilt Institute for Clinical and Translational Research (CTSA award UL1 TR000445 from the National Center for Advancing Translational Sciences); Genome Sciences Resource at VUMC (VANTAGE) for performing cDNA library construction and RNA-seq; VUMC Flow Cytometry Shared Resource, which is supported by the Vanderbilt Ingram Cancer Center (P30 CA68485) and the Vanderbilt Digestive Disease Research Center (DK058404), for performing cell sorting experiments; James G. Patton for suggestions regarding manuscript preparation. We would also like to thank Erin Booton, Brittany Parker, Elleena Benson and Qiang Guan for fish care and maintenance. This work was supported by NIH grants HD054534 and EY024354.

CHAPTER 3

A TRANSCRIPTION FACTOR NETWORK DICTATES MIGRATORY NEURON CELL FATE DECISION IN THE DEVELOPING VERTEBRATE DIENCEPHALON

Introduction

During the development of the nervous system, neurons must be produced in the correct number and then migrate to appropriate positions in the brain to establish precise connectivity to other neurons. One of the best-known examples is the mammalian cortex, where neurons are produced in the ventricular zone, then migrate to the pial surface. In humans, defects in cortical neuron migration result in periventricular heterotopia and lissencephaly, disorders which cause seizures and intellectual disability (Kwan et al., 2012; Liu, 2011).

In the cortex, neurogenesis and migration are separable processes. For example, mutation of *filamin A* affects migration but not specification (Fox and Walsh, 1999; Fox et al., 1998). Conversely, loss of p19Ink4d and p27Kip1 has no effect on migration but reduces neurogenesis because cells remain in the cell cycle (Zindy et al., 1999). Although they can be uncoupled, migration and neurogenesis are often interlinked; for instance, proneural bHLH transcription factors are required for mouse cortical neurogenesis early during development, and later are required for migration of the newly produced neurons (Ge et al., 2006).

The vast number of neuronal subtypes and the difficulty of *in vivo* imaging in the mammalian cortex limit studies of specification and migration. Because of its simplicity and transparency, the zebrafish pineal complex provides advantages for such experiments. The pineal complex is found in the dorsal diencephalon and consists of only 4 types of cells: migratory parapineal neurons and non-migratory projection neurons, rod photoreceptors, and cone photoreceptors (Concha and Wilson, 2001; Halpern et al., 2003; Mano and Fukada, 2007). All four cell types are generated from the pineal complex anlage, with parapineal cells arising in the anterior anlage and projection neurons and photoreceptors developing from the posterior anlage (Clanton et al., 2013; Concha et al., 2003). The pineal complex anlage forms on the dorsal surface of the brain, and it is among the first areas of the brain to undergo neurogenesis and migration (Wilson and Easter, 1991; Wilson et al., 1990), making it amenable to *in vivo* manipulation and imaging.

Parapineal cells are particularly intriguing because they migrate asymmetrically, starting at the midline and moving to the left side of the brain (Concha et al., 2003; Snelson et al., 2008b). Subsequently, the parapineal neurons induce cells in the adjacent left habenular nucleus to differentiate with different characteristics from the right habenula, thus imposing asymmetry on an important conduction pathway involved in fear and anxiety responses (Agetsuma et al., 2010; Gamse et al., 2003; Gamse et al., 2005). As a result, the parapineal neurons provide a unique inroad for understanding the development of asymmetry in the vertebrate CNS. As brain asymmetry is a conserved feature of the brain throughout the vertebrate lineage, it likely confers a sizable competitive advantage by increasing the capacity for, and speed of, multi-tasking (Dadda

and Bisazza, 2006; Goto et al., 2010; Halpern et al., 2005; Lust et al., 2011; Patrick and Elias, 2009; Rogers et al., 2004; Vallortigara et al., 2011). Anatomical asymmetries in the cortex are established during fetal development (Bajic et al., 2012; Hill et al., 2010; Sun et al., 2005). Notably, neurodevelopmental disorders including schizophrenia are linked to reduced or absent hemispheric asymmetry (Abdul-Rahman et al., 2012; Bleich-Cohen et al., 2012; Oertel-Knochel and Linden, 2011; Oertel-Knöchel et al., 2013). However, little progress has been made in identifying how asymmetry arises in the cortex. This is perhaps because hemispheric differences may arise from relatively subtle left-right differences in neurogenesis and migration that are subsequently amplified, just as the asymmetry produced by leftward migration of a small number of parapineal cells is amplified in the habenular nuclei. Since the dorsal diencephalic system (pineal complex and habenulae) is the best understood genetic model of asymmetric brain development, it could reveal important principles about how left-right differences are established in the CNS such as the cortex.

Multiple signaling pathways and transcription factors have been linked to specification and migration of parapineal versus other cell types in the pineal complex anlage. The decision of a posterior cell to become a photoreceptor versus a projection neuron is governed by crosstalk between the BMP and the Notch signaling pathways (Cau et al., 2008; Quillien et al., 2011). Proliferation of both photoreceptors and projection neurons requires the homeobox transcription factor Floating head (Flh) (Masai et al., 1997). In the anterior region of the pineal anlage, the T-box transcription factor Tbx2b is required to specify bipotential parapineal/cone photoreceptor precursors, which are then directed to a parapineal fate by Fgf signaling (Clanton et al., 2013; Snelson et al.,

2008b). The Mediator complex component Med12 appears to coordinate Tbx2b and Fgf signaling (Wu et al., 2013). In addition, Tbx2b and Fgf activity are required for parapineal cells to migrate from the midline to the left side of the brain (Clanton et al., 2013; Regan et al., 2009; Snelson et al., 2008b). However, other factors appear to limit the number of parapineal cells that can be specified, since overexpression of parapineal promoting factors, such as Fgf8a, cannot induce supernumerary parapineal cells (Clanton et al., 2013). One factor limiting parapineal specification is Pitx2c; inactivation of this transcription factor leads to the formation of ~40% more parapineal neurons than WT, and this enlarged parapineal is capable of inducing left habenular characteristics in both the left and right habenulae (Garric et al., 2014).

To further investigate the factors that limit specification of the migratory parapineal neurons, we performed literature searches for other genes that might be involved. We identified and inactivated two transcription factors that are expressed in the very early pineal complex anlage, Flh and the orphan nuclear hormone receptor Nr2e3. We found that Flh acted in a dose-dependent fashion to prevent pineal anlage cells from differentiating as parapineal neurons. Flh activated *nr2e3* expression, which blocks parapineal specification during late stages of development. The supernumerary parapineal neurons in *flh* mutants required Tbx2b activity to migrate, but Tbx2b did not have an instructive role in parapineal specification. We conclude that a network of transcription factors dynamically regulates the number of asymmetrically migrating parapineal neurons.

Materials and methods

Zebrafish strains and maintenance

Zebrafish were raised at 28.5°C on a regular light/dark (14 hours/10 hours) cycle. Embryos were obtained from natural matings and staged according to hours- or days-post-fertilization (hpf or dpf). The following fish lines were used: AB* (Walker, 1999), *tbx2b*^{c144} (Snelson et al., 2008b), Tg[*foxd3:gfp*]^{zf104} (Gilmour et al., 2002), *flh*^{n1} (Talbot et al., 1995), Tg[*cfos:gal4vp16*]^{s1145t} (Scott et al., 2007), Tg[*uas:eGFP*]^{VU294} (this study) and Tg[*krt4:egfp*]^{sqet11} (Parinov et al., 2004).

In situ hybridization

Whole-mount chromogenic RNA *in situ* hybridization was performed as described previously (Gamse et al., 2003), using reagents from Roche Applied Bioscience. Hybridized probes were detected using alkaline phosphatase-conjugated antibodies (Roche) and visualized by 4-nitro blue tetrazolium (NBT; Roche) and 5-bromo-4-chloro-3-indolyl-phosphate (BCIP; Roche) staining for single labeling, or NBT/BCIP followed by iodonitrotetrazolium (INT) and BCIP staining for double labeling.

Whole-mount double fluorescent RNA *in situ* hybridization was performed as previously described with addition of 5% dextran sulfate added to the hybridization buffer (Lauter et al., 2011), using reagents from Sigma. Hybridized probes were detected using alkaline phosphatase-conjugated antibodies (Roche) and visualized by FastRed or Fast Blue for single labeling; or FastRed and FastBlue for double labeling. For double labeling, the alkaline phosphatase (from the first visualization step) was acid inactivated

by a 10 minutes wash in 0.1M glycine HCl pH 2.0 followed by 2 x 10 minutes PBSTr (0.1% Triton-X100 in 1X PBS) washes. Embryos were then incubated in the second alkaline phosphatase conjugated antibody (anti-DIG-AP or anti-Fluor-AP) (1:5000, Roche) overnight at 4°C. The following day, the probe was visualized using either FastRed or FastBlue.

Information on the probes is in Table 5. For chromogenic *in situ* labeling, bright-field images of glycerol-cleared samples were captured with a Leica 6000M compound microscope. For fluorescent *in situ* labeling, glycerol-cleared samples were imaged on a PerkinElmer RS3 spinning disk confocal microscope with a 40X oil-immersion objective. Images were analyzed with Volocity software (PerkinElmer).

Table 5: Templates and enzymes used to synthesize antisense RNA probe

Plasmid name	Reference	Enzyme used to linearized plasmid	RNA polymerase
pBS-*ascl1a*	Allende and Weinberg, 1994	BamHI	T7
pBS-*flh*	Talbot et al., 1995	EcoRI	T7
pBS-*gfi1ab*	Dufourcq et al., 2004	SacII	T3
pRK5-*nr2e3*	Chen et al., 2005	NotI	T7
pENTR-D/TOPO-*sox1a*	Okuda et al., 2006	NotI	T7
pCRII-*tbx2b*	Snelson et al., 2008b	BamHI	T7

Immunofluorescence

Samples for whole-mount immunofluorescence labeling were fixed overnight at 4°C in 4% PFA and processed as previously described (Snelson et al., 2008b). Information on the primary and secondary antibodies used is in 6. To visualize cell nuclei, samples were incubated with ToPro3 (Invitrogen, 1:10,000). Fluorescent *in situ* (FISH)/immunofluorescence double labeling was performed as previously described

(Doll et al., 2011). Samples were cleared in glycerol and imaged on a PerkinElmer RS3 spinning disk confocal microscope with a 40X oil-immersion objective. Images were analyzed with Volocity software (PerkinElmer).

Table 6: List of primary and secondary antibodies

Primary antibody	**Concentration**	**Source**	**References**
Mouse anti-Opsin-1	1:500	DSHB	Concha et al., 2000
Mouse anti-Arrestin 3a	1:500	DSHB	Larison and Bremiller, 1990
Mouse anti-4C12	1:100	James Fadool Laboratory	Morris et al., 2005
Mouse anti-HuC/D	1:200	Invitrogen	Cau et al., 2008
Rabbit anti-Nr2e3	1:150	Jeremy Nathans Laboratory	Chen et al., 2005
Mouse anti-acetylated tubulin	1:500	Sigma-Aldrich	N/A
Rabbit anti-GFP	1:500	Torrey Pines Biolabs	N/A
Secondary antibody	**Concentration**	**Source**	
Goat anti-rabbit Alexa 488	1:300	Invitrogen	
Goat anti-mouse Alexa 568	1:300	Invitrogen	

Morpholino injections

Embryos were injected at the one-cell stage. The following morpholinos were used in this study: *tbx2b* splice-blocking morpholino, 5'-AAAATATGGGTACATACCTTGTC-GT-3'; *nr2e3* splice blocking morpholino, 5'-ATACGCAAGTTGTTTTCTCACCTGT-3' (targets the exon 2/intron 2 junction).

Cloning

nr2e3 was cloned by PCR from the pRK5-nr2e3 plasmid (Chen et al., 2005) using Phusion polymerase (Thermo Scientific) and the following primers: forward, 5' CACCATGGAGGATCCGATGTCAGA 3' and reverse, 5' GTTTTTGAACATGTCACACA 3'. The PCR product was purified with a Mini Elute Gel Purification Kit (Qiagen) and ligated into pENTR-D/Topo vector (Invitrogen).

nr2e3 mRNA overexpression

nr2e3 mRNA was transcribed *in vitro* using the mMessage mMachine transcription kit (Ambion) from the pRK5-*nr2e3* template (linearized with HpaI, transcribed with SP6 polymerase). mRNA was injected into one-cell stage embryos.

Semi-quantitative RT-PCR

RT-PCRs were performed on total RNA isolated from embryos with Trizol (Invitrogen). Reverse transcription was performed with random hexameric primers, followed by PCR amplification using primers to amplify sequence from *nr2e3* (F, 5'-TCCTGAACACGGGACTTCTT-3'; R, 5'-TTCAGCTTGAAGGCATTTCT-3'). Band intensity quantification was performed with Quantity One (Bio-Rad) software.

Results

Flh *transcriptionally regulates tbx2b*

The homeodomain containing transcription factor Floating head (Flh) is necessary for the progression of pineal neurogenesis. In *flh*^{n1} mutants, the initiation of pineal neurogenesis begins normally, but fails to proceed beyond the 18 somite stage (ss) (Masai et al., 1997). The T-box transcription factor 2b (Tbx2b) has also been shown to be important for the specification and migration of parapineal cells. In *tbx2b*^{c144} mutants, fewer parapineal cells are specified; and those cells also fail to migrate away from the midline (Snelson et al., 2008b). Expression patterns of these two transcription factors overlap during parapineal development, although *flh* expression seems more restricted to the posterior region relative to *tbx2b* (Snelson et al., 2008b). Two contradictory results regarding the relationship between Flh and (Tbx2b) have been reported. A study by Cau and Wilson suggested that *tbx2b* is transcriptionally regulated by Flh (2003). However, it is difficult to interpret the finding as the authors examined *tbx2b* expression in *flh*^{n1} mutants at 24 hours post fertilization (hpf), a stage at which reduced pineal number phenotype can be observed using the pro-neural marker *ascl1a/ash1a* and the pineal complex marker *otx5* (Cau and Wilson, 2003). On the other hand, Snelson and others reported no change in *tbx2b* expression in *flh*^{n1} at 6 ss (Snelson et al., 2008a). At this early time point, *tbx2b* expressing domains have not yet fused at the midline and the data are also difficult to interpret. In order to determine whether *tbx2b* is transcriptionally regulated by Flh, we decided to examine its expression at 10 ss. At this stage, the presumptive pineal complex anlage is contiguous at the midline and pineal neurogenesis is still developing normally in *flh*^{nl} mutants. We found *tbx2b* expression to be reduced in

flh^{nl} as compared to WT (Figure 14A). In contrast, *flh* expression was not reduced in *tbx2b*^{c144} (Figure 14B). The data suggests that *tbx2b* is downstream of and is transcriptionally regulated by Flh.

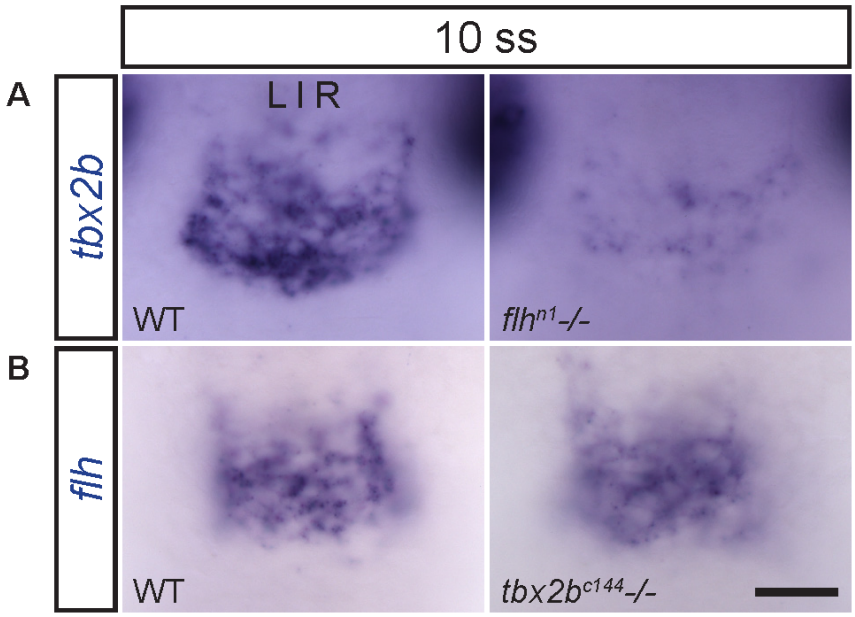

Figure 14: Flh is transcriptionally upstream of *tbx2b*.
At 10 ss, *tbx2b* expression level is reduced in *flh*^{n1} -/- as compared to WT (A). Conversely, expression level of *flh* is unaltered in *tbx2b*^{c144} -/- as compared to WT (B). Scale bar = 30 μM.

Flh *inhibits specification of parapineal cells in a dose-dependent manner*

We performed *in situ* hybridization and found that *flh* was expressed throughout parapineal development (Figure 15). If Flh is genetically upstream of *tbx2b*, then it is reasonable to predict that loss of Flh should also lead to reduced numbers of parapineal cells that do not migrate. To our surprise, we found dramatically greater number of parapineal cells in *flh*^{n1} mutants using all of the currently known markers of parapineal cells including *sox1a* (early differentiation marker), *gfi1ab* (late differentiation marker), and Tg(*krt4:eGFP)*^{sqet11} (the transgenic line that expresses eGFP in parapineal cells by 5 dpf) (Figure 16A). Furthermore, we found that the increase in parapineal cell number was dependent on the levels of Flh. Embryos with only one mutated copy of Flh have a parapineal number phenotype that was intermediate of those of WT and *flh*^{nl} (Figure 16B, Table 7). We conclude that Flh inhibits parapineal specification in a dose-dependent manner. This finding is consistent with a previous report that *flh* is downregulated in parapineal cells (Concha et al., 2003).

Additionally, Flh is essential for the formation of the notochord, the physical and chemical barrier between the left and right body axis (Talbot et al., 1995). To ensure that the observed phenotype was due to Flh activity, and not due to compromised midline structures, we also quantified the number of parapineal cells in *ntl* morphant embryos, which like *flh*^{n1} mutants also lack the notochord. We saw no change in the total number of parapineal cells in *ntl* morphants, as compared to NIC (Figure 17). Thus, an increase in parapineal number was not a result of having a compromised midline structure.

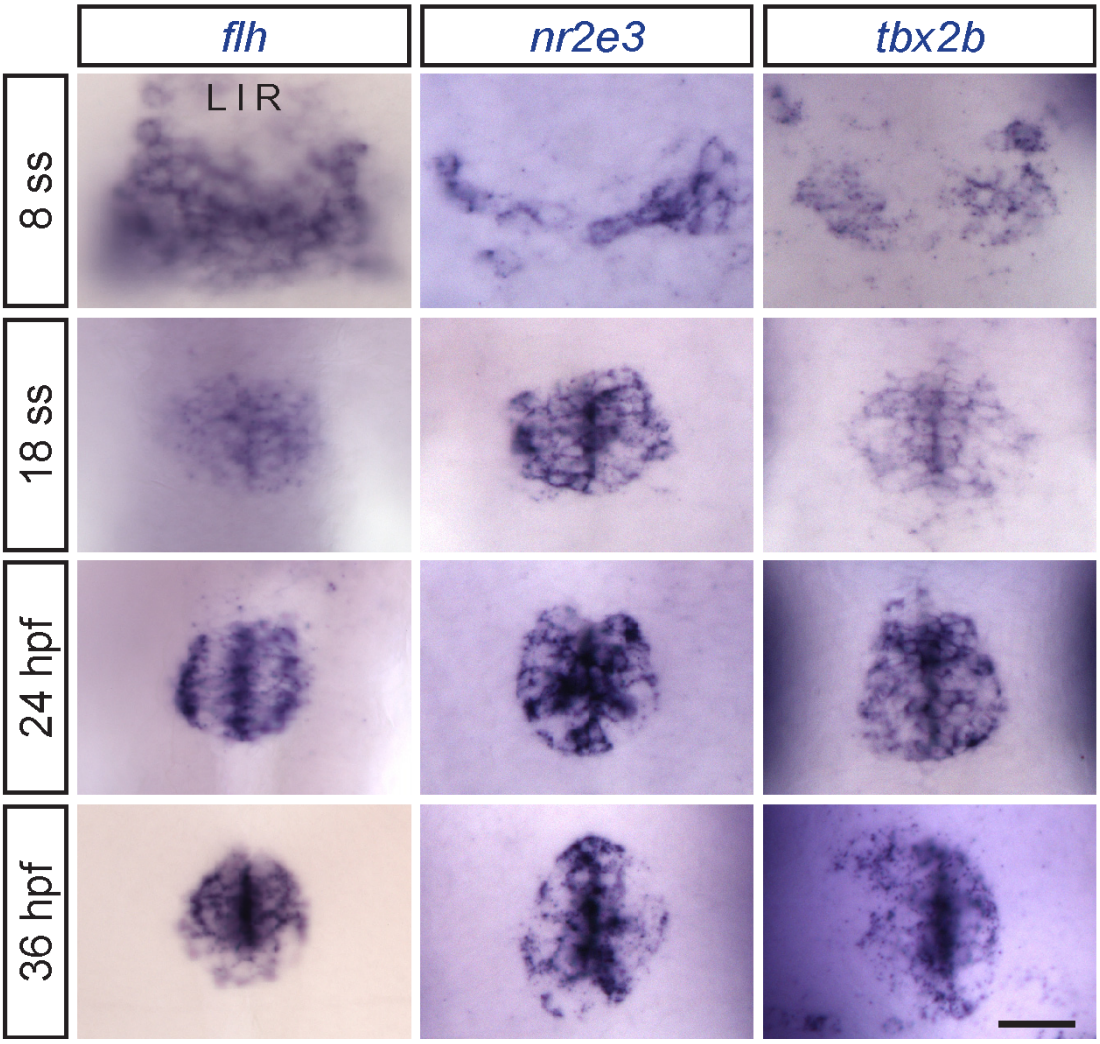

Figure 15: *flh, nr2e3, and tbx2b* expression during parapineal development. Dorsal views of single *in situ* hybridization of *flh, nr2e3,* and *tbx2b* at indicated stages. Scale bars = 30 μM

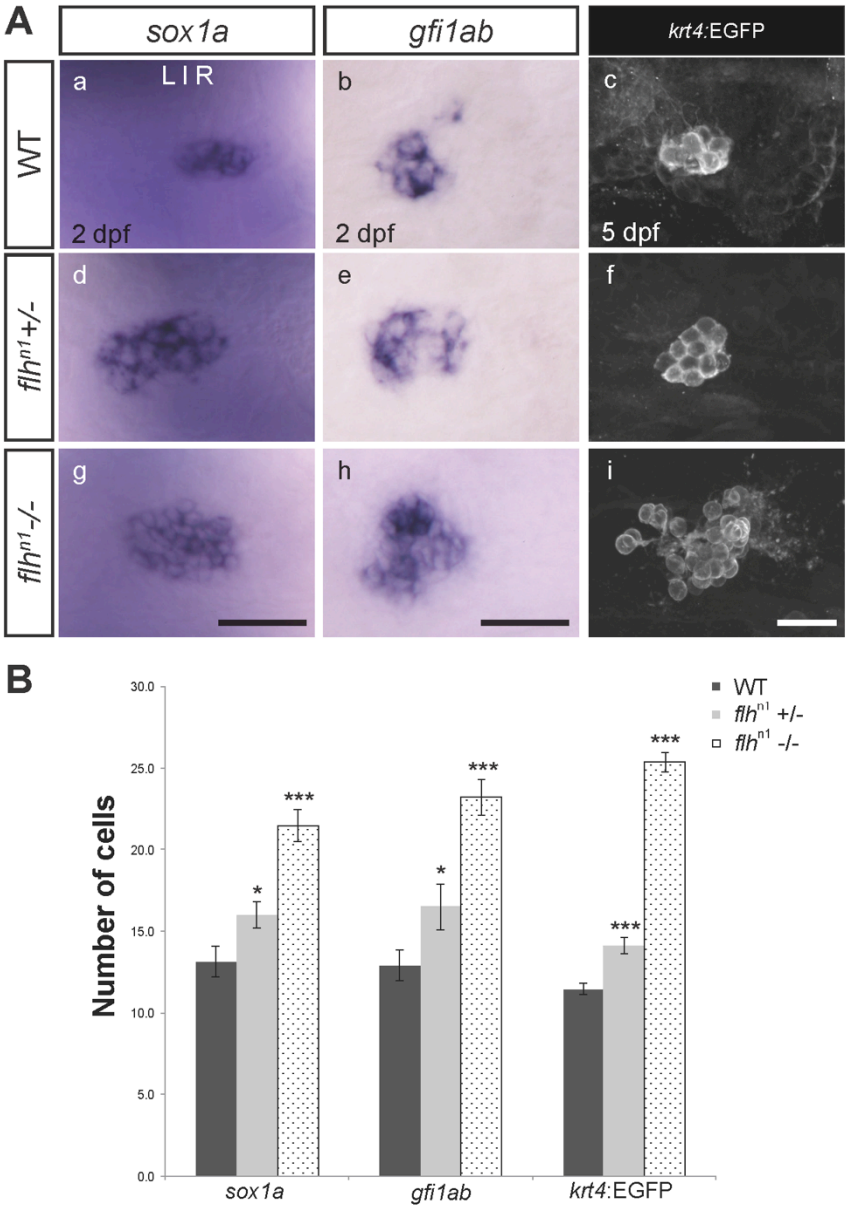

Figure 16: Flh inhibits specification of parapineal cells in a dose-dependent manner. (A) Dorsal views of *in situ* hybridization (*sox1a* and *gfi1ab*) or antibody labeling (*krt4*:EGFP) of the epithalamus under the indicated genetic backgrounds. Greater numbers of parapineal cells were observed in *flh*^{n1}+/- (d-f) and *flh*^{n1}-/- (g-i) as compared to WT (a-c) using an early differentiation marker (*sox1a*), and late differentiation markers (*gfi1ab* and *krt4*:EGFP) of parapineal cells at the indicated stages. Scale bars = 30 μM. (B) Bar chart summarizing the number of cells expressing different markers of parapineal cells. T-Test (Excel) as compared to WT, P-value < 0.05 (*), P-value <0.001 (***).

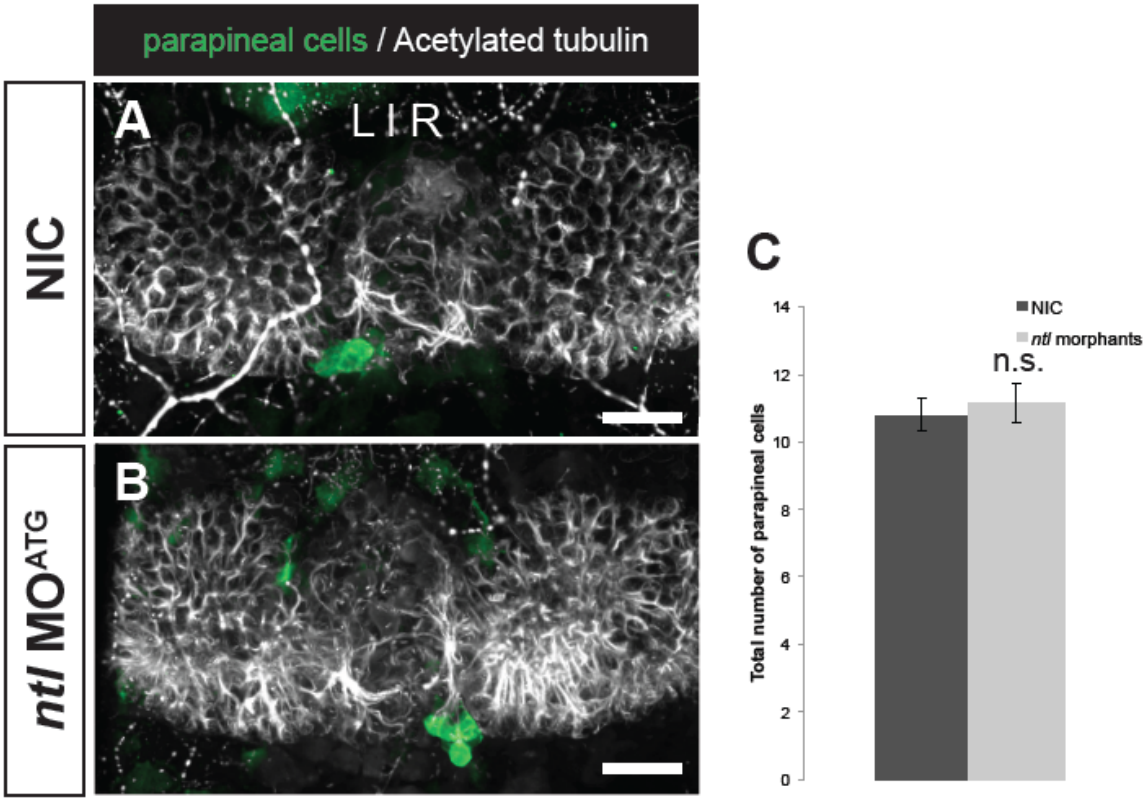

Figure 17. Embryos with compromised midline structures did not have increased numbers of parapineal cells.
Dorsal views of antibody labeled NIC (A) and *ntl* morphants (B). Parapineal laterality is randomized in *ntl* morphants due to bilateral expression of Nodal signaling in the epithalamus due to lack of notochord. However, the number of parapineal cells was unchanged. (C) Bar graph depicting the average number of parapineal cells (plus or minus standard error) at 5dpf. T-Test (Excel), P-value > 0.05 (n.s., not statistically significant), as compared to NIC. Scale bar=30μM.

Table 7. Number of labeled cells present in the pineal complex of Flh deficient embryos

Gene/Protein (cell types labeled)	Stage	Genotype	Number of Cells[a]	n[b]	N[c]	p-value[d]
sox1a	2 dpf	WT	13.1 ± 1.0	8	1	
(parapineal cells)		*flh*^{n1}+/-	16.0 ± 0.8	7	1	0.042*
		flh^{n1}	21.5 ± 1.0	25	2	8.22 x 10^{-5}*
gfi1ab	2 dpf	WT	12.9 ± 1.0	10	1	
(parapineal cells)		*flh*^{n1}+/-	16.5 ± 1.4	10	1	0.0497*
		flh^{n1}	23.2 ± 1.1	15	2	1.01 x 10^{-6}*
GFP in Tg(*krt4:EGFP*)^{sqet11}	5 dpf	WT	11.5 ± 0.4	46	5	
(parapineal cells)		*flh*^{n1}+/-	14.1 ± 0.5	46	5	5.24 x 10^{-5}*
		flh^{n1}	25.4 ± 0.6	70	7	1.12 x 10^{-34}*
Rhodopsin antibody	2 dpf	WT	10.8 ± 1.0	12	1	
(rod outer segments)		*flh*^{n1}+/-	8.0 ± 0.8	12	1	0.045*
		flh^{n1}	0.1 ± 0.1	10	1	1.01 x 10^{-8}*
4C12 antibody	2 dpf	WT	25.6 ± 2.1	25	3	
(rod photoreceptors)		*flh*^{n1}+/-	16.2 ± 2.6	24	3	0.006*
		flh^{n1}	0.7 ± 0.3	22	3	1.93 x 10^{-14}*
Arr3a antibody	2 dpf	WT	23.5 ± 1.1	20	2	
(red-green double cone cells)		*flh*^{n1}+/-	15.8 ± 0.7	20	2	1.32 x 10^{-6}*
		flh^{n1}	0.5 ± 0.2	18	2	1.29 x 10^{-20}*
HuC/D antibody	2 dpf	WT	30.4 ± 1.0	10	1	
(projection neurons)		*flh*^{n1}+/-	26.6 ± 1.1	10	1	0.022*
		flh^{n1}	9.4 ± 0.7	10	1	1.03 x 10^{-12}*
GFP in Tg(*foxd3:GFP*)^{zf104}	2 dpf	WT	63.1 ± 1.0	70	6	
(pineal complex cells, except rods)		*flh*^{n1}+/-	55.2 ± 1.3	66	6	3.57 x 10^{-6}*
		flh^{n1}	25.6 ± 0.6	62	6	1.07 x 10^{-61}*
To-Pro	2 dpf	WT	75.8 ± 3.2	8	1	
(nuclei stain)		*flh*^{n1}+/-	68.1 ± 3.0	8	1	0.101
		flh^{n1}	29.6 ± 0.8	5	1	2.32 x 10^{-7}*

[a]Average number of cells labeled at indicated stage, plus or minus standard error

[b]Number of samples examined

[c]Number of experiments examined

[d]P-value determined from two-tailed t-test (as compared to NIC), *marks significant difference

[e]Embryos have been injected with 6ng of *nr2e3* splice morpholino

dpf, days post fertilization

NIC, non-injected controls

Tbx2b *and* Flh *have opposite roles during parapineal specification*

Since *tbx2b* was transcriptionally regulated by Flh and given the unexpected increase in parapineal number in *flh*^{n1} mutants, we performed an epistasis experiment to better understand the genetic interaction between these two transcription factors. We observed an additive phenotype in *flh*^{n1}/*tbx2b* morphant embryos (i.e. intermediate number of parapineal cells) (Figure 18A, Figure 18B). Loss of *tbx2b* led to a reduction in

parapineal cell number in both *flh*^{n1} mutants and their siblings. The number of parapineal cells observed in *flh*^{n1}/*tbx2b* morphant embryos was similar to the number observed in WT embryos (Figure 18B). Thus, while Tbx2b appeared to play a role in parapineal specification, it appeared to do so in a permissive manner.

Interestingly, parapineal migration depended on the presence of functional Tbx2b. A defect in parapineal migration was observed in *tbx2b* morphants, but not in *flh*^{n1} (Figure 18A, Figure 18C). *flh*^{n1} mutants exhibit a midline defect, leading to bilateral expression of Nodal signaling (Concha et al., 2000; Gamse et al., 2003). As a result, the laterality of parapineal placement is randomized. However, parapineal cells still migrate. While Flh transcriptionally regulated *tbx2b,* normal parapineal migration was observed in *flh*^{n1} mutants, apparently due to residual amount of *tbx2b* remaining (Figure 14). Consistent with this hypothesis, parapineal cells in *flh*^{n1}/*tbx2b* morphant embryos failed to migrate (Figure 18A, Figure 18C).

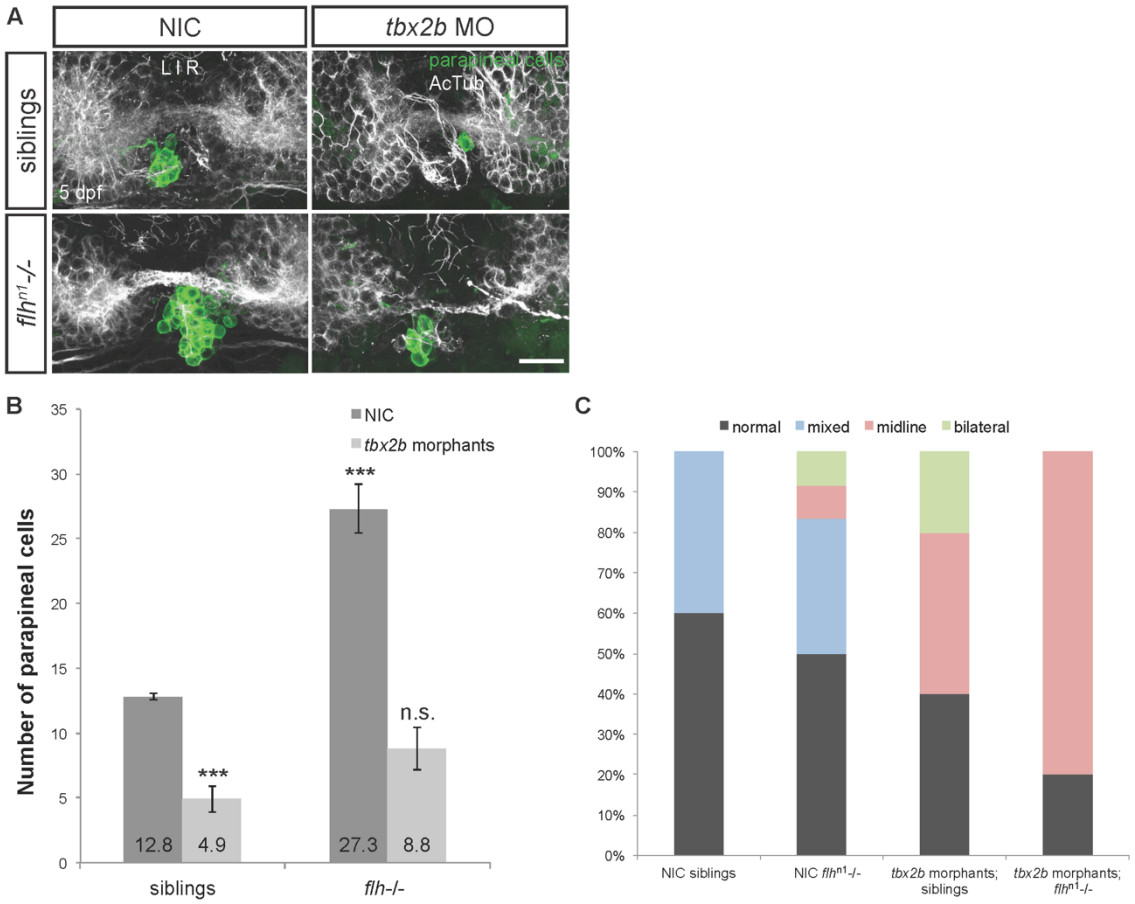

Figure 18: Flh acts in parallel with Tbx2b to specify parapineal fate.
(A) Dorsal views of antibody labeling of parapineal cells (krt4:eGFP) and acetylated tubulin, which marks axons and dendrites. Loss of *flh* function resulted in greater number of parapineal cells. Parapineal cells in *tbx2b* morphants or *tbx2b* morphants/*flh*^{n1} mutants did not migrate correctly and remained within the pineal organ region (as marked by acetylated tubulin). WT numbers of parapineal cells were observed in *tbx2b* morphants/*flh*^{n1} mutants. (B) Bar charts showing the number of krt4:eGFP positive cells (parapineal cells) in *flh*^{n1}-/- mutants or siblings (WT and *flh*^{n1}+/-) that were either non-injected control embryos (NIC) or injected with *tbx2b* morpholino. Loss of *tbx2b* function suppressed *flh*^{n1}-/- parapineal specification phenotype, as well as the migration of parapineal neurons. (C) Bar chart showing the percentage of embryos that have normal, bilateral, mixed (some cells migrate and some do not), or midline (cells remain near the midline) migration phenotypes. Loss of *tbx2b* function led to a greater percentage of embryos that have incorrectly migrated parapineal cells. T-Test (Excel) as compared to NIC;siblings, P-value < 0.001 (***), P-value > 0.05 (n.s., not significant). Scale bars = 30 μM

Flh ***promotes specification of non-migrating pineal cell types***

The pineal complex is made up of migrating (parapineal neurons) and non-migrating cell types (i.e. projection neurons, rod photoreceptors, and cone photoreceptors). Because Flh is required for the progression of pineal neurogenesis and loss of Flh leads to an overall reduction of pineal complex cells (Masai et al., 1997; Snelson et al., 2008a), its role in the specification of each pineal cell type was not previously considered. Since we have established that Flh acts in a dose-dependent manner during parapineal specification, we hypothesized that Flh will also act in a similar manner during specification of other pineal cell types. Thus, we compared the number of rods, cones, and projection neurons between wildtypes and Flh heterozygous. While the total number of pineal complex cell types remained the same between WT and Flh+/- (marked by the nuclei stain ToPro), we observed a reduced number of rods (Rhodopsin, 4C12), red/green cones (Arr3a), and projection neurons (HuC/D) in Flh+/- embryos (Figure 19, Table 7). Together, these data suggests that in addition to its role in the progression of pineal neurogenesis, Flh also plays a role in specifying each cell type present in the pineal organ.

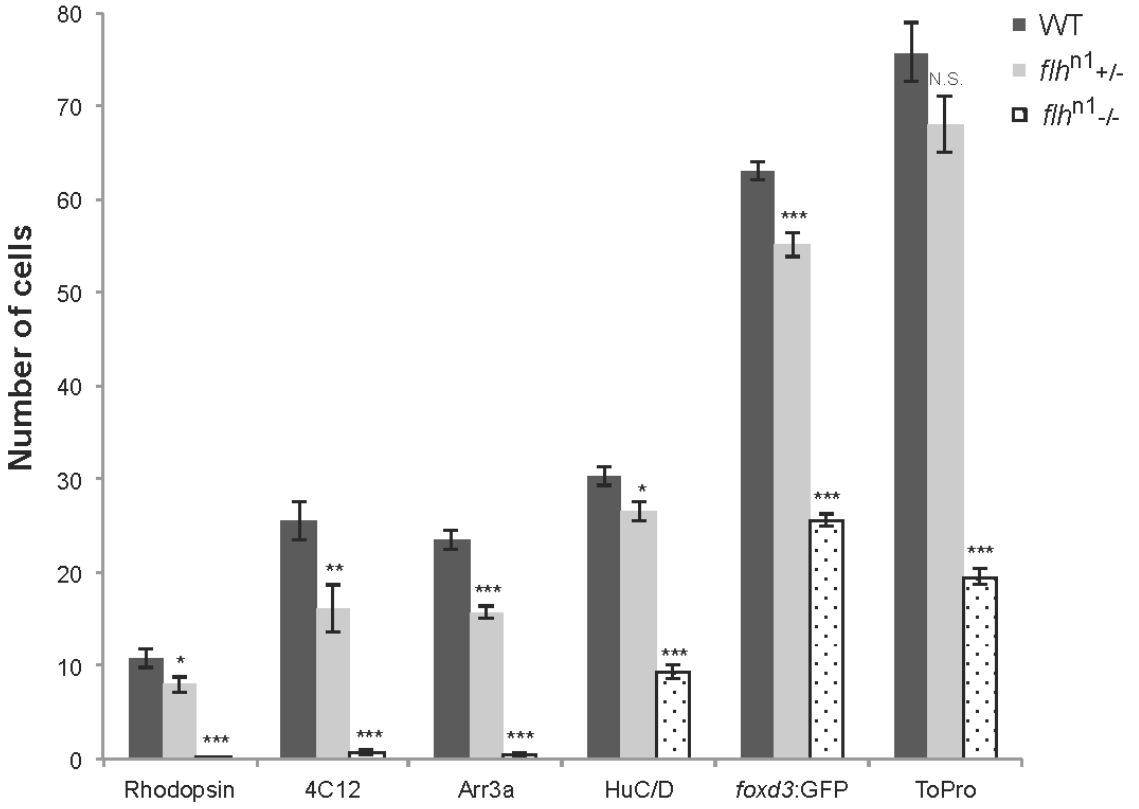

Figure 19: Flh promotes the specification of non-migrating cell types in the pineal complex.

Bar chart depicts the number of cells expressing markers for rod photoreceptors (Rhodopsin and 4C12), cone photoreceptors (Arr3a), projection neurons (HuC/D), pineal complex cells except rods (*foxd3*:GFP), and the total number of nuclei in the pineal complex (ToPro) at 2 dpf in WT, *flh*^{n1} +/-, and *flh*^{n1} -/-. At this stage, the total number of pineal complex cells was not different between WT and *flh*^{n1} +/-. However, other non-migrating pineal cell types were significantly reduced in *flh*^{n1} +/- compared to WT. T-Test (Excel) as compared to WT, P-value < 0.05 (*), P-value < 0.01 (**), P-value <0.001 (***), P-value > 0.05 (n.s., not significant).

Nr2e3 ***promotes pineal rod photoreceptor differentiation and inhibits parapineal fate***

Through literature searches, we hypothesized that the orphan nuclear receptor Nr2e3 (Nuclear receptor subfamily 2, group E, member 3) may also play a role in cell type specification in the pineal complex. In the zebrafish, *nr2e3* is only expressed in the pineal complex and in the retina (Kitambi and Hauptmann, 2007). Tbx2b promotes UV cone fate and represses rod photoreceptor differentiation in the zebrafish retina (Alvarez-Delfin et al., 2009). On the other hand, the role of Nr2e3 in promoting retinal rod photoreceptor differentiation is well established (Cheng et al., 2011; Peng et al., 2005); its role in repressing retinal cone photoreceptor has also been suggested (Chen et al., 2005). Similar to *tbx2b* and *flh*, *in situ* hybridization also demonstrated that *nr2e3* expression was restricted to the developing pineal complex in the epithalamus (Figure 15). Thus, we hypothesized that opposite roles of Tbx2b and Nr2e3 in promoting or repressing cell fates in the retina may persist during pineal complex development.

Accordingly, we tested whether Nr2e3 promotes pineal rod photoreceptor specification. Splice-blocking morpholino was used to eliminate Nr2e3 function. No overall differences in phenotype were observed in *nr2e3* morphants (Figure 20A), arguing against non-specific effect from the morpholino. This morpholino is predicted to work by retention of intron 2, leading to a premature stop codon. Semi-quantitative RT-PCR demonstrated retention of the intron (Figure 20B). Furthermore, Nr2e3 protein was reduced in *nr2e3* morphants (Figure 21A, Figure 21B). In the pineal complex, the role of Nr2e3 is consistent with its role in the retina. We found that loss of *nr2e3* function led to a reduction in the number of rod photoreceptors (Rhodopsin, 4C12) (Figure 21A, Figure 21B). Interestingly, we were not able to induce greater number of rod photoreceptors or

Nr2e3 expressing cells by overexpressing *nr2e3* (Figure 21B). This suggests that some other mechanisms control the production of the minimum number of parapineal neurons and that Nr2e3 functions to regulate this number. Aside from rod photoreceptors, other cell types in the pineal organ remained unaffected by loss of *nr2e3* (Table 8, Figure 21A). However, a small but significant increase in the number of parapineal cells was observed in *nr2e3* morphants, as compared to non-injected controls (NIC) at 5dpf ($p<0.001$) (Table 8, Figure 21A, Figure 21C). Intriguingly, unlike what is observed in *tbx2b*^{c144}, the increased in parapineal number in *nr2e3* morphants was not observed at early stages, (Table 9). This suggests that Nr2e3 plays a later role in parapineal specification.

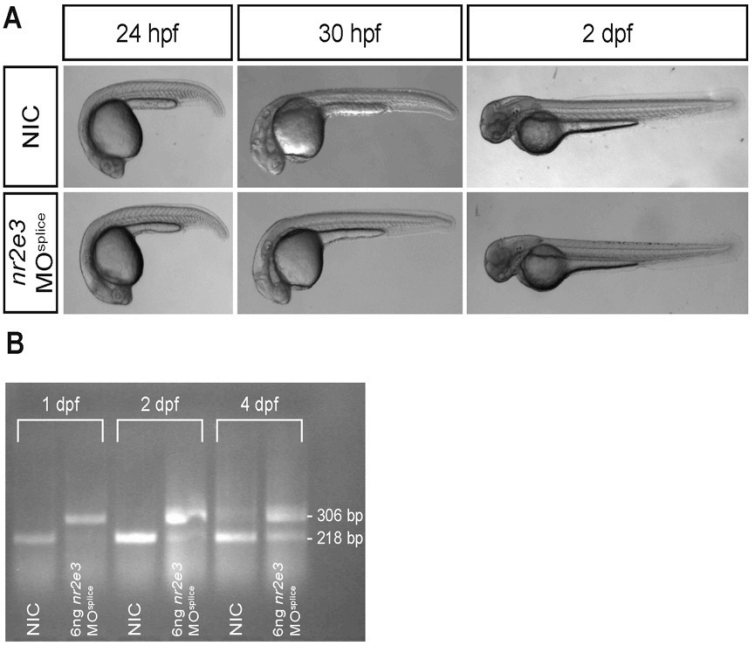

Figure 20: *nr2e3* morpholino prevents normal splicing of *nr2e3* mRNA. (A) *nr2e3* splice morpholino did not cause overall morphological defects. (B) *nr2e3* splice morpholino caused the retention of intron 2, which led to a premature stop codon in *nr2e3* transcript.

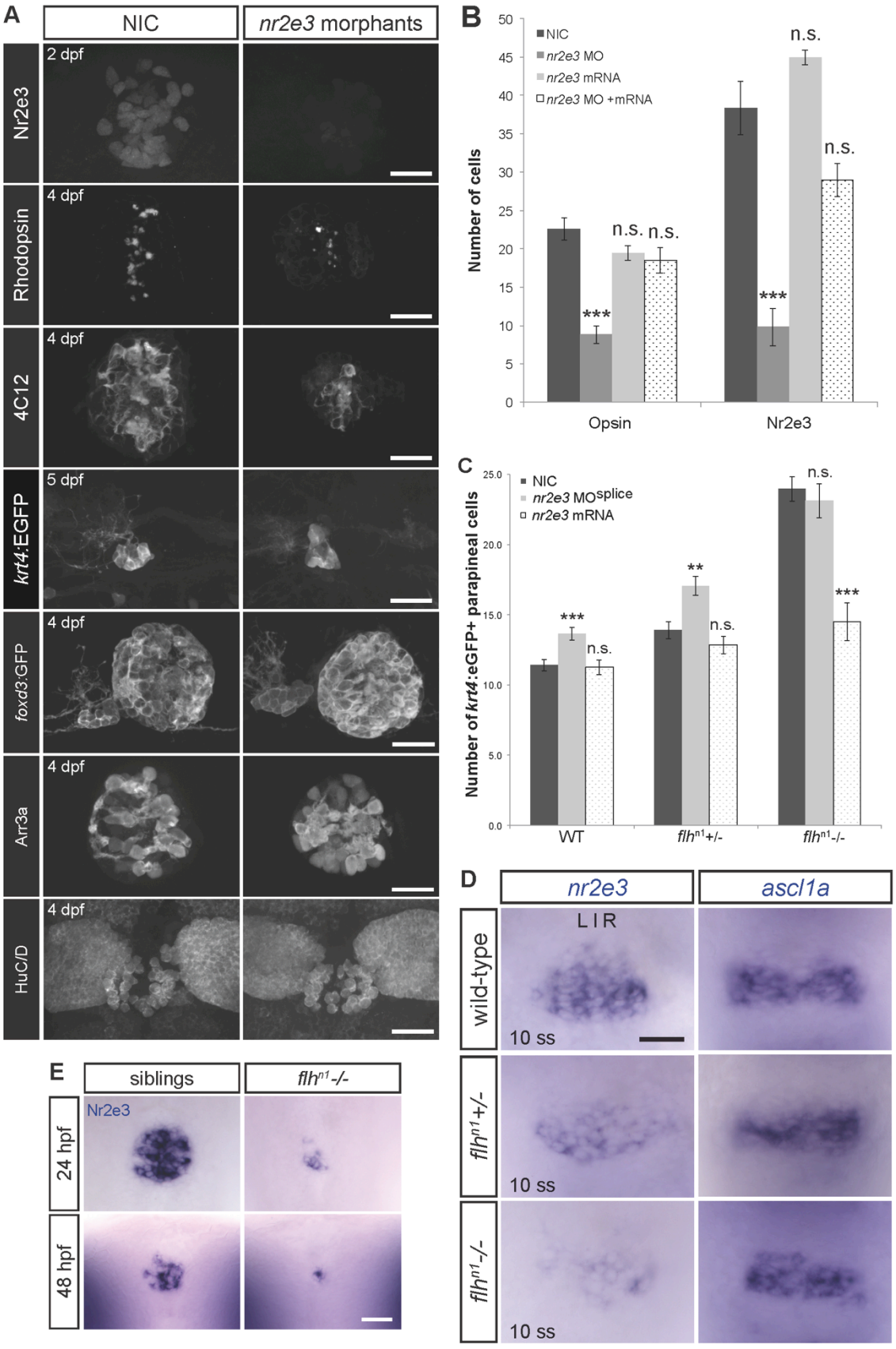
A
NIC
nr2e3 morphants
Nr2e3
Rhodopsin
4C12
krt4:EGFP
foxd3:GFP
Arr3a
HuC/D
2 dpf
4 dpf
4 dpf
5 dpf
4 dpf
4 dpf
4 dpf
B
NIC
nr2e3 MO
nr2e3 mRNA
nr2e3 MO +mRNA
Number of cells
n.s.
***
n.s.
n.s.
***
n.s.
Opsin
Nr2e3
C
NIC
nr2e3 MOsplice
nr2e3 mRNA
Number of krt4:eGFP+ parapineal cells
***
n.s.
**
n.s.
n.s.
***
WT
flh n1+/-
flh n1-/-
D
nr2e3
ascl1a
wild-type
L I R
10 ss
flh n1+/-
10 ss
flh n1-/-
10 ss
E
siblings
flh n1-/-
24 hpf
48 hpf
Nr2e3

Figure 21: Flh regulates parapineal neuron specification in part by upregulation of *nr2e3.*

(A) Antibody labeling demonstrating that Nr2e3 protein and rod markers (Rhodopsin and 4C12) are reduced in *nr2e3* morphants as compared to NIC at 4 dpf. In contrast, the number of parapineal cells (*krt4*:eGFP) is increased in *nr2e3* morphants (5 dpf). The number of red/green cone cells (Arr3a), projection neurons (HuC/D), and approximate total pineal complex (except rods, *foxd3*:GFP) cells remain unchanged in *nr2e3* morphants. (B) Bar charts showing the number of Opsin or Nr2e3 positive cells in NIC, *nr2e3* morphants, *nr2e3* mRNA overexpressed, or *nr2e3* morphants/*nr2e3* mRNA overexpressed embryos. (C) Bar charts showing the number of *krt4*:eGFP positive cells (parapineal cells) in WT, *flh*^{n1}+/-, and *flh*^{n1}-/- that have either been non-injected (NIC), injected with *nr2e3* splice morpholino (*nr2e3* MO^{splice}), or injected with *nr2e3* mRNA. (D) *In situ* hybridization showing either *nr2e3* or *ascl1a* expression in wild-type, *flh*^{n1}+/-, or *flh*^{n1}-/- at 10 ss. While *nr2e3* expression is reduced in *flh* deficient embryos, no change is observed in the expression of pro-neural marker, *ascl1a,* suggesting that reduced *nr2e3* expression is not due to reduced number of cells. (E) *In situ* hybridization showing reduced *nr2e3* expression at 24 and 48 hpf in *flh*^{n1}-/-. T-Test (Excel) as compared to corresponding NIC, P-value < 0.05 (*), P-value < 0.01 (**), P-value < 0.001 (***), P-value > 0.05 (n.s., not significant). Dorsal views. Scale bars = 30 μM

Table 8. Number of labeled cells present in the pineal complex of *nr2e3* morphants

Gene/Protein (cell types labeled)	Stage	Condition	Number of Cells[a]	n[b]	N[c]	p-value[d]
GFP in Tg(*krt4:EGFP*)^{sqet11}	5 dpf	NIC	11.8 ± 0.3	76	8	
(parapineal cells)		*nr2e3* morphants[e]	13.9 ± 0.3	75	8	3.08×10^{-6}*
Rhodopsin antibody	4 dpf	NIC	27.6 ± 1.6	10	1	
(rod outer segments)		*nr2e3* morphants[e]	14.2 ± 2.1	10	1	7.97×10^{-5}*
4C12 antibody	4 dpf	NIC	74.0 ± 4.7	10	1	
(rod photoreceptors)		*nr2e3* morphants[e]	51.8 ± 4.1	9	1	0.003*
Arr3a antibody	4 dpf	NIC	27.6 ± 2.2	14	2	
(red-green double cone cells)		*nr2e3* morphants[e]	26.3 ± 2.0	10	2	0.667
HuC/D antibody	4 dpf	NIC	42.8 ± 1.2	12	2	
(projection neurons)		*nr2e3* morphants[e]	39.5 ± 1.9	10	2	0.134
GFP in Tg(*foxd3:GFP*)^{zf104}	4 dpf	NIC	87.0 ± 2.5	36	3	
(parapineal and pineal cells)		*nr2e3* morphants[e]	85.7 ± 3.2	30	3	0.739

[a]Average number of cells labeled at indicated stage, plus or minus standard error

[b]Number of samples examined

[c]Number of experiments examined

[d]P-value determined from two-tailed t-test (as compared to NIC), *marks significant difference

[e]Embryos have been injected with 6ng of *nr2e3* splice morpholino

dpf, days post fertilization

NIC, non-injected controls

Table 9. Number of *sox1a* positive parapineal cells in *nr2e3* morphants and/or *tbx2b*^{c144} mutants

Stage	Embryo	Number of Cells[a]	n[b]	p-value[c]
32 hpf	NIC	6.5 ± 0.5	11	n/a
	nr2e3 morphants[d]	8.8 ± 3.0	4	0.065
	tbx2b^{c144}-/-	1.3 ± 0.5	13	9.52 x 10^{-8}*
	nr2e3 morphants[d]; tbx2b^{c144}-/-	6.6 ± 1.3	7	0.867
2 dpf	NIC	10.5 ± 0.5	24	n/a
	nr2e3 morphants[d]	10.1 ± 0.6	15	0.688
	tbx2b^{c144}-/-	3.6 ± 0.8	7	2.89 x 10^{-7}*
	nr2e3 morphants[d]; tbx2b^{c144}-/-	n.d.		n/a

[a]Average number of cells labeled, plus or minus one standard error
[b]Number of samples examined
[c]P-value determined from two-tailed t-test (as compared to WT), *marks significant difference
hpf, hours post fertilization
dpf, days post fertilization
n.d. no data

To better understand the relationship between Tbx2b and Nr2e3, we performed an epistasis experiment and found that they act in opposite manners regarding parapineal specification. In *tbx2b*^{c144}/*nr2e3* morphant embryos, partial suppression of *tbx2b*^{c144} specification phenotype was observed (i.e. number of parapineal cells is partially rescued) (Figure 22A, Figure 22B). However, similar to what was observed in *flh*^{n1}/*tbx2b* morphants, parapineal migration was not rescued in *tbx2b*^{c144}/*nr2e3* morphant embryos (Figure 22A and data not shown). This observation further supports the idea that Tbx2b is necessary for parapineal migration.

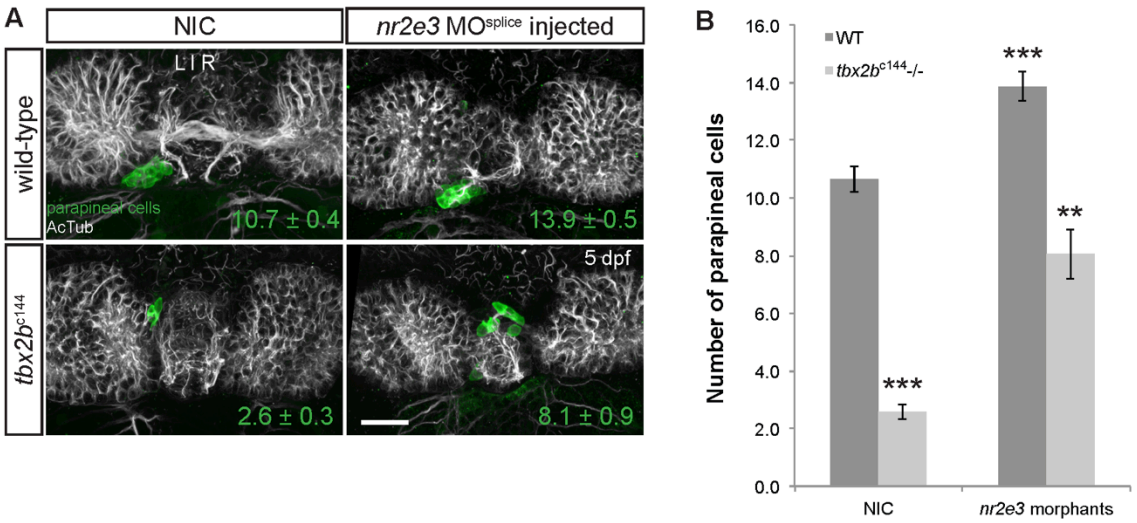

Figure 22. Tbx2b is necessary for parapineal migration.
(A) Dorsal views of antibody labeling of parapineal cells (*krt4*:eGFP) and acetylated tubulin (marks axons and dendrites). Parapineal cells in *tbx2b*^{c144} or *tbx2b*^{c144}/*nr2e3* morphants did not migrate correctly and remained within the pineal organ region (as marked by acetylated tubulin). (B) Bar charts showing the number of *krt4*:eGFP positive cells (parapineal cells) in non-injected embryos (NIC) or *nr2e3* morphants that either have both WT (WT) or two mutated copies of *tbx2b* (*tbx2b*^{c144}-/-). Loss of *nr2e3* function partially suppressed *tbx2b*^{c144} parapineal specification phenotype, but did not suppress the migration defect phenotype. T-Test (Excel) as compared to NIC;WT, P-value < 0.01 (**), P-value < 0.001 (***). Scale bars = 30 μM

Nr2e3 ***acts downstream of*** **Flh** ***to regulate the number of parapineal cells***

Because both Flh and Nr2e3 inhibited parapineal fate, we wanted to determine if they acted in the same genetic pathway. First, we showed that *nr2e3* is transcriptionally regulated by Flh. At 10 ss, *nr2e3* expression was reduced in *flh*^{n1}. In contrast, expression of the pro-neural gene *ascl1a* remained unaffected, demonstrating that loss of *nr2e3* was not due to loss of total number of pineal complex cells (Figure 21D).

Next, we showed that the increase in parapineal cell number in *flh*^{n1} could be partially suppressed by *nr2e3* overexpression. While *nr2e3* mRNA overexpression led to a partial suppression of *flh*^{n1} parapineal phenotype ($p=0.01$ compared to WT, NIC; $p<0.001$ compared to *flh*^{n1}, NIC), it did not lead to a further reduction in number of parapineal cells in WT embryos ($p=0.81$) (Figure 21C). Further reduction of *nr2e3* via morpholino injection did not lead to a greater increase in parapineal number in *flh*^{n1} mutants ($p=0.56$), but did lead to a greater increase in parapineal number in *flh*^{n1} heterozygous embryos ($p=0.001$) (Figure 21C). Together, these data strongly suggest that Nr2e3 acts downstream of Flh to inhibit parapineal fate.

Flh, Nr2e3, ***and*** **Tbx2b** ***expression during parapineal development display subtle, but significant differences***

flh, nr2e3, and *tbx2b* were expressed similarly in the pineal complex during parapineal development (Figure 15). We next sought to determine if the spatial regulation of these transcription factors could explain how these three genes could combine to generate precise numbers of parapineal cells. In order to resolve the expression patterns of these genes relative to one another, we performed double fluorescent *in situ*

hybridization experiments. *flh* and *nr2e3* appeared to be expressed within the same domain (Figure 23A, Figure 23d, Figure 25). However, the *tbx2b* positive domain seemed to be expanded anteriorly relative to *flh* (Figure 23B, Figure 23E) and *nr2e3* (Figure 23C, Figure 23F, Figure 24, Figure 25).

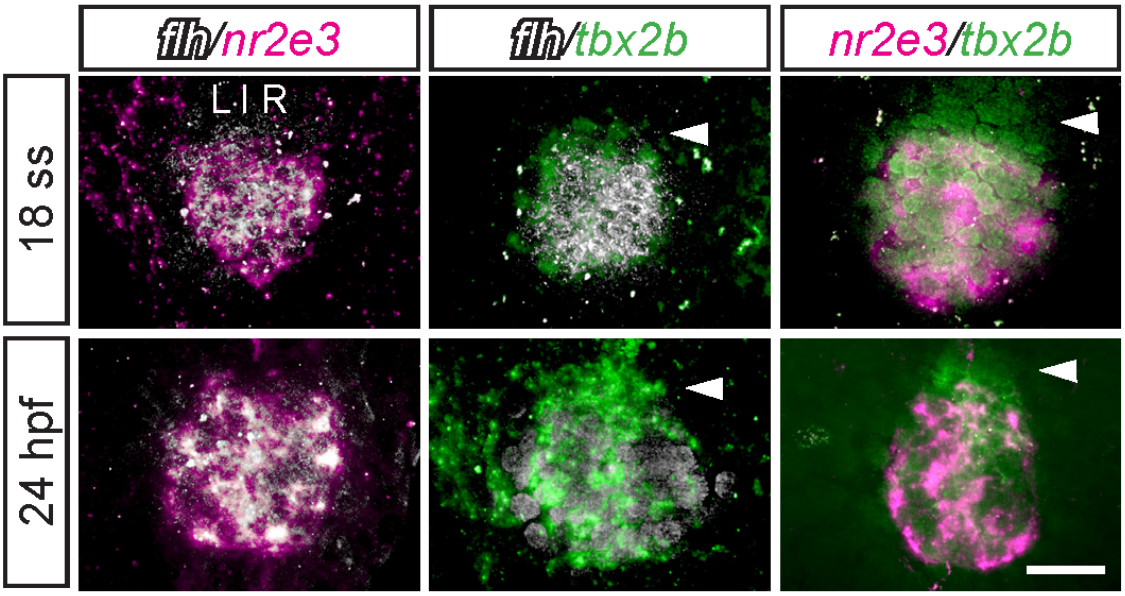

Figure 23: *flh, nr2e3, and tbx2b* expression during parapineal development display subtle, but significant differences.
tbx2b expression was expanded in the anterior region (arrowheads), relative to *flh* or *nr2e3* expression patterns. Dorsal views of double fluorescent *in situ* hybridization of *flh/nr2e3, flh/tbx2b,* and *nr2e3/tbx2b* at indicated stages. Scale bar = 30 μM

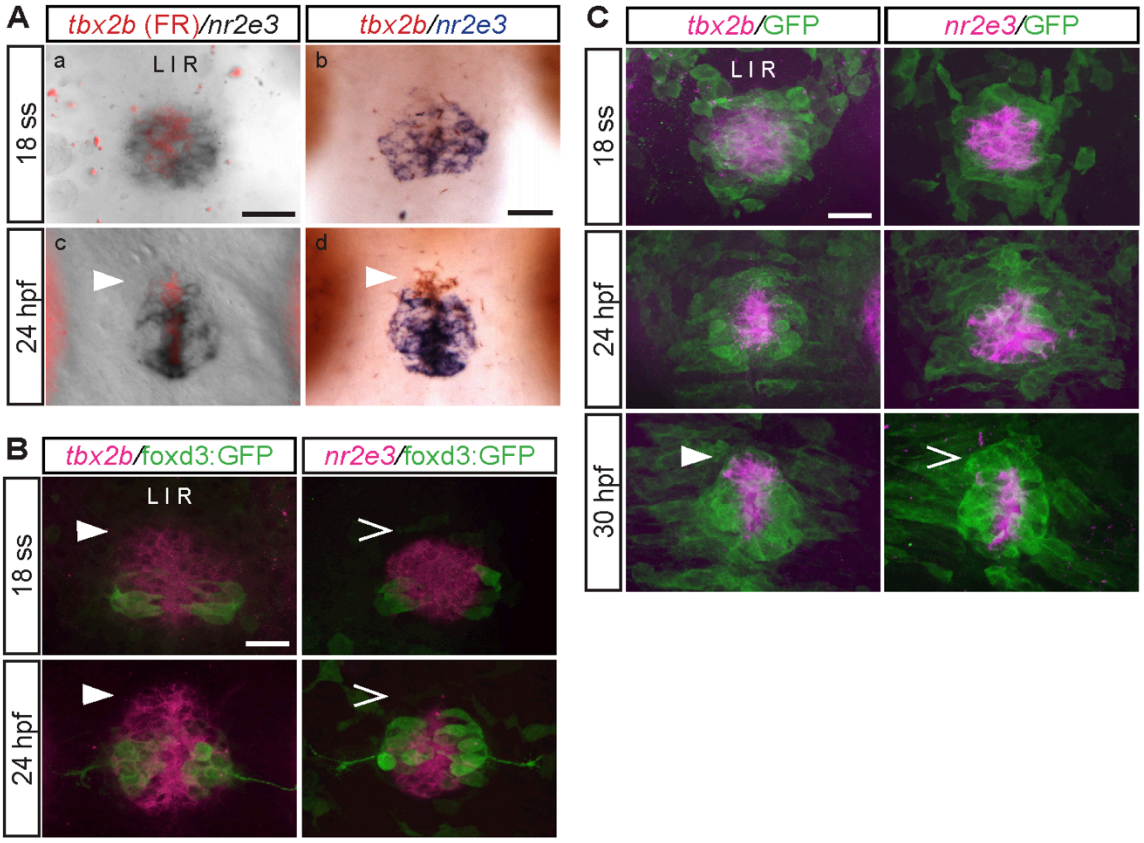

Figure 24: *nr2e3* and *tbx2b* expression during parapineal development display subtle, but significant differences.
tbx2b expression was expanded in the anterior region (arrowheads), relative to *nr2e3* expression patterns. This difference was subtle at 18 ss and became more apparent at 24 hpf. (A) Double ISH of *tbx2b* and *nr2e3* at indicated stages. (a,c) *tbx2b* was developed using fast red reagents and imaged using fluorescence filter; *nr2e3* was developed using NBT/BCIP and imaged under bright field. (b,d) *tbx2b* (developed using INT/BCIP) and *nr2e3* (developed using NBT/BCIP) were imaged under bright field. (B) Double fluorescent ISH labeling (*tbx2b* or *nr2e3*) and antibody labeling (AB) (*foxd3*:GFP). At these stages, *foxd3*:GFP is expressed in the projection neurons. (C) Double labeling with fluorescent ISH (*tbx2b* or *nr2e3*) and AB (*s1145t*:GFP). At these stages, *s1145t*:GFP is expressed throughout the pineal anlage. Scale bars=30 μM

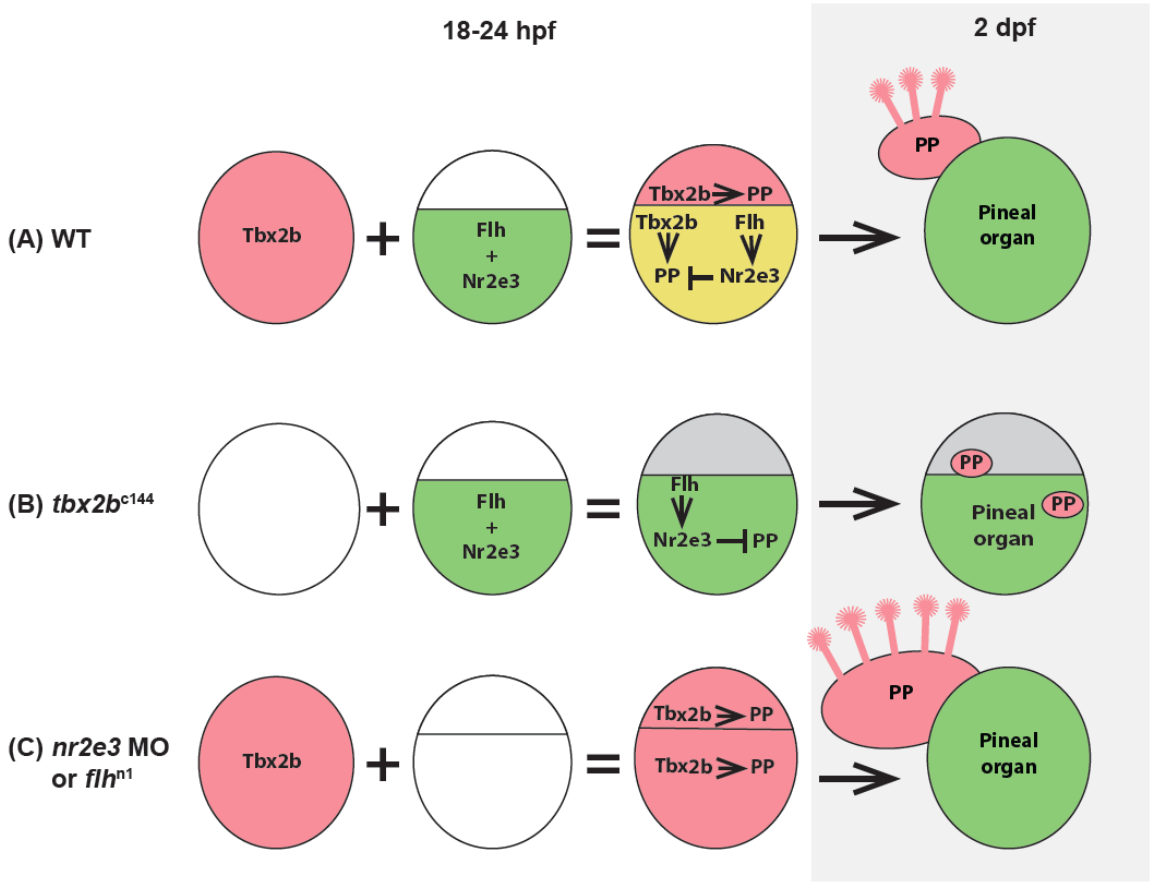

Figure 25. Proposed model of genetic interaction between Tbx2b, Nr2e3, and Flh during parapineal specification.
(A) In wild-type embryos, Tbx2b is expressed throughout the pineal anlage during parapineal specification step while Nr2e3 and Flh expressed are more restricted to the posterior region. Together, this generates a Tbx2b positive domain in the anterior region. Cells in this domain are competent to become parapineal cells. (B) In *tbx2b*^{c144} mutants, only parapineal inhibition factors (Flh and Nr2e3) are present, reducing the population of cells competent to be specified as parapineal cells. Reduced number of parapineal cells is observed. (C) In *nr2e3* morphants or *flh*^{n1} mutants, a population of cells competent to become parapineal cells is expanded due to lack of the inhibition factors Flh or Nr2e3. Greater number of parapineal cells is observed. Abbreviations: hours post fertilization (hpf), days post fertilization (dpf), morphants (MO), parapineal (PP).

Discussion

Understanding how cells become migratory or not can have significant implications on normal development as well as in metastatic cancers (Lauffenburger and Horwitz, 1996; Liotta et al., 1991). The pineal complex consists of migratory (parapineal) and non-migratory (pineal) cell types that originate from the same anlage (Clanton et al., 2013). After specification, parapineal cells migrate unilaterally away from the pineal organ in a consistent manner (Snelson et al., 2008b). Thus, the pineal complex can be used to study how a subset of the cell population can become migratory. Previous work has shown that the transcription factor Tbx2b is necessary for proper specification and migration of parapineal cells (Snelson et al., 2008b). However, it was unclear how Tbx2b functions. Through literature searches, we have identified and tested two other key transcription factors that also function to specify correct number of parapineal cells: Flh and Nr2e3. Using knockdown and overexpression studies, we determined that Nr2e3 was positively regulated by Flh and could inhibit parapineal cell fate. Furthermore, we showed that while Tbx2b is necessary for proper parapineal migration, its role in parapineal specification was permissive, as loss of Tbx2b function together with loss of either of the inhibitory factors (Nr2e3 or Flh) still resulted in a number of correctly specified parapineal cells that did not migrate correctly. This is consistent with a role for Tbx2b during neural plate formation, where it mediates cell migration in a cell autonomous manner (Fong et al., 2005). The elucidation of Tbx2b responsive genes that play a direct role in parapineal migration will help us better understand how parapineal cells become migratory. Transcriptome analysis between NIC and *tbx2b* morphant pineal cells has yielded several genes that were upregulated by Tbx2b (Chapter 2). Functional

characterization of these target genes may yield significant insight into the mechanisms of parapineal migration.

Our data suggest that correct parapineal specification is achieved via spatial differences in *tbx2b, nr2e3,* and *flh* expression patterns, in which *tbx2b* is relatively expanded anteriorly (Figure 25). This observation is significant because while the origin of parapineal precursors is unknown, previous lineage labeling experiments demonstrate that by 24 hpf, parapineal precursors are located in the anterior region of the pineal anlage (Clanton et al., 2013; Concha et al., 2003). Therefore, this supports a model in which the correct number of parapineal cells results from the Tbx2b-positive domain being more anteriorly expressed as relative to the parapineal inhibitory factors such as Flh and Nr2e3.

Similar to its role in the retina, Nr2e3 also functions to promote rod photoreceptor specification in the pineal complex. Nr2e3 loss-of-function (LOF) results in a small, but significant increase in parapineal cell number at late stage (5 dpf). Overexpression of *nr2e3* mRNA suppresses *flh*^{n1} parapineal phenotype and *nr2e3* is transcriptionally regulate by Flh. One possible explanation for the finding that the Nr2e3 LOF parapineal phenotype was not observed at early stages is due to continued production of Nr2e3 by Flh.

In addition to its role in the progression of pineal neurogenesis (Masai et al., 1997), Flh inhibited parapineal fate (this study). This observation was completely unexpected, as a previous study has reported that Flh does not control parapineal fate (Snelson et al., 2008a). We have also observed that in some embryos, the parapineal cells in *flh*^{n1} mutants formed two separate clusters, suggesting there might be two different

populations. Birthdating analysis, such as BrdU or EdU labeling, should reveal if the supernumerary parapineal cells in *flh*^{n1} mutants were all born at the same time.

We found that Flh also controls the specification of other non-migratory pineal cell types including rods, cones, and projection neurons. Being able to induce photoreceptor or inhibit parapineal fates via mosaic overexpression of Flh will provide greater insight into permissive versus instructive roles for Flh. Furthermore, we demonstrated that Flh transcriptionally regulated both *tbx2b* and *nr2e3*. This is very intriguing, as *tbx2b* and *nr2e3* have very different roles in specifying pineal complex cell types: Tbx2b had a permissive role in parapineal specification and promotes cone maintenance genes (Chapter 2). In contrast, Nr2e3 inhibited parapineal fate and promotes rod photoreceptor differentiation. Together, these observations showed that Flh can control specification of both migratory and non-migratory pineal complex cell types and might be a master regulator of transcription factors that defines pineal cell identity.

Acknowledgements

I thank Benjamin J. Dean and Joshua A. Clanton for performing, imaging, and analyzing double fluorescence *in situ* hybridization experiments; Robert Taylor for use of Tg(*uas:eGFP*)^{vu294} fishes.

CHAPTER 4

DISCUSSION AND FUTURE DIRECTIONS

The zebrafish pineal complex offers a unique opportunity to study the question of how a subset of cells from a common anlage is fated to become migratory. Within the pineal complex, formation of the parapineal organ is most intriguing: parapineal neurons are specified from the same anlage as the non-migratory pineal neurons. The parapineal neuron cluster then migrates unilaterally away from the midline to lie adjacent to the flanking habenular nuclei. Proper migration of parapineal neurons is essential in establishing left-right asymmetries in the zebrafish diencephalon, which have important implications in proper neuronal functions and behavior. Therefore, understanding how parapineal neurons form and migrate will not only provide insight into understanding neuronal fate determination, but also left-right asymmetry formation. In this body of work, I have investigated the roles of the T-box transcription factor Tbx2b during parapineal development. I found that together with Flh and Nr2e3, Tbx2b was a part of a transcription factor network that interacted to regulate the number and migration of parapineal neurons.

Tbx2b plays a permissive role during parapineal specification

Previous study showed reduced numbers of parapineal cells that do not migrate in *tbx2b*^{c144} mutants, suggesting that Tbx2b is necessary for parapineal specification and migration (Snelson et al., 2008b). Through literature searches, I have identified and

characterized the roles of two transcription factors, Flh and Nr2e3, during parapineal development and found that they both have an inhibitory role. Using genetic epistasis experiments, as well as mosaic overexpression studies, I have determined that Tbx2b acts in a permissive manner during parapineal specification. First, mosaic overexpression of fluorescently tagged Tbx2b in the pineal complex via Gal4/UAS system could not induce parapineal fate (Figure 26). More characterization of the UAS:Tbx2b overexpression constructs will need to be performed to ensure that this is not due to non-functional Tbx2b protein. However, the fluorescently tagged overexpressed Tbx2b protein was localized in the nuclei, consistent with Tbx2b being a transcription factor (Figure 26). Secondly, relatively normal numbers of parapineal cells were still observed in embryos with reduced or absent Tbx2b activity, as long as an inhibitory factor (Nr2e3 or Flh) was also absent. Thus, one of Tbx2b functions could be to inhibit expression of Nr2e3 or Flh. However, expression of *nr2e3* mRNA was reduced in *tbx2b*^{c144} mutants (Figure 27A); and the number of cells that express Nr2e3 protein was reduced in *tbx2b*^{c144} mutants (Figure 27B). These seemingly paradoxical findings led us to begin exploring a genetic interaction system known as an *incoherent type I feed forward system* (Figure 28). In this system, Tbx2b promotes both parapineal fate as well as Nr2e3 expression. Nr2e3 inhibits parapineal specification, but at a much less effective level as Tbx2b promotion of parapineal specification at an earlier stage. At a later stage, Nr2e3 levels are sufficient to allow for it to outcompete Tbx2b and inhibit parapineal fates and promote rod fate. The fact that I did not see an increase in *sox1a* positive cell number in *nr2e3* morphants at earlier stages supports this model (Table 9). Furthermore, I have demonstrated that two genes identified from RNA-seq experiments to be downstream of Tbx2b, *pde6c* and

gnat2, were increased in *nr2e3* morphants as compared to wildtypes at 2 dpf, but they were indistinguishable at 1 dpf (Figure 29). In the future, a photoactivatable morpholino could be used to temporally control the knockdown of *nr2e3* and further test this idea.

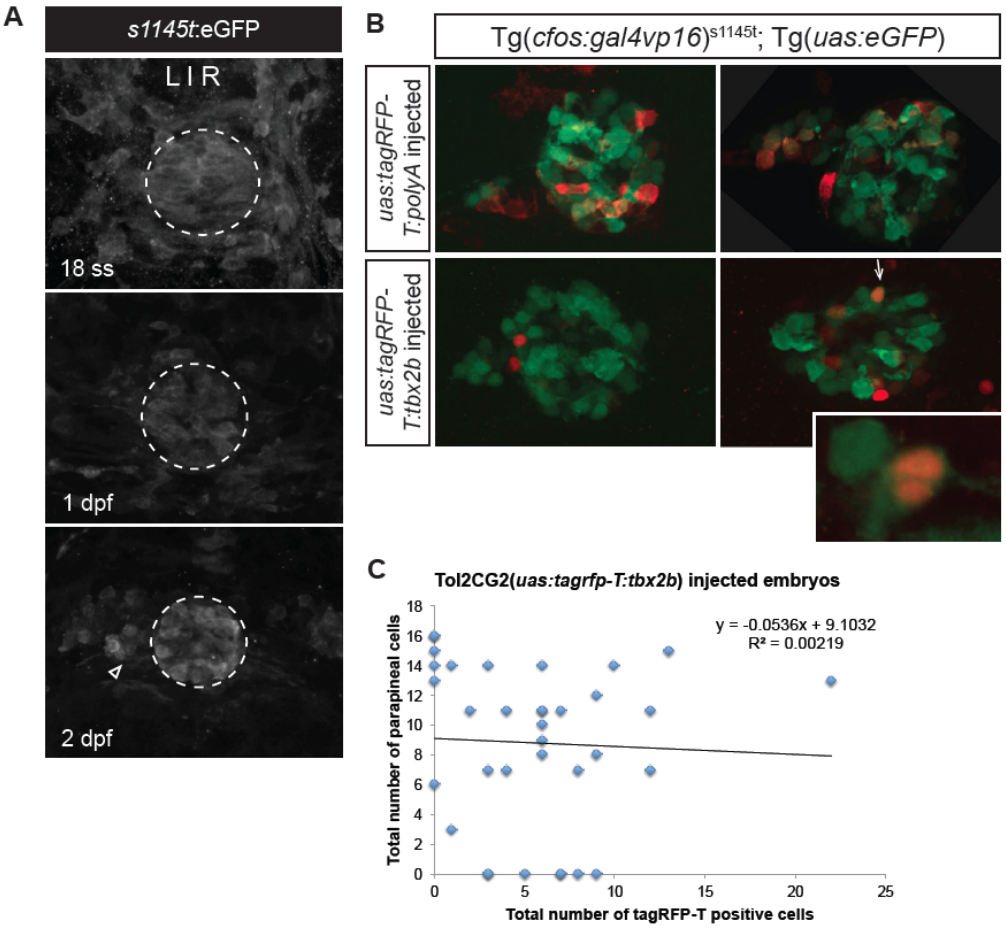

Figure 26: Mosaic overexpression of Tbx2b cannot induce parapineal fate. (A) Tg(*cfos*:*gal4vp16*)^{s1145t} could be used to drive gene expression in the pineal complex. Dorsal views showing immunofluorescent images at indicated stages of Tg(*cfos*:*gal4vp16*)^{s1145t}; Tg(*uas:eGFP*) embryos. The expression was strong in the pineal complex (dotted circles) and the parapineal organ (open arrow heads) at later stages, but was also expressed in other parts of the zebrafish brain. (B) Immunofluorescent images of *s1145t*:eGFP embryos injected with either *uas:tagRFP-T:polyA* or *uas:tagRFP-T:tbx2b*. tagRFP:Tbx2b fusion protein appeared to be localized in the nuclei. (C) Scatter plot showing there was no correlation (Excel, Pearson's correlation, R^2=0.00219) between the total number of cells expression tagRFP:Tbx2b fusion protein and the total number of parapineal cells.

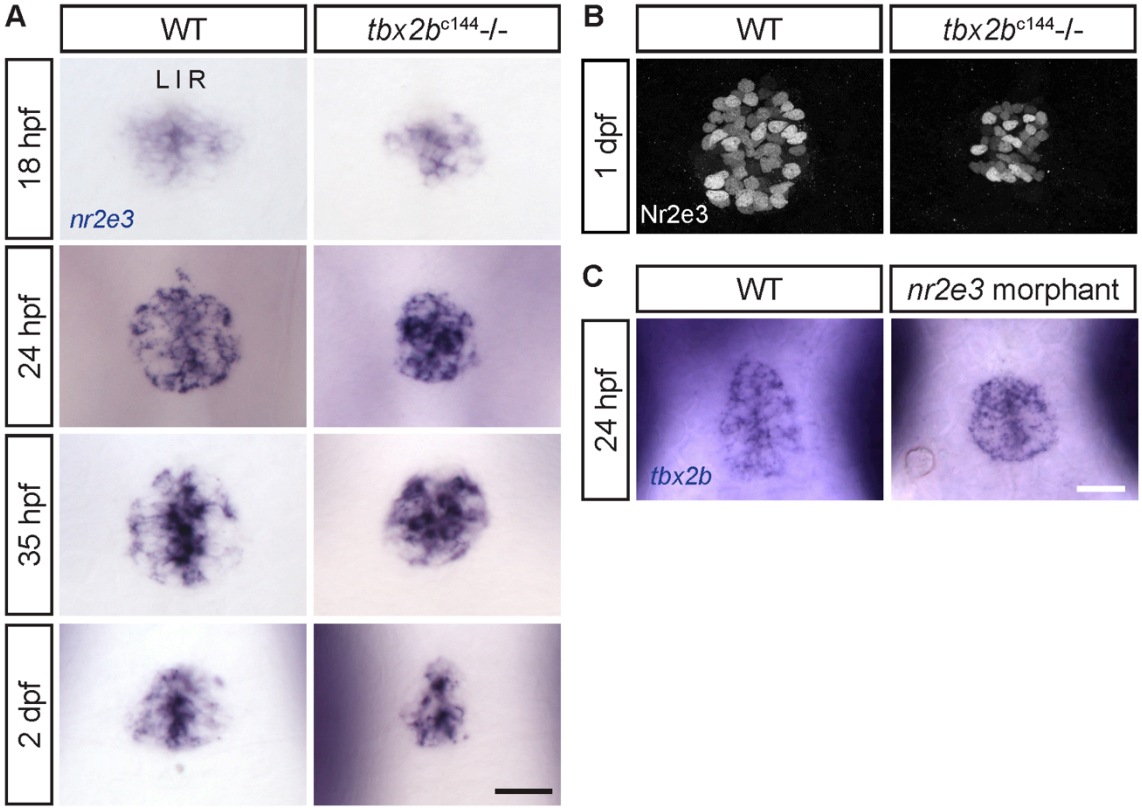

Figure 27: Tbx2b upregulates Nr2e3 expression.
(A) *In situ* hybridization showing representative images of *nr2e3* expression in WT or *tbx2b*^{c144}-/- pineal complex at indicated stages. *nr2e3* mRNA expression was reduced in *tbx2b*^{c144}-/-. Dorsal views. (B) Antibody labeling showing smaller number of cells expression Nr2e3 protein in the pineal organ. Dorsal views. (C) *In situ* hybridization showing representative images of *tbx2b* expression in WT and *nr2e3* morphants pineal complex at 24 hpf. Scale bars=30μM

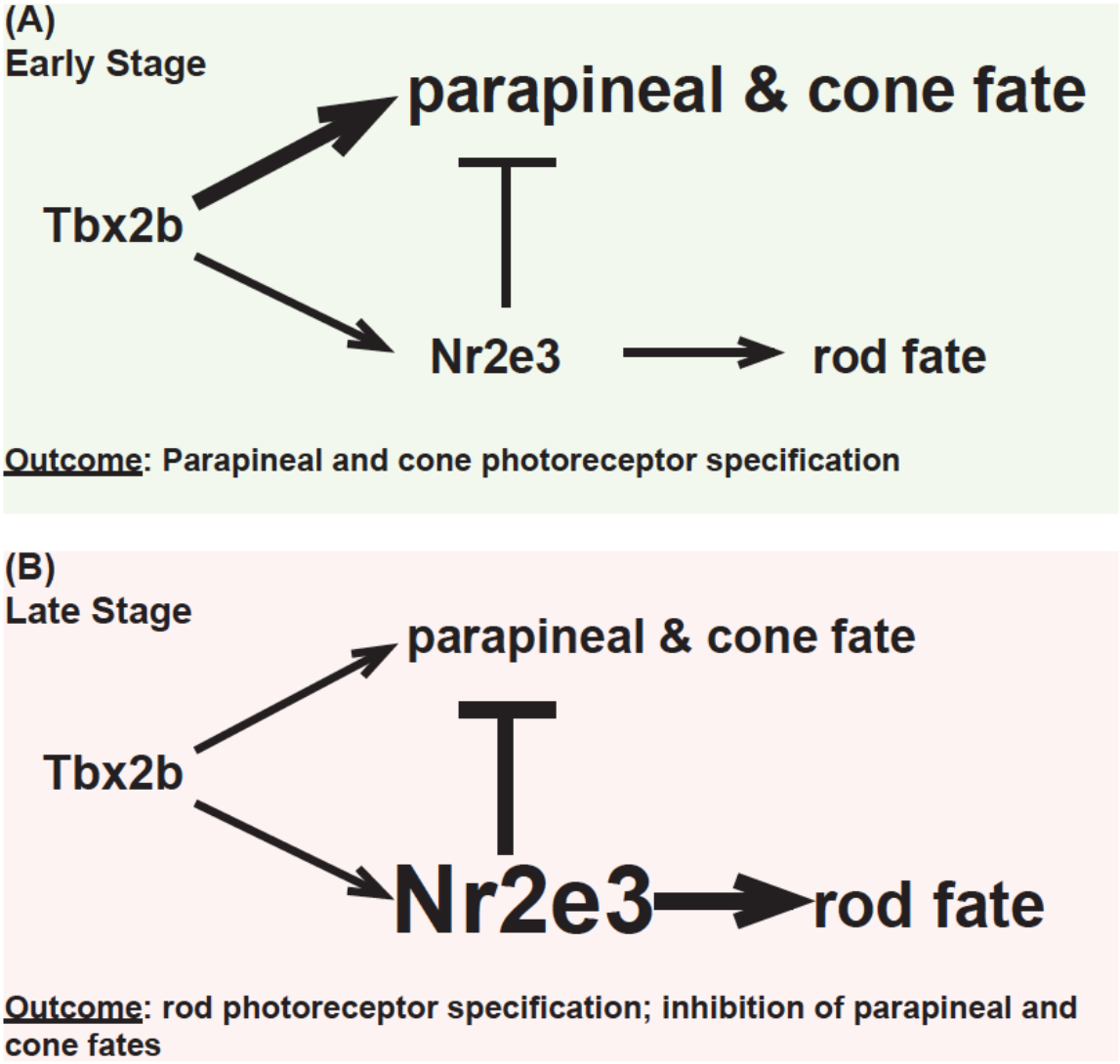

Figure 28: Model of incoherent type I feed forward system during pineal complex development.
Tbx2b upregulates the expression of Nr2e3 as well as genes related to cone functions. (A) At an early stage, Nr2e3 is not accumulated enough to induce rod fate or inhibit cone/parapineal fates. The outcome is parapineal and cone photoreceptor specification. (B) At a late stage, high level of Nr2e3 is accumulated. Nr2e3 can now out compete Tbx2b's function. The outcome is rod photoreceptor specification and inhibition of parapineal and cone fates.

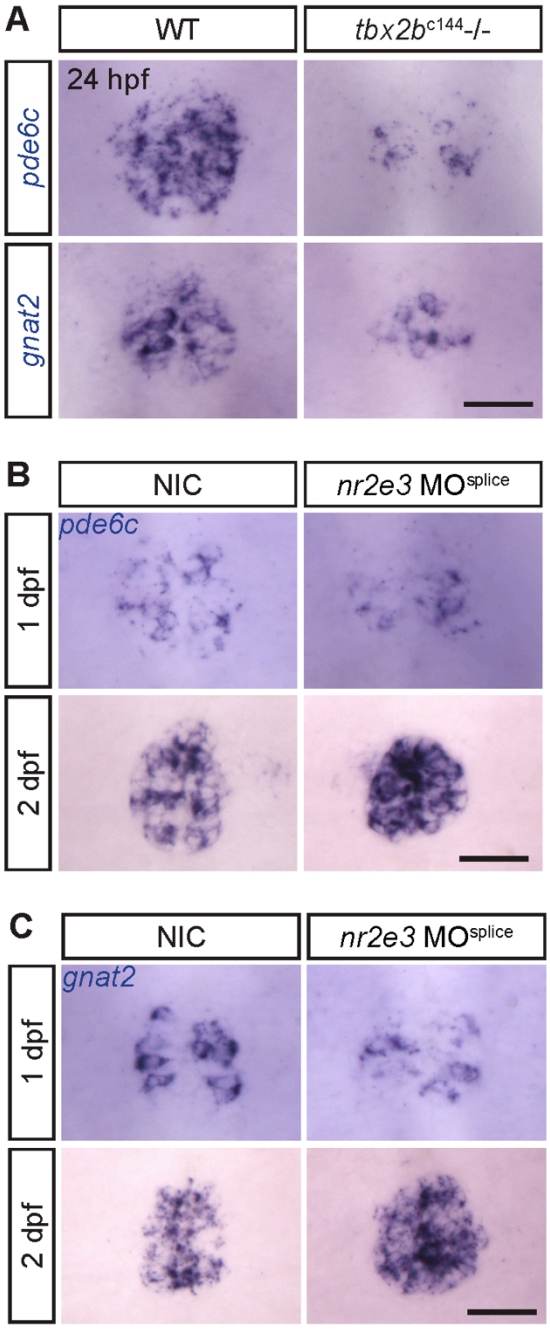

Figure 29: Tbx2b responsive genes are upregulated at a later stage in *nr2e3* morphants.
(A) Representative *in situ* hybridization images of *pde6c* and *gnat2* in WT or *tbx2b*^{c144}-/- at 24 hpf. *pde6c* and *gnat2* were transcriptionally upregulated by Tbx2b. (B) Representative *in situ* hybridization images of *pde6c* expression in NIC and *nr2e3* morphants at indicated stages. (C) Representative *in situ* hybridization images of *gnat2* expression in NIC and *nr2e3* morphants at indicated stages. Dorsal views. Scale bar=30μM

Spatial regulation of *tbx2b, nr2e3,* and *flh* expression is essential in generating correct number of parapineal cells

Using gene knockdown approaches, I have shown that Flh and Nr2e3 were inhibitory to parapineal specification. Loss of Flh or Nr2e3 function resulted in supernumerary parapineal neurons. To elucidate the possible mechanism that regulates the correct number of parapineal cells, I started to examine the expression patterns of these three transcription factors more closely. Preliminary data from double fluorescent *in situ* hybridization suggested that the inhibitory factors *nr2e3* and *flh* were more restricted posteriorly, and that there was a *tbx2b* positive, *nr2e3* and *flh* negative domain in the anterior-most region of the pineal anlage during parapineal specification (Figure 23, Figure 25). This finding is significant because previous lineage labeling experiments have placed parapineal precursors in the anterior region of the pineal anlage by 24 hpf (Clanton et al., 2013; Concha et al., 2003). Similarly, I have found that parapineal precursors were left-biased by 24-26 hpf (Figure 30). To get better resolution of the expression patterns, I am now working to optimize the labeling using next-generation *in situ* hybridization chain reaction techniques (ISHCR) (Choi et al., 2014; Choi et al., 2010). Because of the nature of developing double fluorescence *in situ* hybridizations, which only allow for the development of a single signal at a time, the second signal(s) is always reduced at subsequent step(s). Use of ISHCR allows for all signals to be developed at the same time. This should then enable weaker signals to be more visible. Preliminary results from use of this technique have shown that there was a *tbx2b* positive, *nr2e3* and *flh* negative, domain in the anterior region (Figure 31).

While it is possible that some parapineal inductive cue exists within the pineal anlage, the data support the existence of an external cue from outside of the pineal complex that is instructive in inducing parapineal fate.

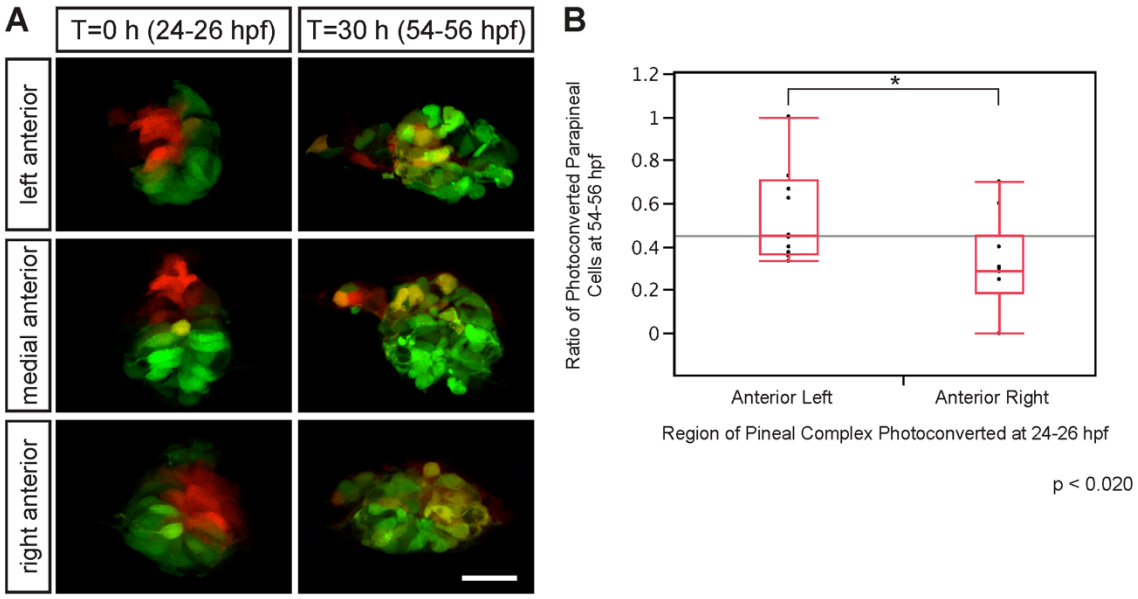

Figure 30: Parapineal precursors placement is left biased by 24-26 hpf. (A) Representative images of Tg(*cfos:gal4vp16*)^{s1145t};Tg(*uas:kaede*) in live embryos at indicated stages. Kaede was photoconverted from green to red fluorescence at 24-26 hpf (T=0 hour post photoconversion) at the region indicated. At T=30 hours post photoconversion (54-56 hpf), position of red Kaede positive cells were noted and quantified in (B). Dorsal view. Scale bar=30μM By 24-26 hpf, placement of parapineal precursors was left biased. T-test (Excel), P < 0.02.

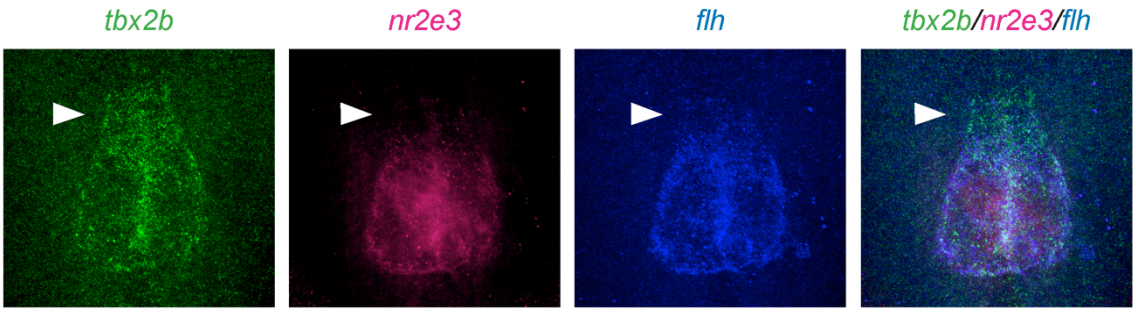

Figure 31: Preliminary results from *in situ* hybridization chain reaction experiments.
tbx2b (green), *nr2e3* (magenta), and *flh* (blue) expression at 24 hpf using *in situ* hybridization chain reaction protocol with reagents from Molecular Probe (California Institute of Technology). The anterior domain was *tbx2b* positive and *nr2e3/flh* negative (arrow heads). Mostly, *nr2e3* and *flh* expression seemed to overlap.

Tbx2b is necessary for parapineal migration

Several lines of evidence suggest that Tbx2b is necessary for parapineal migration. First, in mosaic overexpression studies, some of the cells that expressed the fluorescently tagged Tbx2b migrated away from the pineal organ, but did not turn on the marker of parapineal cells, Tg(*foxd3:gfp)* (Figure 26). Second, in *flh*^{n1} mutants/*tbx2b* morphants or *nr2e3* morphants/*tbx2b*^{c144} mutants, parapineal cells were still specified, but they did not migrate correctly (Figure 18, Figure 22).

To determine how Tbx2b controls parapineal migration, the elucidation of Tbx2b responsive genes is necessary. The transcriptome analyses between WT and *tbx2b*-deficient pineal complex cells have yielded a subset of genes that might be worth pursuing further (Chapter 2). The G-protein gamma subunits *gngt1* and *gngt2a* were downregulated in the pineal complex of *tbx2b*-deficient embryos (Figure 32A, Figure 32B). They are of interest because they have been shown to be involved in primordial

germ cell migration (Mulligan and Farber, 2011; Mulligan et al., 2010). Functional characterization of one or both of these genes should determine if they are important for parapineal migration. We were surprised that the transcriptome analyses did not yield more obvious targets. However, it is important to point out that the differential expression analysis was reported using a single program, Cuffdiff2 (Trapnell et al., 2013). Since each program performs the calculation to determine whether or not a gene is differentially expressed differently, it would be worthwhile to reanalyze the data using other available programs to see if additional candidates might arise.

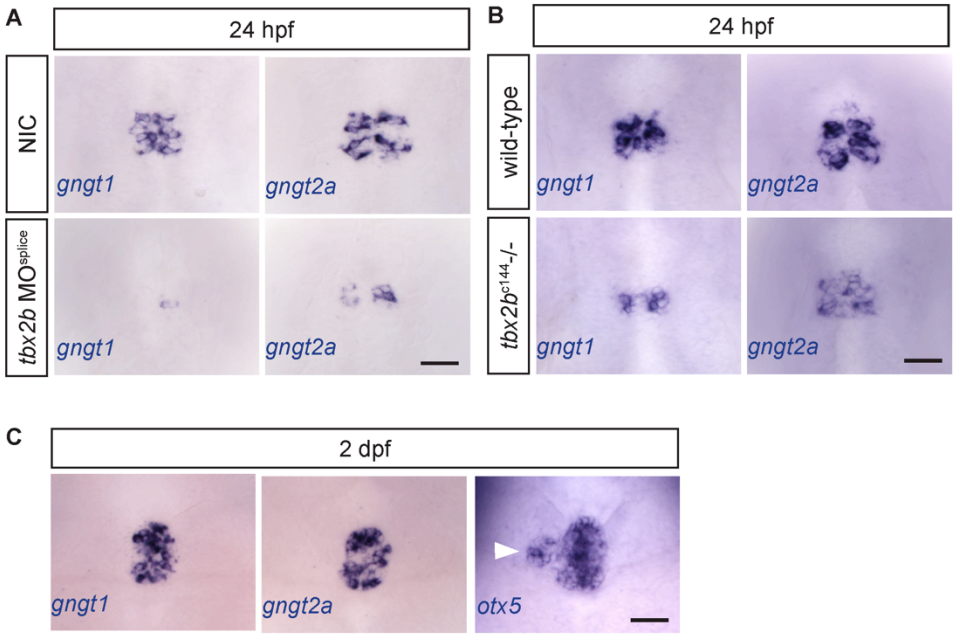

Figure 32: G-protein gamma subunits are downregulated in *tbx2b*-deficient embryos.
(A) Representative images of *in situ* hybridization (ISH) showing expression of *gngt1* or *gngt2a* in NIC and *tbx2b* morphant embryos at 24 hpf. (B) Representative images of ISH showing expression of *gngt1* or *gngt2a* in WT and *tbx2b*^{c144}-/- mutant embryos at 24 hpf. In both *tbx2b*-deficient conditions, expression of *gngt1* and *gngt2a* are reduced as compared to controls. (C) Representative images of ISH showing expression of *gngt1, gngt2a,* and *otx5* in WT embryos at 2 dpf. At this stage, *gngt1* and *gngt2a* were not expressed in matured parapineal cells (arrow head). Dorsal views. Scale bars=30μM

Correct number of parapineal cells is important for asymmetry formation in the habenulae

The parapineal organ is unilaterally placed and sends projections into the flanking habenular nucleus. However, nothing is known about how the parapineal organ influences asymmetries observed in habenular nuclei and the downstream connections to the IPN. Currently, the lack of a parapineal-specific promoter makes it impossible to directly test the function of neurons within the parapineal organ. Should a mechanism in which a particular gene or chemical can be either induced or expressed specifically within the parapineal neurons become available in the future, many questions can be addressed. For an example, is it electrical or chemical signals from the parapineal neurons that direct asymmetry formation?

A recent study by Garric and others (2014) showed that parapineal size does influence asymmetry formation in the habenulae. *pitx2c* morphant embryos have about 40 percent greater numbers of parapineal cells as compared to WT. In these embryos, asymmetry within the habenular nuclei is reduced due to an increase in left-sided characteristics (greater expression of Kctd12.1) in the right habenula. The authors did not address how this may affect the efferent connections into the IPN nor how the increase in symmetry affects behavior. However, this work provided more evidence that tightly regulating the number of parapineal cells is important in establishing left-right brain asymmetries.

In *flh*^{n1} mutants, about 2-fold more parapineal cells are observed as compared to WT. Consistent with the previous finding, our preliminary study also demonstrated

increased left sided characteristics (greater expression of Kctd12.1 expression) in the right habenula and reduced habenular asymmetries in *flh*^{n1} mutants (Figure 33).

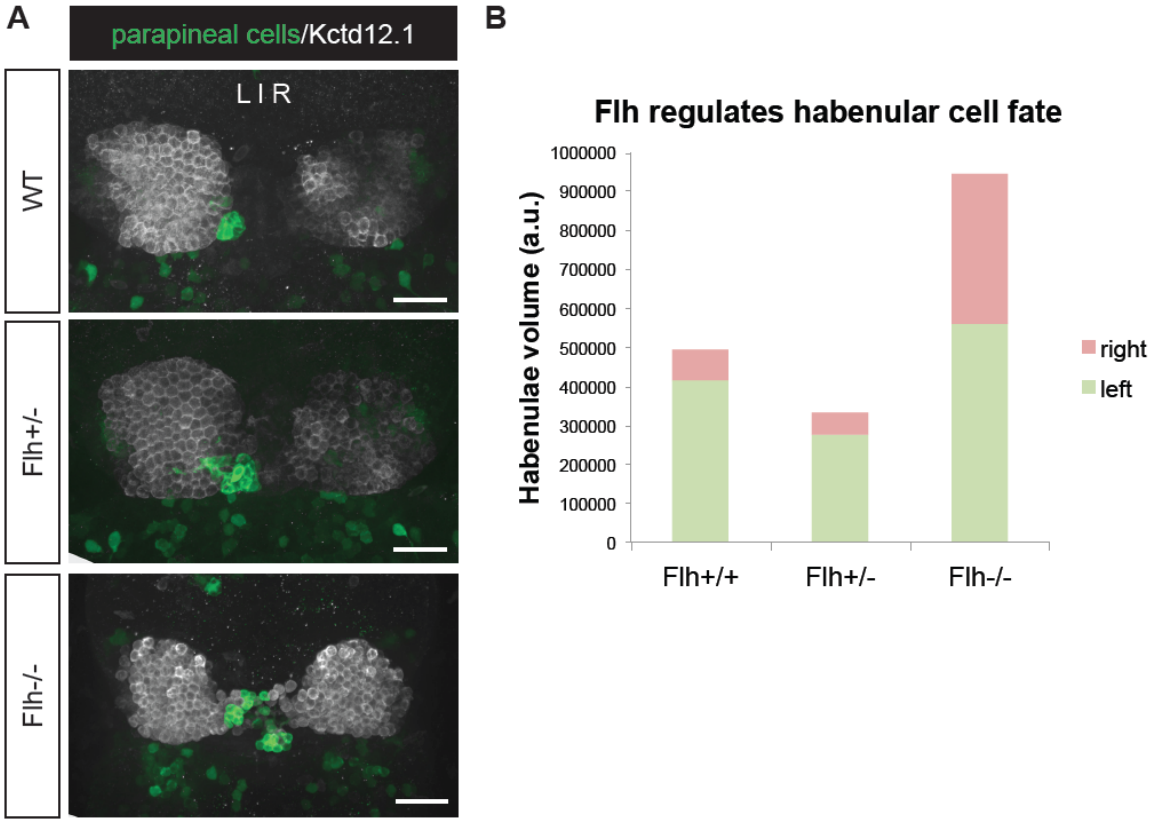

Figure 33: Decreased habenular asymmetry is observed in Flh-/- embryos. (A) Representative images of antibody labeling of *krt4*:eGFP (parapineal cells) and Kctd12.1 protein in the zebrafish epithalamus. Dorsal views, 5 dpf. Scale bars=30μM. (B) Normally, Kctd12.1 protein is more highly expressed in the left habenula as compared to the right (Flh+/+;WT). Kctd12.1 positive cell volume was more symmetrically expressed in Flh-/- mutants due to increase in Kctd12.1 expression in the right habenula.

The *incoherent type I feed forward system* as a genetic interaction system that controls cone versus rod photoreceptor differentiation

While studying the roles of Tbx2b and Nr2e3 during parapineal development, I made an interesting observation: while Tbx2b and Nr2e3 had opposite role in parapineal specification, Tbx2b seemed to positively regulate *nr2e3* expression (Figure 27). While this interaction was initially very hard to explain, it led us to propose an *incoherent type I feed forward system* as the genetic interaction system that controls parapineal numbers (discussed above). However, the best studied roles of Nr2e3, and to a lesser extent, Tbx2b are in rod and cone photoreceptor specification, respectively (Alvarez-Delfin et al., 2009; Chen et al., 2005). Because of this, we believe that this *feed forward system* may also control photoreceptor specification as well.

The question of how a correct ratio between cones and rods is achieved remains a very active topic in the field (Emerson et al., 2013). One of the proposed treatments for those who suffered from degenerative eye disease such as retinitis pigmentosa or macular degeneration is transplantation of photoreceptor precursors into the retina (Lamba et al., 2009; MacLaren et al., 2006). However, very limited number of cones, which are required for color vision, is usually generated from these precursors. Thus, understanding how cones are generated and maintained can have significant impact on human health.

The pineal organ shares cell types similarities with the retina and has fully functional photoreceptors (Mano and Fukada, 2007). Thus, it can be used as a model to study how the number of rod versus cone photoreceptors is correctly proportioned. Also, the zebrafish pineal organ, which has only two main photoreceptor subtypes: red/green cones and rods (Cau et al., 2008; Clanton et al., 2013; Lu et al., 2013), offers some

advantages over use of the zebrafish retina. It is relatively simple and unlike the photoreceptors of the retina, which are located behind the lens are aqueous humor, the photoreceptors of the pineal organ is located at the most dorsal aspect of the zebrafish head, making it very amenable to live and fixed imaging in whole embryos.

We propose that Tbx2b promotes both cone specification as well as Nr2e3 expression. Nr2e3 inhibits cone specification, but at a much less effective level as Tbx2b promotion of cone specification at an earlier stage. At later stages, Nr2e3 levels are sufficient to allow for Nr2e3 to outcompete Tbx2b and begins to outright inhibit cone fates and promote rod fate (Figure 28). In support of this model, several genes that control photoreceptor functions and maintenance were downregulated in *tbx2b* knockdown condition (Table 2). I have also demonstrated that two genes that have known roles in cone function and maintenance, *pde6c* and *gnat2,* were downstream of Tbx2b and were increased in *nr2e3* morphants as compared to wildtypes at a late stage (2 dpf), but they were indistinguishable at an early stage (1 dpf). To further test this idea, we have planned to use photoactivatable morpholino to temporally control the knockdown of *nr2e3*; use a combination of morpholino knockdown and mosaic overexpression approaches to manipulate Tbx2b and/or Nr2e3 levels.

Concluding remarks

This work has yielded significant insight into the roles of Tbx2b during parapineal development using both the candidate gene approach resulting from literature searches as well as the non-biased, transcriptome analysis approach. Through the candidate approach, I was able to determine that Tbx2b acted in a permissive manner during parapineal

specification, but it was necessary for proper parapineal migration. Further, I have characterized the inhibitory roles of Flh and Nr2e3 during formation of parapineal neurons. Using RNA-sequencing to perform differential expression analysis between wild-type and *tbx2b*-deficient pineal complex cells has yielded many targets that were downstream of Tbx2b. Together, these studies also provided a novel insight into a potential genetic interaction system between Tbx2b and Nr2e3 during cone versus rod photoreceptor differentiation.

REFERENCES

Abdul-Rahman, M. F., Qiu, A., Woon, P. S., Kuswanto, C., Collinson, S. L. and Sim, K. (2012). Arcuate fasciculus abnormalities and their relationship with psychotic symptoms in schizophrenia. *PLoS ONE* **7**, e29315.

Agetsuma, M., Aizawa, H., Aoki, T., Nakayama, R., Takahoko, M., Goto, M., Sassa, T., Amo, R., Shiraki, T., Kawakami, K., et al. (2010). The habenula is crucial for experience-dependent modification of fear responses in zebrafish. *Nature Publishing Group* **13**, 1354–1356.

Aizawa, H., Bianco, I. H., Hamaoka, T., Miyashita, T., Uemura, O., Concha, M. L., Russell, C., Wilson, S. W. and Okamoto, H. (2005). Laterotopic representation of left-right information onto the dorso-ventral axis of a zebrafish midbrain target nucleus. *Curr Biol* **15**, 238–243.

Aizawa, H., Goto, M., Sato, T. and Okamoto, H. (2007). Temporally regulated asymmetric neurogenesis causes left-right difference in the zebrafish habenular structures. *Dev Cell* **12**, 87–98.

Allende, M. L. and Weinberg, E. S. (1994). The expression pattern of two zebrafish achaete-scute homolog (ash) genes is altered in the embryonic brain of the cyclops mutant. *Dev Biol* **166**, 509–530.

Alvarez-Delfin, K., Morris, A. C., Snelson, C. D., Gamse, J. T., Gupta, T., Marlow, F. L., Mullins, M. C., Burgess, H. A., Granato, M. and Fadool, J. M. (2009). Tbx2b is required for ultraviolet photoreceptor cell specification during zebrafish retinal development. *Proc Natl Acad Sci USA* **106**, 2023–2028.

Amo, R., Aizawa, H., Takahoko, M., Kobayashi, M., Takahashi, R., Aoki, T. and Okamoto, H. (2010). Identification of the zebrafish ventral habenula as a homolog of the mammalian lateral habenula. *J Neurosci* **30**, 1566–1574.

Anders, S. and Huber, W. (2010). Differential expression analysis for sequence count data. *Genome Biol*.

Anfora, G., Frasnelli, E., Maccagnani, B., Rogers, L. J. and Vallortigara, G. (2010). Behavioural and electrophysiological lateralization in a social (Apis mellifera) but not in a non-social (Osmia cornuta) species of bee. *Behav Brain Res* **206**, 236–239.

Bajic, D., Canto Moreira, N., Wikström, J. and Raininko, R. (2012). Asymmetric development of the hippocampal region is common: a fetal MR imaging study. *AJNR Am J Neuroradiol* **33**, 513–518.

Barth, K. A., Kishimoto, Y., Rohr, K. B., Seydler, C., Schulte-Merker, S. and Wilson, S. W. (1999). Bmp activity establishes a gradient of positional information throughout the entire neural plate. *Development* **126**, 4977–4987.

Barth, K. A., Miklosi, A., Watkins, J., Bianco, I. H., Wilson, S. W. and Andrew, R. J. (2005). fsi zebrafish show concordant reversal of laterality of viscera, neuroanatomy, and a subset of behavioral responses. *Curr Biol* **15**, 844–850.

Bertolucci, C. and Foà, A. (2004). Extraocular photoreception and circadian entrainment in nonmammalian vertebrates. *Chronobiology international* **21**, 501–519.

Bisgrove, B. W., Essner, J. J. and Yost, H. J. (1999). Regulation of midline development by antagonism of lefty and nodal signaling. *Development* **126**, 3253–3262.

Bleich-Cohen, M., Sharon, H., Weizman, R., Poyurovsky, M., Faragian, S. and Hendler, T. (2012). Diminished language lateralization in schizophrenia corresponds to impaired inter-hemispheric functional connectivity. *Schizophr Res* **134**, 131–136.

Bolger, A. M., Lohse, M. and Usadel, B. (2014). Trimmomatic: a flexible trimmer for Illumina sequence data. *Bioinformatics*.

Cahill, G. M. (1996). Circadian regulation of melatonin production in cultured zebrafish pineal and retina. *Brain Res* **708**, 177–181.

Campione, M., Steinbeisser, H., Schweickert, A., Deissler, K., van Bebber, F., Lowe, L. A., Nowotschin, S., Viebahn, C., Haffter, P., Kuehn, M. R., et al. (1999). The homeobox gene Pitx2: mediator of asymmetric left-right signaling in vertebrate heart and gut looping. *Development* **126**, 1225–1234.

Carl, M., Bianco, I. H., Bajoghli, B., Aghaallaei, N., Czerny, T. and Wilson, S. W. (2007). Wnt/Axin1/beta-catenin signaling regulates asymmetric nodal activation, elaboration, and concordance of CNS asymmetries. *Neuron* **55**, 393–405.

Cau, E. and Wilson, S. W. (2003). Ash1a and Neurogenin1 function downstream of Floating head to regulate epiphysial neurogenesis. *Development* **130**, 2455–2466.

Cau, E., Quillien, A. and Blader, P. (2008). Notch resolves mixed neural identities in the zebrafish epiphysis. *Development* **135**, 2391–2401.

Chen, J., Rattner, A. and Nathans, J. (2005). The rod photoreceptor-specific nuclear receptor Nr2e3 represses transcription of multiple cone-specific genes. *J Neurosci* **25**, 118–129.

Chen, P., Hao, W., Rife, L., Wang, X. P., Shen, D., Chen, J., Ogden, T., Van Boemel, G. B., Wu, L., Yang, M., et al. (2001). A photic visual cycle of rhodopsin regeneration is dependent on Rgr. *Nat. Genet.* **28**, 256–260.

Cheng, H., Khan, N. W., Roger, J. E. and Swaroop, A. (2011). Excess cones in the retinal degeneration rd7 mouse, caused by the loss of function of orphan nuclear receptor Nr2e3, originate from early-born photoreceptor precursors. *Hum Mol Genet* **20**, 4102–4115.

Chi, N. C., Shaw, R. M., De Val, S., Kang, G., Jan, L. Y., Black, B. L. and Stainier, D. Y. R. (2008). Foxn4 directly regulates tbx2b expression and atrioventricular canal formation. *Genes Dev* **22**, 734–739.

Choi, H. M. T., Beck, V. A. and Pierce, N. A. (2014). Next-generation in situ hybridization chain reaction: higher gain, lower cost, greater durability. *ACS Nano* **8**, 4284–4294.

Choi, H. M. T., Chang, J. Y., Le A Trinh, Padilla, J. E., Fraser, S. E. and Pierce, N. A. (2010). Programmable in situ amplification for multiplexed imaging of mRNA expression. *Nat. Biotechnol.* **28**, 1208–1212.

Clanton, J. A., Hope, K. D. and Gamse, J. T. (2013). Fgf signaling governs cell fate in the zebrafish pineal complex. *Development* **140**, 323–332.

Collery, R., McLoughlin, S., Vendrell, V., Finnegan, J., Crabb, J. W., Saari, J. C. and Kennedy, B. N. (2008). Duplication and divergence of zebrafish CRALBP genes uncovers novel role for RPE- and Muller-CRALBP in cone vision. *Invest Ophthalmol Vis Sci* **49**, 3812–3820.

Concha, M. L. and Wilson, S. W. (2001). Asymmetry in the epithalamus of vertebrates. *J. Anat.* **199**, 63–84.

Concha, M. L., Burdine, R. D., Russell, C., Schier, A. F. and Wilson, S. W. (2000). A nodal signaling pathway regulates the laterality of neuroanatomical asymmetries in the zebrafish forebrain. **28**, 399–409.

Concha, M. L., Russell, C., Regan, J. C., Tawk, M., Sidi, S., Gilmour, D. T., Kapsimali, M., Sumoy, L., Goldstone, K., Amaya, E., et al. (2003). Local tissue interactions across the dorsal midline of the forebrain establish CNS laterality. *Neuron* **39**, 423–438.

Dadda, M. and Bisazza, A. (2006). Does brain asymmetry allow efficient performance of simultaneous tasks? *Animal Behaviour* **72**, 523–529.

Dadda, M., Domenichini, A., Piffer, L., Argenton, F. and Bisazza, A. (2010). Early differences in epithalamic left-right asymmetry influence lateralization and personality of adult zebrafish. *Behav Brain Res* **206**, 208–215.

Danesin, C. and Houart, C. (2012). A Fox stops the Wnt: implications for forebrain development and diseases. *Curr. Opin. Genet. Dev.* **22**, 323–330.

Doll, C. A., Burkart, J. T., Hope, K. D., Halpern, M. E. and Gamse, J. T. (2011). Subnuclear development of the zebrafish habenular nuclei requires ER translocon function. *Dev Biol* **360**, 44–57.

Domenichini, A., Dadda, M., Facchin, L., Bisazza, A. and Argenton, F. (2011). Isolation and genetic characterization of mother-of-snow-white, a maternal effect

allele affecting laterality and lateralized behaviors in zebrafish. *PLoS ONE* **6**, e25972.

Dreosti, E., Vendrell Llopis, N., Carl, M., Yaksi, E. and Wilson, S. W. (2014). Left-Right Asymmetry Is Required for the Habenulae to Respond to Both Visual and Olfactory Stimuli. *Curr Biol*.

Dufourcq, P., Rastegar, S., Strähle, U. and Blader, P. (2004). Parapineal specific expression of gfi1 in the zebrafish epithalamus. *Gene Expr Patterns* **4**, 53–57.

Dworkin, S. and Jane, S. M. (2013). Novel mechanisms that pattern and shape the midbrain-hindbrain boundary. *Cell. Mol. Life Sci.* **70**, 3365–3374.

Elmore, M. H., Gibbons, J. G. and Rokas, A. (2012). Assessing the genome-wide effect of promoter region tandem repeat natural variation on gene expression. *G3 (Bethesda)* **2**, 1643–1649.

Emerson, M. M., Surzenko, N., Goetz, J. J., Trimarchi, J. and Cepko, C. L. (2013). Otx2 and Onecut1 promote the fates of cone photoreceptors and horizontal cells and repress rod photoreceptors. *Dev Cell* **26**, 59–72.

Essner, J. J., Amack, J. D., Nyholm, M. K., Harris, E. B. and Yost, H. J. (2005). Kupffer's vesicle is a ciliated organ of asymmetry in the zebrafish embryo that initiates left-right development of the brain, heart and gut. *Development* **132**, 1247–1260.

Essner, J. J., Branford, W. W., Zhang, J. and Yost, H. J. (2000). Mesendoderm and left-right brain, heart and gut development are differentially regulated by pitx2 isoforms. *Development* **127**, 1081–1093.

Essner, J. J., Vogan, K. J., Wagner, M. K., Tabin, C. J., Yost, H. J. and Brueckner, M. (2002). Conserved function for embryonic nodal cilia. *Nature* **418**, 37–38.

Facchin, L., Burgess, H. A., Siddiqi, M., Granato, M. and Halpern, M. E. (2009). Determining the function of zebrafish epithalamic asymmetry. *Philos Trans R Soc Lond, B, Biol Sci* **364**, 1021–1032.

Fleisch, V. C., Schonthaler, H. B., Lintig, von, J. and Neuhauss, S. C. F. (2008). Subfunctionalization of a retinoid-binding protein provides evidence for two parallel visual cycles in the cone-dominant zebrafish retina. *J Neurosci* **28**, 8208–8216.

Fodor, E., Zsigmond, Á., Horváth, B., Molnár, J., Nagy, I., Tóth, G., Wilson, S. W. and Varga, M. (2013). Full transcriptome analysis of early dorsoventral patterning in zebrafish. *PLoS ONE* **8**, e70053.

Fong, S. H., Emelyanov, A., Teh, C. and Korzh, V. (2005). Wnt signalling mediated by Tbx2b regulates cell migration during formation of the neural plate. *Development* **132**, 3587–3596.

Fox, J. W. and Walsh, C. A. (1999). Periventricular heterotopia and the genetics of neuronal migration in the cerebral cortex. *The American Journal of Human Genetics* **65**, 19–24.

Fox, J. W., Lamperti, E. D., Ekşioğlu, Y. Z., Hong, S. E., Feng, Y., Graham, D. A., Scheffer, I. E., Dobyns, W. B., Hirsch, B. A., Radtke, R. A., et al. (1998). Mutations in filamin 1 prevent migration of cerebral cortical neurons in human periventricular heterotopia. *Neuron* **21**, 1315–1325.

Gamse, J. T., Kuan, Y.-S., Macurak, M., Brösamle, C., Thisse, B., Thisse, C. and Halpern, M. E. (2005). Directional asymmetry of the zebrafish epithalamus guides dorsoventral innervation of the midbrain target. *Development* **132**, 4869–4881.

Gamse, J. T., Shen, Y.-C., Thisse, C., Thisse, B., Raymond, P. A., Halpern, M. E. and Liang, J. O. (2002). Otx5 regulates genes that show circadian expression in the zebrafish pineal complex. *Nat. Genet.* **30**, 117–121.

Gamse, J. T., Thisse, C., Thisse, B. and Halpern, M. E. (2003). The parapineal mediates left-right asymmetry in the zebrafish diencephalon. *Development* **130**, 1059–1068.

Garric, L., Ronsin, B., Roussigne, M., Booton, S., Gamse, J. T., Dufourcq, P. and Blader, P. (2014). Pitx2c ensures habenular asymmetry by restricting parapineal cell number. *Development* **141**, 1572–1579.

Ge, W., He, F., Kim, K. J., Blanchi, B., Coskun, V., Nguyen, L., Wu, X., Zhao, J., Heng, J. I.-T., Martinowich, K., et al. (2006). Coupling of cell migration with neurogenesis by proneural bHLH factors. *Proc Natl Acad Sci USA* **103**, 1319–1324.

Gibbons, J. G., Beauvais, A., Beau, R., McGary, K. L., Latgé, J.-P. and Rokas, A. (2012). Global transcriptome changes underlying colony growth in the opportunistic human pathogen Aspergillus fumigatus. *Eukaryotic Cell* **11**, 68–78.

Gilmour, D. T., Maischein, H.-M. and Nüsslein-Volhard, C. (2002). Migration and function of a glial subtype in the vertebrate peripheral nervous system. *Neuron* **34**, 577–588.

Goff, L., Trapnell, C. and Kelley, D. (2012). cummeRbund: Analysis, exploration, manipulation, and visualization of Cufflinks high-throughput sequencing data. 1–65.

Goto, K., Kurashima, R., Gokan, H., Inoue, N., Ito, I. and Watanabe, S. (2010). Left-right asymmetry defect in the hippocampal circuitry impairs spatial learning and working memory in iv mice. *PLoS ONE* **5**, e15468.

Grindberg, R. V., Yee-Greenbaum, J. L., McConnell, M. J., Novotny, M., O'Shaughnessy, A. L., Lambert, G. M., Araúzo-Bravo, M. J., Lee, J., Fishman, M., Robbins, G. E., et al. (2013). RNA-sequencing from single nuclei. *Proc Natl Acad Sci USA* **110**, 19802–19807.

Gross, J. M. and Dowling, J. E. (2005). Tbx2b is essential for neuronal differentiation along the dorsal/ventral axis of the zebrafish retina. *Proc Natl Acad Sci USA* **102**, 4371–4376.

Halpern, M. E., Güntürkün, O., Hopkins, W. D. and Rogers, L. J. (2005). Lateralization of the vertebrate brain: taking the side of model systems. *J Neurosci* **25**, 10351–10357.

Halpern, M. E., Liang, J. O. and Gamse, J. T. (2003). Leaning to the left: laterality in the zebrafish forebrain. **26**, 308–313.

Herbert, M. R., Ziegler, D. A., Deutsch, C. K., O'Brien, L. M., Kennedy, D. N., Filipek, P. A., Bakardjiev, A. I., Hodgson, J., Takeoka, M., Makris, N., et al. (2005). Brain asymmetries in autism and developmental language disorder: a nested whole-brain analysis. *Brain* **128**, 213–226.

Hill, J., Dierker, D., Neil, J., Inder, T., Knutsen, A., Harwell, J., Coalson, T. and Van Essen, D. (2010). A surface-based analysis of hemispheric asymmetries and folding of cerebral cortex in term-born human infants. *J Neurosci* **30**, 2268–2276.

Inbal, A., Kim, S.-H., Shin, J. and Solnica-Krezel, L. (2007). Six3 represses nodal activity to establish early brain asymmetry in zebrafish. *Neuron* **55**, 407–415.

Jerome-Majewska, L. A., Jenkins, G. P., Ernstoff, E., Zindy, F., Sherr, C. J. and Papaioannou, V. E. (2005). Tbx3, the ulnar-mammary syndrome gene, and Tbx2 interact in mammary gland development through a p19Arf/p53-independent pathway. *Dev Dyn* **234**, 922–933.

Jiang, H. and Wong, W. H. (2008). SeqMap: mapping massive amount of oligonucleotides to the genome. *Bioinformatics* **24**, 2395–2396.

Jiang, L., Romero-Carvajal, A., Haug, J. S., Seidel, C. W. and Piotrowski, T. (2014). Gene-expression analysis of hair cell regeneration in the zebrafish lateral line. *Proc Natl Acad Sci USA* **111**, E1383–92.

Kim, D., Pertea, G., Trapnell, C., Pimentel, H., Kelley, R. and Salzberg, S. L. (2013). TopHat2: accurate alignment of transcriptomes in the presence of insertions, deletions and gene fusions. *Genome Biol* **14**, R36.

Kitambi, S. S. and Hauptmann, G. (2007). The zebrafish orphan nuclear receptor genes nr2e1 and nr2e3 are expressed in developing eye and forebrain. *Gene Expr Patterns* **7**, 521–528.

Krishnan, S., Mathuru, A. S., Kibat, C., Rahman, M., Lupton, C. E., Stewart, J., Claridge-Chang, A., Yen, S.-C. and Jesuthasan, S. (2014). The right dorsal habenula limits attraction to an odor in zebrafish. *Curr Biol* **24**, 1167–1175.

Kronmüller, K.-T., Schröder, J., Köhler, S., Götz, B., Victor, D., Unger, J., Giesel, F.,

Magnotta, V., Mundt, C., Essig, M., et al. (2009). Hippocampal volume in first episode and recurrent depression. *Psychiatry Res* **174**, 62–66.

Kwan, K. Y., Sestan, N. and Anton, E. S. (2012). Transcriptional co-regulation of neuronal migration and laminar identity in the neocortex. *Development* **139**, 1535–1546.

Lamba, D. A., Karl, M. O. and Reh, T. A. (2009). Strategies for retinal repair: cell replacement and regeneration. *Prog Brain Res* **175**, 23–31.

Larison, K. D. and Bremiller, R. (1990). Early onset of phenotype and cell patterning in the embryonic zebrafish retina. *Development* **109**, 567–576.

Lauffenburger, D. A. and Horwitz, A. F. (1996). Cell migration: a physically integrated molecular process. *Cell* **84**, 359–369.

Lauter, G., Söll, I. and Hauptmann, G. (2011). Two-color fluorescent in situ hybridization in the embryonic zebrafish brain using differential detection systems. *BMC Dev Biol* **11**, 43.

Lee, A., Mathuru, A. S., Teh, C., Kibat, C., Korzh, V., Penney, T. B. and Jesuthasan, S. (2010). The habenula prevents helpless behavior in larval zebrafish. *Curr Biol* **20**, 2211–2216.

Leonard, C. M. and Eckert, M. A. (2008). Asymmetry and dyslexia. *Dev Neuropsychol* **33**, 663–681.

Lewis, M. M., Smith, A. B., Styner, M., Gu, H., Poole, R., Zhu, H., Li, Y., Barbero, X., Gouttard, S. and McKeown, M. J. (2009). Asymmetrical lateral ventricular enlargement in Parkinson's disease. *European Journal of Neurology* **16**, 475–481.

Liang, J. O., Etheridge, A., Hantsoo, L., Rubinstein, A. L., Nowak, S. J., Izpisúa Belmonte, J. C. and Halpern, M. E. (2000). Asymmetric nodal signaling in the zebrafish diencephalon positions the pineal organ. *Development* **127**, 5101–5112.

Liotta, L. A., Steeg, P. S. and Stetler-Stevenson, W. G. (1991). Cancer metastasis and angiogenesis: an imbalance of positive and negative regulation. *Cell* **64**, 327–336.

Liu, J. S. (2011). Molecular genetics of neuronal migration disorders. *Curr Neurol Neurosci Rep* **11**, 171–178.

Long, S., Ahmad, N. and Rebagliati, M. (2003). The zebrafish nodal-related gene southpaw is required for visceral and diencephalic left-right asymmetry. *Development* **130**, 2303–2316.

Lu, P.-N., Lund, C., Khuansuwan, S., Schumann, A., Harney-Tolo, M., Gamse, J. T. and Liang, J. O. (2013). Failure in closure of the anterior neural tube causes left isomerization of the zebrafish epithalamus. *Dev Biol* **374**, 333–344.

Lust, J. M., Geuze, R. H., Groothuis, A. G. G. and Bouma, A. (2011). Functional cerebral lateralization and dual-task efficiency-testing the function of human brain lateralization using fTCD. *Behav Brain Res* **217**, 293–301.

MacLaren, R. E., Pearson, R. A., MacNeil, A., Douglas, R. H., Salt, T. E., Akimoto, M., Swaroop, A., Sowden, J. C. and Ali, R. R. (2006). Retinal repair by transplantation of photoreceptor precursors. *Nature* **444**, 203–207.

Mano, H. and Fukada, Y. (2007). A median third eye: pineal gland retraces evolution of vertebrate photoreceptive organs. *Photochem Photobiol* **83**, 11–18.

Manoli, M. and Driever, W. (2012). Fluorescence-Activated Cell Sorting (FACS) of Fluorescently Tagged Cells from Zebrafish Larvae for RNA Isolation. *Cold Spring Harbor Protocols* **2012**, pdb.prot069633–pdb.prot069633.

Martin, M. (2011). Cutadapt removes adapter sequences from high-throughput sequencing reads. *EMBnet.journal* **17**, 10–12.

Masai, I., Heisenberg, C. P., Barth, K. A., Macdonald, R., Adamek, S. and Wilson, S. W. (1997). floating head and masterblind regulate neuronal patterning in the roof of the forebrain. *Neuron* **18**, 43–57.

Mesbah, K., Rana, M. S., Francou, A., van Duijvenboden, K., Papaioannou, V. E., Moorman, A. F., Kelly, R. G. and Christoffels, V. M. (2012). Identification of a Tbx1/Tbx2/Tbx3 genetic pathway governing pharyngeal and arterial pole morphogenesis. *Hum Mol Genet* **21**, 1217–1229.

Mesulam, M.-M., Weintraub, S., Rogalski, E. J., Wieneke, C., Geula, C. and Bigio, E. H. (2014). Asymmetry and heterogeneity of Alzheimer's and frontotemporal pathology in primary progressive aphasia. *Brain* **137**, 1176–1192.

Morris, A. C., Schroeter, E. H., Bilotta, J., Wong, R. O. L. and Fadool, J. M. (2005). Cone survival despite rod degeneration in XOPS-mCFP transgenic zebrafish. *Invest Ophthalmol Vis Sci* **46**, 4762–4771.

Mortazavi, A., Williams, B. A., McCue, K., Schaeffer, L. and Wold, B. (2008). Mapping and quantifying mammalian transcriptomes by RNA-Seq. *Nat. Methods* **5**, 621–628.

Mulligan, T. and Farber, S. A. (2011). Central and C-terminal domains of heterotrimeric G protein gamma subunits differentially influence the signaling necessary for primordial germ cell migration. *Cell. Signal.* **23**, 1617–1624.

Mulligan, T., Blaser, H., Raz, E. and Farber, S. A. (2010). Prenylation-deficient G protein gamma subunits disrupt GPCR signaling in the zebrafish. *Cell. Signal.* **22**, 221–233.

Murayama, E., Herbomel, P., Kawakami, A., Takeda, H. and Nagasawa, H. (2005).

Otolith matrix proteins OMP-1 and Otolin-1 are necessary for normal otolith growth and their correct anchoring onto the sensory maculae. *Mech Dev* **122**, 791–803.

Nadauld, L. D., Chidester, S., Shelton, D. N., Rai, K., Broadbent, T., Sandoval, I. T., Peterson, P. W., Manos, E. J., Ireland, C. M., Yost, H. J., et al. (2006). Dual roles for adenomatous polyposis coli in regulating retinoic acid biosynthesis and Wnt during ocular development. *Proc Natl Acad Sci USA* **103**, 13409–13414.

Nagashima, M., Mawatari, K., Tanaka, M., Higashi, T., Saito, H., Muramoto, K.-I., Matsukawa, T., Koriyama, Y., Sugitani, K. and Kato, S. (2009). Purpurin is a key molecule for cell differentiation during the early development of zebrafish retina. *Brain Res* **1302**, 54–63.

Nagashima, M., Saito, J., Mawatari, K., Mori, Y., Matsukawa, T., Koriyama, Y. and Kato, S. (2010). A hypoplastic retinal lamination in the purpurin knock down embryo in zebrafish. *Adv. Exp. Med. Biol.* **664**, 517–524.

Oertel, V., Knöchel, C., Rotarska-Jagiela, A., Schönmeyer, R., Lindner, M., van de Ven, V., Haenschel, C., Uhlhaas, P., Maurer, K. and Linden, D. E. J. (2010). Reduced laterality as a trait marker of schizophrenia--evidence from structural and functional neuroimaging. *J Neurosci* **30**, 2289–2299.

Oertel-Knochel, V. and Linden, D. E. J. (2011). Cerebral Asymmetry in Schizophrenia. *Neuroscientist* **17**, 456–467.

Oertel-Knöchel, V., Knöchel, C., Matura, S., Prvulovic, D., Linden, D. E. J. and van de Ven, V. (2013). Reduced functional connectivity and asymmetry of the planum temporale in patients with schizophrenia and first-degree relatives. *Schizophr Res* **147**, 331–338.

Okuda, Y., Yoda, H., Uchikawa, M., Furutani-Seiki, M., Takeda, H., Kondoh, H. and Kamachi, Y. (2006). Comparative genomic and expression analysis of group B1 sox genes in zebrafish indicates their diversification during vertebrate evolution. *Dev Dyn* **235**, 811–825.

Ozsolak, F. and Milos, P. M. (2011). RNA sequencing: advances, challenges and opportunities. *Nat Rev Genet* **12**, 87–98.

Palmer, A. R. (2004). Symmetry breaking and the evolution of development. *Science* **306**, 828–833.

Parinov, S., Kondrichin, I., Korzh, V. and Emelyanov, A. (2004). Tol2 transposon-mediated enhancer trap to identify developmentally regulated zebrafish genes in vivo. *Dev Dyn* **231**, 449–459.

Patrick, R. E. and Elias, L. J. (2009). Navigational conversation impairs concurrent distance judgments. *Accid Anal Prev* **41**, 36–41.

Peng, G.-H., Ahmad, O., Ahmad, F., Liu, J. and Chen, S. (2005). The photoreceptor-specific nuclear receptor Nr2e3 interacts with Crx and exerts opposing effects on the transcription of rod versus cone genes. *Hum Mol Genet* **14**, 747–764.

Puelles, E. (2007). Genetic control of basal midbrain development. *J. Neurosci. Res.* **85**, 3530–3534.

Quillien, A., Blanco-Sanchez, B., Halluin, C., Moore, J. C., Lawson, N. D., Blader, P. and Cau, E. (2011). BMP signaling orchestrates photoreceptor specification in the zebrafish pineal gland in collaboration with Notch. *Development* **138**, 2293–2302.

Ramsköld, D., Wang, E. T., Burge, C. B. and Sandberg, R. (2009). An abundance of ubiquitously expressed genes revealed by tissue transcriptome sequence data. *PLoS Comput Biol* **5**, e1000598.

Rebagliati, M. R., Toyama, R., Fricke, C., Haffter, P. and Dawid, I. B. (1998). Zebrafish nodal-related genes are implicated in axial patterning and establishing left-right asymmetry. *Dev Biol* **199**, 261–272.

Regan, J. C., Concha, M. L., Roussigne, M., Russell, C. and Wilson, S. W. (2009). An Fgf8-dependent bistable cell migratory event establishes CNS asymmetry. *Neuron* **61**, 27–34.

Renninger, S. L., Gesemann, M. and Neuhauss, S. C. F. (2011). Cone arrestin confers cone vision of high temporal resolution in zebrafish larvae. *Eur. J. Neurosci.* **33**, 658–667.

Robinson, J. T., Thorvaldsdóttir, H., Winckler, W., Guttman, M., Lander, E. S., Getz, G. and Mesirov, J. P. (2011). Integrative genomics viewer. *Nat. Biotechnol.* **29**, 24–26.

Robinson, M. D., McCarthy, D. J. and Smyth, G. K. (2009). edgeR: a Bioconductor package for differential expression analysis of digital gene expression data. *Bioinformatics* **26**, 139–140.

Rogers, L. J. (2008). Development and function of lateralization in the avian brain. *Brain Res. Bull.* **76**, 235–244.

Rogers, L. J. (2014). Asymmetry of brain and behavior in animals: Its development, function, and human relevance. *Genesis (New York, NY : 2000)* **52**, 555–571.

Rogers, L. J., Zucca, P. and Vallortigara, G. (2004). Advantages of having a lateralized brain. *Proc Biol Sci* **271 Suppl 6**, S420–2.

Roussigne, M., Bianco, I. H., Wilson, S. W. and Blader, P. (2009). Nodal signalling imposes left-right asymmetry upon neurogenesis in the habenular nuclei. *Development* **136**, 1549–1557.

Sampath, K., Rubinstein, A. L., Cheng, A. M., Liang, J. O., Fekany, K., Solnica-Krezel, L., Korzh, V., Halpern, M. E. and Wright, C. V. (1998). Induction of the zebrafish ventral brain and floorplate requires cyclops/nodal signalling. *Nature* **395**, 185–189.

Sarmah, B., Latimer, A. J., Appel, B. and Wente, S. R. (2005). Inositol polyphosphates regulate zebrafish left-right asymmetry. *Dev Cell* **9**, 133–145.

Saxena, A., Wagatsuma, A., Noro, Y., Kuji, T., Asaka-Oba, A., Watahiki, A., Gurnot, C., Fagiolini, M., Hensch, T. K. and Carninci, P. (2012). Trehalose-enhanced isolation of neuronal sub-types from adult mouse brain. *BioTechniques* **52**, 381–385.

Schier, A. F. (2003). Nodal signaling in vertebrate development. *Annu Rev Cell Dev Biol* **19**, 589–621.

Schonthaler, H. B., Lampert, J. M., Isken, A., Rinner, O., Mader, A., Gesemann, M., Oberhauser, V., Golczak, M., Biehlmaier, O., Palczewski, K., et al. (2007). Evidence for RPE65-independent vision in the cone-dominated zebrafish retina. *Eur. J. Neurosci.* **26**, 1940–1949.

Scott, E. K., Mason, L., Arrenberg, A. B., Ziv, L., Gosse, N. J., Xiao, T., Chi, N. C., Asakawa, K., Kawakami, K. and Baier, H. (2007). Targeting neural circuitry in zebrafish using GAL4 enhancer trapping. *Nat. Methods* **4**, 323–326.

Snelson, C. D. and Gamse, J. T. (2009). Building an asymmetric brain: development of the zebrafish epithalamus. **20**, 491–497.

Snelson, C. D., Burkart, J. T. and Gamse, J. T. (2008a). Formation of the asymmetric pineal complex in zebrafish requires two independently acting transcription factors. *Dev Dyn* **237**, 3538–3544.

Snelson, C. D., Santhakumar, K., Halpern, M. E. and Gamse, J. T. (2008b). Tbx2b is required for the development of the parapineal organ. *Development* **135**, 1693–1702.

Sperry, R. W. (1961). Cerebral Organization and Behavior: The split brain behaves in many respects like two separate brains, providing new research possibilities. *Science* **133**, 1749–1757.

Stockhammer, O. W., Rauwerda, H., Wittink, F. R., Breit, T. M., Meijer, A. H. and Spaink, H. P. (2010). Transcriptome analysis of Traf6 function in the innate immune response of zebrafish embryos. *Mol Immunol* **48**, 179–190.

Stryer, L. (1991). Visual excitation and recovery. *J Biol Chem* **266**, 10711–10714.

Sun, T., Patoine, C., Abu-Khalil, A., Visvader, J., Sum, E., Cherry, T. J., Orkin, S. H., Geschwind, D. H. and Walsh, C. A. (2005). Early asymmetry of gene transcription in embryonic human left and right cerebral cortex. *Science* **308**, 1794–

1798.

Sun, Y.-F., Lee, J.-S. and Kirby, R. (2010). Brain imaging findings in dyslexia. *Pediatr Neonatol* **51**, 89–96.

Sutherland, R. J. (1982). The dorsal diencephalic conduction system: a review of the anatomy and functions of the habenular complex. *Neurosci Biobehav Rev* **6**, 1–13.

Suzuki-Hirano, A. and Shimogori, T. (2009). The role of Fgf8 in telencephalic and diencephalic patterning. *Semin. Cell Dev. Biol.* **20**, 719–725.

Talbot, W. S., Trevarrow, B., Halpern, M. E., Melby, A. E., Farr, G., Postlethwait, J. H., Jowett, T., Kimmel, C. B. and Kimelman, D. (1995). A homeobox gene essential for zebrafish notochord development. *Nature* **378**, 150–157.

Tang, F., Barbacioru, C., Wang, Y., Nordman, E., Lee, C., Xu, N., Wang, X., Bodeau, J., Tuch, B. B., Siddiqui, A., et al. (2009). mRNA-Seq whole-transcriptome analysis of a single cell. *Nat. Methods* **6**, 377–382.

Taylor, R. W., Hsieh, Y.-W., Gamse, J. T. and Chuang, C.-F. (2010). Making a difference together: reciprocal interactions in C. elegans and zebrafish asymmetric neural development. *Development* **137**, 681–691.

Thisse, C. and Thisse, B. (1999). Antivin, a novel and divergent member of the TGFbeta superfamily, negatively regulates mesoderm induction. *Development* **126**, 229–240.

Toga, A. W. and Thompson, P. M. (2003). Mapping brain asymmetry. *Nat Rev Neurosci* **4**, 37–48.

Trapnell, C., Hendrickson, D. G., Sauvageau, M., Goff, L., Rinn, J. L. and Pachter, L. (2013). Differential analysis of gene regulation at transcript resolution with RNA-seq. *Nat. Biotechnol.* **31**, 46–53.

Trapnell, C., Roberts, A., Goff, L., Pertea, G., Kim, D., Kelley, D. R., Pimentel, H., Salzberg, S. L., Rinn, J. L. and Pachter, L. (2012). Differential gene and transcript expression analysis of RNA-seq experiments with TopHat and Cufflinks. *Nat Protoc* **7**, 562–578.

Treutlein, B., Brownfield, D. G., Wu, A. R., Neff, N. F., Mantalas, G. L., Espinoza, F. H., Desai, T. J., Krasnow, M. A. and Quake, S. R. (2014). Reconstructing lineage hierarchies of the distal lung epithelium using single-cell RNA-seq. *Nature*.

Vallortigara, G. and Rogers, L. J. (2005). Survival with an asymmetrical brain: advantages and disadvantages of cerebral lateralization. *Behav Brain Sci* **28**, 575–89; discussion 589–633.

Vallortigara, G., Chiandetti, C. and Sovrano, V. A. (2011). Brain asymmetry (animal). *Wiley Interdisciplinary Reviews: Cognitive Science* **2**, 146–157.

Vallortigara, G., Rogers, L. J. and Bisazza, A. (1999). Possible evolutionary origins of cognitive brain lateralization. *Brain Res. Brain Res. Rev.* **30**, 164–175.

Venkateswaran, A., Sekhar, K. R., Levic, D. S., Melville, D. B., Clark, T. A., Rybski, W. M., Walsh, A. J., Skala, M. C., Crooks, P. A., Knapik, E. W., et al. (2013). The NADH Oxidase ENOX1, a Critical Mediator of Endothelial Cell Radiosensitivity, is Crucial for Vascular Development. *Cancer Res*.

Vesterlund, L., Jiao, H., Unneberg, P., Hovatta, O. and Kere, J. (2011). The zebrafish transcriptome during early development. *BMC Dev Biol* **11**, 30.

Walker, C. (1999). Haploid screens and gamma-ray mutagenesis. *Methods Cell Biol* **60**, 43–70.

Wells, Q. S., Becker, J. R., Su, Y. R., Mosley, J. D., Weeke, P., D'Aoust, L., Ausborn, N. L., Ramirez, A. H., Pfotenhauer, J. P., Naftilan, A. J., et al. (2013). Whole exome sequencing identifies a causal RBM20 mutation in a large pedigree with familial dilated cardiomyopathy. *Circ Cardiovasc Genet* **6**, 317–326.

Wilson, S. W. and Easter, S. S. (1991). Stereotyped pathway selection by growth cones of early epiphysial neurons in the embryonic zebrafish. *Development* **112**, 723–746.

Wilson, S. W., Ross, L. S., Parrett, T. and Easter, S. S. (1990). The development of a simple scaffold of axon tracts in the brain of the embryonic zebrafish, Brachydanio rerio. *Development* **108**, 121–145.

Wu, S.-Y., de Borsetti, N. H., Bain, E. J., Bulow, C. R. and Gamse, J. T. (2013). Mediator Subunit 12 coordinates intrinsic and extrinsic control of epithalamic development. *Dev Biol*.

Wurst, W. and Bally-Cuif, L. (2001). Neural plate patterning: upstream and downstream of the isthmic organizer. *Nat Rev Neurosci* **2**, 99–108.

Xu, J., Dodd, R. L., Makino, C. L., Simon, M. I., Baylor, D. A. and Chen, J. (1997). Prolonged photoresponses in transgenic mouse rods lacking arrestin. *Nature* **389**, 505–509.

Zhang, J., Talbot, W. S. and Schier, A. F. (1998). Positional cloning identifies zebrafish one-eyed pinhead as a permissive EGF-related ligand required during gastrulation. *Cell* **92**, 241–251.

Zindy, F., Cunningham, J. J., Sherr, C. J., Jogal, S., Smeyne, R. J. and Roussel, M. F. (1999). Postnatal neuronal proliferation in mice lacking Ink4d and Kip1 inhibitors of cyclin-dependent kinases. *Proc Natl Acad Sci USA* **96**, 13462–13467.